A COMPREHENSIVE ANALYSIS OF SURFACE ELECTROMYOGRAPHY FOR CONTROL OF LOWER LIMB EXOSKELETON

ABDELHAKIM DEBOUCHA

Thesis submitted in fulfillment of the requirements
For the Degree of Doctor of Philosophy

Faculty of Manufacturing Engineering
UNIVERSITY MALAYSIA PAHANG

AUGUST 2016

UNIVERSITY MALAYSIA PAHANG

DECLARATION OF THESIS AND COPYRIGHT

Author's full name : Abdelhakim Deboucha

Date of birth : MAY 01, 1982

Title : A COMPREHENSIVE ANALYSIS OF SURFACE ELECTROMYOGRAPHY FOR CONTROL OF LOWER LIMB EXOSKELETON

Academic Session : 2015/2016

I declare that this thesis is classified as:

☐ **CONFIDENTIAL** (Contain confidential information under the Official Secret Act 1972)*

☐ **RESTRICTED** (Contain restricted information as specified by the organization where research was done)

☐ **OPEN ACCESS** I agree that my thesis to be published as online open access (Full text)

I acknowledge that Universiti Malaysia Pahang reserve the right as follows:

1. The Thesis is the Property of Universiti Malaysia Pahang
2. The Library of Universiti Malaysia Pahang has the right to make copies for the purpose of research only
3. The Library has the right to make copies of the thesis for academic exchange.

Certified By:

_____ _____

(Student's Signature) (Signature of Supervisor)

D Abdelhakim

(New IC/Passport Number) (Name of Supervisor)

Date: Date:

NOTES : *If the thesis is CONFIDENTIAL or RESTRICTED, please attach with the letter from the organization with period and reasons for confidentiality or restriction.

SUPERVISOR'S DECLARATION

We hereby declare that we have checked this thesis and in our opinion, this thesis is adequate in terms of scope and quality for the award of the degree of Doctor of Philosophy in Mechatronics Engineering.

_____

(Supervisor's Signature)

Name of Supervisor:

Position:

Date: _____

_____

(Co-Supervisor's Signature)

Name of Co-Supervisor:

Position:

Date: _____

STUDENT'S DECLARATION

I hereby declare that the work in this thesis is my original work except for quotations and citation which have been duly acknowledged. I also declare that it has not been previously or concurrently submitted for any other degree at Universiti Malaysia Pahang or any other institutions.

_____

(Author's Signature)

Name : ABDELHAKIM DEBOUCHA

ID Number : PMA12002

Date : 22 AUGUST, 2016

DEDICATION

To one whose prayers is the secret of my success and whose affection is the cure to my wounds to the most and the dearest loved ones

My Beloved Mother, My Wife and our angel: Abdulrahman.

I dedicate this work

ACKNOWLEDGMENT

In the name of Allah, the most Beneficent, the most Merciful, lord of the universe, Praise is to Allah who gave me the power, the strength, the motivation, help and the patience to complete this study after so many hurdles and obstacles, and blessings and peace be upon our final prophet and messenger Muhammad (peace be upon him) who was sent by Allah to be a great teacher of human kind. Firstly and above all, I would like to thank Allah for giving me health and all the internal resources needed for the fulfillment of completing the journey of the PhD program.

I would like to express my heartiest thanks to my supervisor, Professor Dr. Zahari Taha, for receiving me with open arms, support, advice and devotion of time, throughout my research. I learnt from him on how to arrange my research and how to innovate my ideas to achieve my goal with highest accuracy and longer time. He has been an inspiration in both personal and professional aspects. I owe my deepest appreciation and gratitude to my co-supervisor Dr Nizam Uddin, who has been invaluable as a research partner. Only with his dedication, wisdom, and inspiration, I am forever indebted to him for his good guidance.

I cannot finish my acknowledgements without thanking my family for their affectionate understanding and love throughout my PhD. study; my father, my mother, my brothers, and my sisters. No words could express my deepest gratitude for my family, Their support and efforts have relieved my worries and made me able to concentrate on my research, They have always encouraged me when I encountered difficulties. I would like to share this moment of happiness with them. Special thanks with all my heart to my wife for being the greatest support during my PhD life, which makes my time towards the PhD program as smooth as possible.

Last but not least, I would like to thank everybody who was important to the successful realization of the thesis, as well as express my apology that I could not mention personally one by one. The completion of my thesis would not be possible without the help and encouragement of many people.

ABSTRACT

The development of exoskeleton robotic device (ERD) is one of the most applicable devices for rehabilitation purposes and human-assistance. Unlike other control methods applied to industrial robotic systems in the sense of giving specific trajectory to be tracked, ERD physically interacts alongside with the user. To attain high cognitive interaction and safe human-machine system, there is a need to detect the user's movement intention. One of the bio-signals that have been found to reflect directly the individual's motion intention is the Electromyography (EMG). Although these signals are to some extent insulated by myelin, with the remarkable advancement in bio-sensors technology and standard recommendations in signal acquiring processing, it becomes affordable to acquire, analyze, interpret and use them to control robotic devices. Surface Electromyography (sEMG) signal measured by surface electrodes has become of great interest among researchers in both clinical and engineering aspects. To ensure high cognitive user-robotic system, sEMG signal is implemented as control command for ERD. However, this signal is highly sensitive to noises and exhibits additional measurements (crosstalk) contaminated on the signal of interest. In order to add to this area of knowledge, recording and analyzing these signals may give an optimum and safe control performance for ERD. Particular experiments were conducted on the rising from a chair and walking tasks. The experiments were conducted on five subjects where the sEMG signals were recorded over four major muscles of the lower limb (Biceps Femoris (BF), Rectus Femoris (RF), Gastrocnemius (Gas) and Soleus (Sol) muscles) along with the kinematics recordings. A novel algorithm to determine the overlapped crosstalk recordings was developed along with a modified low pass filter that adaptively removes these recordings. A parametric model based on Hill Muscle Model (HMM) to estimate the knee joint moment is developed for both experiments protocols. The parametric model involves the mapping of the sEMG signals to the knee joint moment. Obviously, selecting four muscles to attain a full joint moment and motion is not sufficient, therefore we introduced the net joint moment obtained from the inverse dynamics to optimize the predicted joint moment. Initial estimate of the model is obtained from literature review while the Levenderg-Marquardt (LM) method is applied to solve the nonlinear least squares optimization problem. Results showed that the filter parameters selection could significantly affect the amplitude of the sEMG as well as it may conceal the exact onset/offset time of the signal. The developed algorithm for the crosstalk recordings detection shows ability in determining the presence of the overlapped measurements period. The results of the modified Butterworth filter showed good suppression of the crosstalk and brought the signal of interest into its baseline state. This will increase and ensure the safety of the users of the ERD. For both experiment protocols, the R^2 between the net and the predicted joint moment showed good agreement in the chair-rise protocol (0.99), while the in the walking task the R^2 was (0.91). The RMSE for both protocols were relatively low varying between 6.88 and 8.31. This means the model can accurately predict the knee joint moment.

ABSTRAK

Pembangunan peranti robotik exoskeleton (ERD) adalah salah satu alat yang paling digunakan untuk tujuan pemulihan dan manusia-bantuan. Tidak seperti kaedah kawalan yang lain digunakan untuk sistem robotik industri dalam erti memberi trajektori tertentu yang akan dikesan, ERD fizikal berinteraksi bersama-sama dengan pengguna, dan oleh itu terdapat keperluan untuk mengesan pergerakan niat pengguna. Salah satu bio-isyarat yang telah ditemui untuk mencerminkan langsung gerakan niat individu adalah Electromyography (EMG). Walaupun isyarat ini adalah dalam beberapa jenis terlindung oleh Myelin, dengan kemajuan yang luar biasa dalam teknologi sensor dan cadangan standard dalam pemprosesan, ia menjadi berpatutan untuk memperoleh, menganalisis, mentafsir dan menggunakan mereka untuk mengawal peranti robotik. Surface Electromyography (sEMG) isyarat diukur dengan elektrod permukaan telah menjadi kepentingan besar di kalangan penyelidik dalam kedua-dua aspek klinikal dan kejuruteraan. Untuk memastikan sistem pengguna-robot kognitif yang tinggi, isyarat EMG dilaksanakan sebagai arahan kawalan untuk ERD. Walau bagaimanapun, isyarat ini sangat sensitif kepada bunyi dan mempamerkan ukuran tambahan (crosstalk) yang tercemar pada isyarat yang menarik. Dalam usaha untuk menambah ke kawasan ini pengetahuan, rakaman dan menganalisis isyarat-isyarat ini boleh memberi prestasi kawalan optimum dan selamat untuk ERD. eksperimen tertentu dijalankan ke atas yang semakin meningkat dari kerusi dan berjalan tugas. Kajian ini telah dijalankan ke atas lima mata pelajaran inilah isyarat sEMG dicatatkan lebih empat otot utama anggota badan yang lebih rendah (Biceps Femoris (BF), Rectus Femoris (RF), gastrocnemius (Gas) dan soleus (Sol) otot) bersama-sama dengan kinematik rakaman. algoritma untuk menentukan rakaman crosstalk bertindih telah dibangunkan bersama-sama dengan penapis laluan rendah diubahsuai yang adaptif membuang rakaman ini. model parametrik berdasarkan Hill Muscle Model (HMM) untuk menganggarkan lutut masa ini bersama dibangunkan untuk kedua-dua eksperimen protokol. Model parametrik melibatkan pemetaan isyarat sEMG lutut masa ini bersama. Jelas sekali, memilih empat otot untuk mencapai masa bersama penuh dan gerakan adalah tidak mencukupi, oleh itu kami memperkenalkan masa bersama bersih diperolehi daripada dinamik songsang untuk mengoptimumkan masa bersama yang diramalkan. anggaran awal model yang diperolehi daripada kajian literatur manakala Levenberg-Marquardt (LM) method digunakan untuk menyelesaikan masalah-kurangnya dua pengoptimuman tak linear. Hasil kajian menunjukkan bahawa pemilihan parameter penapis ketara boleh menjejaskan amplitud sEMG dan juga kerana ia boleh menyembunyikan bermulanya tepat / masa yang mengimbangi isyarat. Algoritma dibangunkan untuk mengesan rakaman crosstalk menunjukkan keupayaan dalam menentukan kehadiran tempoh ukuran yang bertindih. Keputusan penapis Butterworth yang diubah suai menunjukkan penindasan baik crosstalk dan membawa isyarat faedah ke dalam keadaan asas itu. Ini akan meningkatkan dan memastikan keselamatan pengguna ERD. Bagi kedua-dua protokol eksperimen, R^2 antara bersih dan masa bersama yang diramalkan menunjukkan perjanjian yang baik dalam protokol kerusi bertingkat (0.99), manakala dalam tugas berjalan R^2 adalah (0.91). The RMSE untuk kedua-dua protokol yang agak rendah yang berbeza-beza di antara 6.88 dan 8.31. Ini bermakna model yang tepat boleh meramalkan lutut masa ini bersama.

TABLE OF CONTENTS

DECLARATION

TITLE PAGE i

ACKNOWLEDGMENT ii

ABSTRACT iii

ABSTRAK iv

TABLE OF CONTENTS v

LIST OF TABLES viii

LIST OF FIGURES ix

LIST OF SYMBOLS xiii

LIST OF ABBREVIATION xiv

CHAPTER 1 INTRODUCTION

1.1 Introduction 1

1.2 Motivation and Significance of the Research 3

1.3 Problem Statement 4

1.4 Research Objectives 5

1.5 Overview of the Thesis 5

CHAPTER 2 LITERATURE REVIEW

2.1 Introduction 7

2.1.1 Rehabilitation Definition 8

2.2 Brief History 10

2.2.1 Exoskeletons 11

2.3 Electromyography 13

2.3.1 sEMG Recording Concept 14

2.3.2 Crosstalk Phenomenon 15

2.4 Usability of sEMG signal in the Control of Assistive Devices 17

2.5 Butterworth Filter for sEMG Filtering Review 22
2.6 Summary 25

CHAPTER 3 METHODOLOGY

3.1 Introduction 27
3.2 Materials 28
3.2.1 Software 28
3.2.2 Synchronized Biomechanics Software 30
3.2.3 Hardware 32
3.3 Experimental Protocol 34
3.4 Data Acquisition 36
3.4.1 Sensor Placement 37
3.4.2 Pre-recording Data Protocol 37
3.4.3 Skin Preparation and Surface Electrodes Placing 37
3.5 Real Time Implementation 38
3.6 Summary 40

CHAPTER 4 sEMG SIGNAL PROCESSING

4.1 Introduction 42
4.2 Data Analysis Procedure 42
4.2.1 sEMG Normalization 42
4.2.2 Baseline Wander 43
4.2.3 DC Components 43
4.2.4 sEMG Features Extraction 44
4.2.5 High Pass Filtering 47
4.2.6 Low Pass Filtering 47
4.3 Onset/Offset of sEMG Detection (offline Detection) 52
4.4 Modified Butterworth Filter for Crosstalk /Unwanted Measurement Removal 53
4.4.1 Recursive Least Squares 54
4.5 sEMG Signal to Muscle Activation Model 57

4.6 Hill's Type Model 59
4.7 Inverse Dynamics Method 64
4.8 Summary 68

CHAPTER 5 RESULTS AND DISCUSSION

5.1 Introduction 69
5.2 Pre-Processing 70
5.3 Butterworth Filter Performance 72
5.3.1 Optimal Filter Order 78
5.3.2 Optimal Cutoff Frequency 80
5.4 Lower Limb Muscle Activities Normalization to Motion Range 81
5.4.1 Sit to Stand Results 82
5.4.2 Stand to Sit Results 85
5.4.3 Walking Results 88
5.5 Crosstalk/Unwanted Recordings Removal 91
5.6 Muscle Activation Dynamics 98
5.7 Hill's Model Output 99
5.8 Inverse Dynamics Results 101
5.8.1 Predicted Joint Moment 103
5.8.2 Real Time Implementation 106
5.9 Summary 107

CHAPTER 6 CONCLUSIONS

6.1 Introduction 108
6.2 Summary of the Research work 108
6.3 Research Contribution 110
6.4 Future Work 110
6.5 Recommendations 110

REFERENCES 112
APPENDICES 123

LIST OF TABLES

Table	Title	Page
2.1	Comparison of prosthesis, orthosis and exoskeleton.	11
2.2	Butterworth Filter Usability in sEMG Filtering	23
3.1	Shimmer EMG sensor specification	32
3.2	Task specification for chair rising experiment protocol	37
4.1	Brief description and the mathematical equations for some of EMG applicable features.	45
4.2	Correlation between sEMG features.	46
4.3	Properties of the selected muscles	62
4.4	Estimated coefficients of the equation (3.45)	63
4.5	Anthropometric data of one subject with weight of 71kg	67
5.1	Maximum values of the filtered sEMG	78
5.2	Wavelet output correlation with Butterworth filter	79
5.3	Computation time difference between wavelet and Butterworth	81
5.4	Hip angles range and movement time during chair rise task	82
5.5	STD during sit to stand task	85
5.6	STD during stand to sit task	87
5.7	Motion range and movement time during walking for one stride	88
5.8	Identified parameters based LS method	105
5.9	R^2 and RMSE values	106

LIST OF FIGURES

Figure	Title	Page
2.1	Assistive Robotics device application overview	8
2.2	Berkeley Lower Extremity Exoskeleton (BLEEX)	12
2.3	Schematic representation of the muscle fiber, the nerve fiber, and the resultant activations.	15
2.4	Example of mixture signal (crosstalk)	17
2.5	Utah prosthesis assembly adapted from [Jacobson. S. C. (1982)]	18
2.6	One channel of the waveform length with the corresponding angle.	20
2.7	sEMG with elbow motion	21
2.6	Simplified control strategy for elbow assistance	21
3.1	Overview block diagram of the study.	28
3.2	Print screen of Real-Term hyperteminal capture software.	29
3.3	Block Diagram for the developed software	30
3.4	sEMG Recording user interface using MATLAB.	31
3.5	Shimmer EMG sensor.	32
3.6	Gyro sensor	33
3.7	Disposal electrodes and the leads used to connect the sensor with the electrodes	33
3.8	Arduino Uno and Adafruit motor shield boards	34
3.9	Chair rising protocol.	35
3.10	Kinematics coordinates.	35
3.11	Representation scheme of human walking gait in one cycle, the gait begins and ends at heel strike.	36
3.12	Experiment set-up for chair rising and walking protocols.	39
3.13	Hardware Configuration	40
4.1	Determination of Butterworth coefficients	48

4.2	Example of Onset/Offset of sEMG (Offline Detection)	53
4.3	Adaptive Butterworth filter stages.	54
4.4	Schematic representation of the steps involved to transform sEMG signal to the muscle force.	57
4.5	A-model: neural activation to muscle activation	58
4.6	Hill's muscle type model.	59
4.7	Relationship between the muscle forces to the fiber length	60
4.8	Segmental model of the chair-rise, the movement is about the knee joint.	65
5.1	Example of a sEMG raw with DC component being removed.	70
5.2	Example of a measured angular velocity achieved during chair rise task for two trials	71
5.3	Example of a resulted hip angle during chair rise task for two trials.	71
5.4	Example of sEMG raw over RF and BF muscles during chair rising task	72
5.5	Butterworth Filter Performance at w_c = 2Hz.	74
5.6	Butterworth Filter Performance at w_c = 5Hz.	75
5.7	Butterworth Filter Performance at w_c = 6Hz.	76
5.8	Butterworth Filter Performance at w_c = 8Hz.	77
5.9	Correlation between the wavelet output at level six and outputs of the Butterworth filter at different order.	79
5.10	Example of the wavelet outputs at scales 5, 6, 7 and 8.	80
5.11	Filters output correlation with the original signal.	81
5.12	Hip angles of five subjects during performing sit to stand task	83
5.13	BF muscle activities normalized to the sit to stand motion range	84
5.14	RF muscle activities normalized to the sit to stand motion range	84
5.15	Schematic representation of the BF and RF muscle activities onset time during sit to stand task with regard to the motion range	86
5.16	Hip angles of five subjects during stand to sit task	86

5.17 BF muscle activities normalized to the stand to sit motion range 86

5.18 RF muscle activities normalized to the stand to sit motion range 87

5.19 Schematic representation of the BF and RF muscle activities during stand to sit task 87

5.20 Hip angles during walking. 89

5.21 Knee angles during walking. 89

5.22 BF muscle activities normalized to one gait cycle 90

5.23 RF muscle activities normalized to one gait cycle 90

5.24 Gastrocnemius muscle activities normalized to one gait cycle 91

5.25 Soleus muscle activities normalized to one gait cycle. 91

5.26 BF and RF sEMG recording with the corresponding angular velocity 93

5.27 Filtered 1st and 2nd bursts of the RF sEMG using 3rd order Butterworth. 94

5.28 Example 1 of the crosstalk removal using adaptive Butterworth filter 95

5.29 Example 2 of the crosstalk removal using adaptive Butterworth filter 96

5.30 Example 3 of the crosstalk removal using adaptive Butterworth filter 97

5.31 sEMG to the muscle activation transformation 98

5.32 Example of the transformation (e(k)) to ($F_m(k)$). 99

5.33 Joint moment generated by the RF and BF muscle during chair-rise task 100

5.34 Net joint moment obtained from the BF, RF and Gas muscles during walking task for one gait cycle 100

5.35 Inverse dynamic of the knee joint moment and the moment produced by the BF and RF muscles during chair-rise 102

5.36 Inverse dynamic joint moment and the selected muscles during walking task 103

5.37 Inverse dynamic net joint moment and the tuned joint moment during chair-rise 104

5.38 Inverse dynamic net joint moment and the tuned joint moment during walking 104

5.39 Knee angles of the individual compared with angle of the exoskeleton during chair-rise task 106

LIST OF SYMBOLS

θ_1	Knee angle
θ_2	Hip angle
A	A model (sEMG to neural activation model)
b_0	Butterworth Coefficient
Cov	Co-variance
N	Number of samples
s	Fourier Transform Operator
Var	Variance
w_c	Angular cut-off frequency
w_s	Angular Sampling frequency
z	z Transform Operator
λ	Wavelet scale
σ_x	Variance for x variable
σ_y	Variance for y variable

LIST OF ABBREVIATIONS

AT	Assistive Technology
BF	Biceps Femoris Muscle
CE	Contractile active element
CoG	Center of Gravity
DCT	Digital Cosine Transform
ECG	Electrocardiogram signal
EMG	Electromyographic
Gas	Gastrocnemius Muscle
HAT	Head, Arms and Trunk
HMI	Human Machine Interface
I/O	Input/Output
ICA	Independent Component Analysis
IEMG	Integral EMG
IIR	Infinite Impulse Response
l^{mt}	Muscle-tendon length
LS	Least Squares
$M.A_i$	Moment arm
MAV	Mean Absolute Value
MMAV1	Modified Mean Absolute Value 1
MMAV2	Modified Mean Absolute Value 2
MRT	Multi Resolution Transform
PCA	Principal Component Analysis
PE	Passive elastic element

QRS	Q wave, R wave and S wave graphical deflections in the ECG signal
RF	Rectus Femoris Muscle
RLS	Recursive Least Squares
RMS	Root Mean Square
sEMG	Surface Electromyography
SNR	Signal to Noise Ratio
STS	Sit to Stand
Sol	Soleus Muscle
SSI	Simple Square Integral
VAR	Variance
WT	Wavelet Transform

UMP

CHAPTER 1

INTRODUCTION

1.1 Introduction

Assistive devices are a particular category of assistive technology (AT). Examining some definitions given for assistive technology reported in (Hersh and Johnson, 2008a, Digiovine et al., 2007 and Pasha and Pasha, 2006), assistive technology is an inclusive term which covers technologies, products, services and systems that could be used by disabled and/or elderly people. Assistive technology could also be defined based either on social use (Barnes, 1994 and Johnstone, 2001) or medical use (WHO, 1980, 2001). Furthermore, the definition of assistive technology could be based on overcoming the barriers/deficits faced by the user him/herself for instance, knee assistive device, and ankle prosthesis. Particularly, assistive technology could be categorized based on its function (Hersh, 2010)

i. Assistive devices, in which are designed to remove barriers faced by disabled and elderly people.
ii. Rehabilitation devices designed to restore the functioning of disabled and/or elderly people experiencing lower or upper extremities impairment.
iii. Medical devices, which are designed to support a range of health care practices and promote healing in people experiencing illness or other forms of ill-health and who may be categorized as patient.

The difference between assistive devices and rehabilitation devices is that assistive devices modify the interaction between the user and the environment in order to remove certain obstacles such as cranks/braces used by elderly and prosthesis used by amputees, whereas rehabilitation devices such as powered exoskeleton alters directly on the individual/patient to overcome some limitations (Hersh and Johnson, 2008a, b). Exoskeletons are intermingled assistive devices in terms that they can be assistive device until the individual recover back his/her motor skill.

The presence of exoskeleton robotic devices in the rehabilitation field and assistive technology opened new direction of interest in the study of their control strategies. Unlike other control methods applied to industrial robotic systems in the sense of giving pre-programmed trajectory to be followed, assistive devices (exoskeletons/orthoses) technologies require parallel physical interaction and close cognitive between the user and the device. In order to ensure a safe physical interaction with high cognitive, there is a need to detect the user's movement intention.

Biology signals are the only means that detect the user's movement intention such as Electroencephalography (EEG), Electromyography (EMG), Mechnanomyogram (MMG), and Electrocorticogram (ECoG) signals. One might refers to the evidence that the first intention can be detected from the central nervous system (CNS) through EEG recordings. However, due to the complexity/analysis in recording/analyzing the EEG signal and the traveling time of the signal pulse from the CNS to the motor nerve of the muscles, researchers are more towards the investigation of the use of EMG signal. This latter seems to enclose the meaning and explanation of a motion generated by the muscles activities. In human skeleton there are about 640 muscles acting as actuators in order to give an amazing flexible motion to human being ("Muscle," 2016). Particularly, there are about 32 major group muscles in the lower extremities that allow human being to move flexibly (Ward et al., 2009).

Advances in assistive robotics together with clinical neuroscience have greatly expanded the development of machines to improve functioning and mobility for individual with disability. These devices can be used during therapy to retrain motor abilities or during every day activities to assist individuals with disabilities (Schulze et al, 2012).

Many promising rehabilitation technologies have to some extent partially failed to achieve successful recovery for the patient due to maybe late intervention, less intensively rehabilitation task and other reasons. It is important then to involve different disciplines in order to complete a successful therapeutic rehabilitation robotic device. Engineers, physiologists and neuroscientists should take part and conduct a close collaboration to design a safe, robust and human friendly machine. Rehabilitation devices are not merely operated by a person, but they must work in concert with the patient as a system. Current researches on designing exoskeletons for rehabilitation purposes have given slightly important enhancement to the patients plying the role of therapist and have push forward the clinician's productivity. As mentioned, using bio-signals are the only interfacing approach to design friendly human-machine.

Despite these advances, capabilities and potentials, still biological signals based control have a long way to go before reaching the realm of professional and commercial applications.

Several researchers such as (Pons, 2010 and Kiguchi and Hayashi, 2012) have significantly deepening our understanding and open interest on the use of surface electromyography to control assistive devices meant to be used as therapeutic robots.

Yet, extracting sufficient neural information using sEMG signal at the peripheral nervous system (PNS) is not mature enough and needs more advanced algorithm.

1.2 Motivation and Significance of the Research

The motivation of this research comes from the fact that elderly are having difficulties in their daily life activities for example standing up/sitting down and their severe impaired gait. With the remarkable increase in the ageing population (United Nation, 2010 and WHO, 2013), spinal cord injury, traumatic brain injury and stroke cases often result in a mobility impairment. With the hope for this population to regain and restore their mobility skills, assistive devices designated for rehabilitation purposes are in high demand. Particularly, powered exoskeletons robots are motivated from the notion that they would give significant assistance to individuals with mobility impairment to be able to walk properly and/or to regain their skills.

1.3 Problem Statement

For less than two decades, Electromyography signals have been started used in controlling assistive devices in the field of rehabilitation due to the evidence that these signals could give an intuitive understanding on the individual's movement intention. This therefore guarantees safety and highly cognitive assistive device. Moreover, these signals could practically estimate the moment generated by muscles in which causes a movement.

Electromyography signal processing techniques have been studied and developed widely for clinical purposes (offline processing). However, this signal is acquired and processed in real time in order to use it as control input for assistive device. Besides, the usability of this signal as control command for rehabilitation/assistive devices has not been sufficiently investigated (Pons, 2010 and Singh et al., 2012). Unwise processing of these signals may give higher probability for the exoskeleton robot to behave differently from the user. Electromyography measurement for a specific muscle is often inevitably full of noises and may be a result of mixtures of signals generated by different active muscles during performing a specific task (Farina et al., 2004). Generally these mixture signals overlapped in time and frequency. This contaminated mixtures need to be identified and removed from the signal of interest.

As the main aim of using sEMG as a control input for ERD is to detect the motion's intention of an individual, the onset/offset parameter of the sEMG signal is crucial and important (Micera et al., 2001 and Kornard, 2006). This parameter could be concealed by the background noises and the effect of low pass filter output (Conforto et al., 1999 and Lee et al., 2007). Thus, designing an optimum filter is required. Furthermore, sEMG signal differs between individuals and even within the same individual in terms of magnitudes and pattern repeatability, delay between recordings, waveform of the signal and accordance with the person motion. Therefore, a rigorous and precise analysis scheme for sEMG signal processing is needed.

The below characteristics are a breif of the sEMG properties:

i. It is hard to obtain similar signals to achieve same task even within the same individual.
ii. Activity level (magnitude) of the sEMG signal keeps changing even within one individual from time-to-time.
iii. sEMG may exhibit a deferent behave as an interfere muscle measurements contaminated on the signal of interest.

1.4 Research Objectives

The main aim of this study is to obtain a suitable surface Electromyography signal for the control of lower extremity exoskeleton robot. For this purpose, several objectives were identified which needed to be tackled to achieve the main aim of the research. These objectives are as follows:

i. To design an optimum digital filter that cleans the noises in surface Electromyography signals.
ii. To detect and eliminate the presence of unwanted/crosstalk recordings from the signal of interest.
iii. To develop a mathematical based on Hill's Muscle Model (HMM) that relates the muscle activities with the joint moment for chair-rise and walking protocols.
iv. To implement the algorithm into a real time system as a preliminary application to an exoskeleton system.

1.5 Overview of the Thesis

The thesis is divided into six chapters. Chapter 1 introduces the use of surface electromyography patterns in control strategies of assistive devices sEMG-based control. It explores the nature and the challenges of using sEMG as control input to the assistive device.

Chapter 2 concentrates on the literature review of the research. In the literature review, sufficient information about the previous research on the field of rehabilitation engineering and the use of sEMG signals in controlling assistive devices is detailed, compared and reviewed.

Chapter 3 covers the research methodology. The chapter provides details on the methods used to identify the recording process of sEMG signals from lower limb muscles; material used to acquire the sEMG/kinematics data and the implementation in real time process using one link exoskeleton.

Chapter 4 reveals the sEMG signal processing part from pre-processing the measured data, filtering effects on the sEMG, normalization of the sEMG in amplitude and time as function of movement range.

Chapter 5 presents the results and discussions. The chapter presents the results of both chair rise and walking experiments in details. The influence of the filter parameters on the sEMG in term of magnitude and time is addressed. The efficiency of the RLS technique in reducing and eliminating the unwanted/crosstalk recordings contaminating the signal of interest is presented. Mathematical model based HMM is developed to relate the sEMG signals with the joint moment. The joint moments is then optimized with the net moment measured from the inverse dynamic of the system.

Chapter 6 contains the conclusion and recommendations for further research. It summarizes the overall findings of the research and highlights the significance of the achieved methodology.

CHAPTER 2

LITERATURE REVIEW

2.1 Introduction

Assistive technology development is aimed for both mental and physical disabilities. Most often, aging population is the largest population subjected to be affected by these disabilities. In fact, according to United Nations Population Division, the world's population aging is growing at a rate of 2.6 % per year, (United Nations 2010). Population of elderly above the age of 65 years old was 4.9% in 1950, 20% in 2007 and is expected to reach 35% in 2050 due to increasing quality of living and healthcare (Dellon et al., 2007). In particular, 8% of Malaysian's Population is well above 60 years old (WHO, 2013).

Physical disability could be classified into two major groups, one is known as Musculo Skeletal Disability (MSD), that is when the person is unable to perform a distinctive activities associated with movements of the body parts. The second is known as Neuro Musculo Disability (NMD), which is defined when the person is not able to perform a controlled movement of affected body parts due to disorder of the nervous system. NMD could be classified into four main categories (cerebral palsy, stroke, traumatic brain injury and spinal cord injury). For instance, in Malaysia, 11% of children aged between 0 to 18 years old were diagnosed with cerebral palsy disabilities according to Malaysia, 2011. All of these disease categories yield a severe abnormality posture and limited range of movement with retardation.

Healthcare providers/caregivers reported that early and appropriate intervention with an intensive rehabilitation task could greatly lessen the time for the patient to recover/rehabilitate the impaired movement or to prevent the patient from being in an obsession state of a permanent disease. This type of intervention is called 'rehabilitation medicine' which is the care given to the patients. According to the world health organization (WHO), the demand for rehabilitation services is increasing, (1.5% of the total population requires rehabilitation services at any country). With the advancement in technology, a new discipline called rehabilitation engineering is increasingly being incorporated into the field of rehabilitation medicine to assist the patient as well as to reduce some of the burden imposed on caregivers. This symbiotic relationship depends on the patient situation and the stage of the disability.

In the next section, we briefly define the rehabilitation process in both disciplines of medicine and engineering.

Figure 2.1 summarizes the general application of the assistive robotic device. It contains the reasons for using exoskeleton and/or assistive devices, to whom the robotic device is developed, and who are the developers.

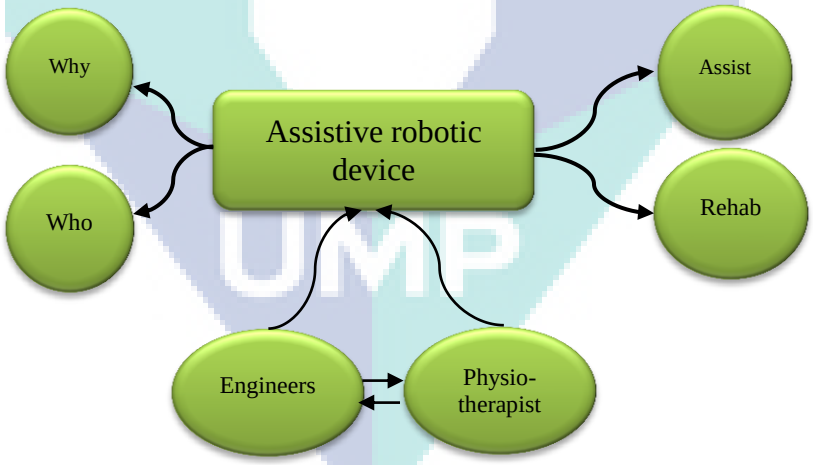

Figure 2.1. Assistive robotics device application overview

2.1.1 Engineering Rehabilitation Definition

The term rehabilitation has a wide range of meaning and it depends on the setting or the place of usage. The word rehabilitation is originally a Latin word, which means,

“to make fit again”. In health-care, rehabilitation provides the interventions that go beyond the medical treatment to give care for those who have injuries, strokes, spinal cord injuries and elderly with lower/upper extremities impairment in order to re-establish themselves back to previous level of health. For physical rehabilitation, physiotherapists are involved in this service.

Physiotherapy is a healthcare profession that provides services to individuals and public to maintain and restore maximum movement and functional ability throughout their lifespan. This includes providing services in circumstances where movements and functions are affected by aging, injury, disease and environmental factors. Physiotherapy is concerned with identifying and maximizing quality of life and movement potential within the spheres of promotion, prevention, intervention and rehabilitation. Even though physiotherapists are well skilled, professionals and well-practiced, with the increase of incidents with different stages of disability, the demand for them is increased. Commonly, one patient may require more than one therapist to aid him/her during the rehabilitation process and also depending on the level of disability with regards to the recovery prediction time (Tilling et al., 2001). Therefore, there is a need to induce engineering technologies into physiotherapist services in order to shorten the impaired motor skill recovering time and give help to the physiotherapists.

From an engineering standpoint, physical rehabilitation is often utilized after major surgery, an accident, or any event that robs the individual mobility. Rehabilitation engineering has been emerged recently with rehabilitation medicine in which could be defined as a systematic application of engineering science to design, develop, adapt, test, evaluate, apply, and distribute technological solutions to problems confronted by individuals with disabilities in functional areas and activities associated with employment, independent living, education, and community integration.

With the remarkable advances in technology, assistive robotics is taking place to playing the role of therapist. Assistive robotics devices are classified as passive, semi-active and active robotic systems (Burgar et al., 2010). In each type of the above mentioned classes, the designed assistive device is categorized as prosthesis, orthosis or exoskeletons robotic system. From the mechatronics standpoint, active prostheses, orthoses, exoskeletons robot are similar at the functional level, but they are slightly different in the control objectives. Orthosis and prostheses are different in the hardware configuration. Orthosis are worn on the existing but impaired limb, and the device weight

is added to the limb weight. Prosthesis is a device that replaces a missing limb. Table 1 may break the difference between robotic devices used in assistive technology for physical disabilities. The objective in rehabilitation devices is the reproduction of motion sequences to facilitate the patient's functional skill recovery. Trajectory-tracking controller is a commonly employed strategy to improve repetitive motion pattern.

Table 2.1
Comparison of prosthesis, orthosis and exoskeleton

Prosthesis	Orthosis	Exoskeleton
• Replace a missing limb	• Worn on an existing limb	• Worn on an existing limb
• Passive, semi-active and active	• Passive, semi-active and active	• Passive, semi-active and active
• Replacing closely to the weight of the missed limb	• The weight is added to the limb.	• The weight is added to the limb.
• Used for assistive purposes.	• Used for assistive, augmenting ability rehabilitation purposes	• Used for assistive, augmenting ability and rehabilitation purposes
	• Reproducing the motion sequences	• Reproducing the motion sequences

2.2 Brief History

The history of assistive technology for physical disabilities can be traced back to the evidence of prosthetic usage dating back as early as the Ancient Egyptians. In one case, it was found that a mummy's big toe had been amputated during its life and supplanted with a carefully crafted wooden toe, which was attached by a series of wooden plates and leather strings. The oldest known leg prosthesis from 300 BCE was discovered in Capua, Italy, and was made out of copper and wood. In the 16th century, prostheses were created from iron for soldiers by the same blacksmiths who crafted their suits of arms. An iron arm had the ability to flex a fully digital hand. By the 19th century, James Potts created a leg with artificial tendons to lift the toe when bending the knee (Dellon and Matsuoka, 2007). It is also reported that some inventions had been done for soldiers (prosthesis equipment) immediately after the World War II. By the early 1970's,

rehabilitation engineering had increasingly taken a wide place in research (Bogue, 2009). Variety aspects of rehabilitation robotics can be found in (Messier, 2010).

In the following section, rehabilitation robotics is discussed to understand the control strategies, methods and techniques that have been applied. The review is not confined only to the lower limb exoskeleton but also various types of prosthesis/exoskeleton.

2.2.1 Exoskeletons

Exoskeletons are wearable devices with close cognitive and physical interaction with the user operator. They are rigid robotics moving in parallel with human limbs mainly used to enhance the ability of human being. Robotic exoskeletons for decades were meant to enhance human power capabilities. Since early 1970's, engineers have started working on the development of exoskeletons to augment human power (Hughes, 1972; Seireg and Grundman, 1981; Ruthenberg et al., 1997 and Zoss et al., 2006). Wearable robotic exoskeletons initially were built to improve the soldier's endurance, speed and load carrying ability.

The Defense Advanced Research Project Agency (DARPA) funded the Berkeley Lower Extremity Exoskeleton (BLEEX) project in 2000 (Figure 2.2). This project has helped renew interest in the development of robotic exoskeletons to assist human locomotion (Sawicki, 2007).

Figure 2.2. Berkeley Lower Extremity Exoskeleton

Source BLEEX, Sawicki 2007

With the advances in actuation technology, control engineering and material sciences have propelled the state-of the art quickly forward (Guizzo and Goldstein, 2005). The benefits and applications of exoskeletons are not limited only for soldiers in military sector. Civilian laborers such as disaster relief workers, wildfire fighters and other personnel emergency could also use exoskeletons to reduce the physical demands of climbing, heavy lifting, or long periods of sustained locomotion.

Recently, exoskeletons are increasingly becoming more accepted in the field of rehabilitation medicine. Typically, robots use trajectory or pattern trajectory to follow (pre-programmed trajectory). However, in human-machine robotics system, the device is more likely to follow the nature of the operator locomotion. To attain a friendly human-machine, an appropriate alternative solution is to connect the control system to biological signals of the operator that is directly linked to the desire of movement.

Obviously, the movement's intention is firstly relayed to the brain (Central Nervous System) level which can be represented by EEG signal. It is known that muscles are the tissues responsible to provide human with locomotion during their contraction. Therefore, researchers are attempting to understand the muscles behavior during movement by examining the sEMG signals.

Before we state the previous work on the use of sEMG as control input for assistive devices, a brief description on the sEMG signal, recording methods and techniques are given first.

2.3 Electromyography

ELECTROMYOGRAM (EMG) is a combination of three words: **ELCTRO** stands for *electric*, **MYO** stands for *Muscle* and **GRAM** stands for *recording*. Electromyography is a collective electric signal (negative and positive values) from muscles produced during their contraction. It is also defined as the summation of the motor unit action potentials occurring during the contraction measured at a given electrode location which is often expressed in millivolts.

The EMG measurement is based on two recording techniques one is known as an invasive technique, which uses intramuscular electrodes (needle electrodes), and the second technique is by using surface electrodes (non-invasive technique). The attribute and the quality of the EMG signal depend on the internal structure of the subject, including the individual skin formation, blood flow velocity, measured skin temperatures and the tissue structure (muscle, fat, *etc.*).

Compared with the needle-based process, surface EMG technique (surface electrodes-EMG-based) is used more frequently because it is preferred by the subjects and because it is a non-invasive and painless technique (Pullma et al., 2000 and Rodríguez-Carreño et al., 2006). Surface electromyography (sEMG) signal represents the characteristics of the muscle function and provide information on the muscle activities. sEMG signal is highly prone to noise interference that may reshape and alter the signal such as baseline drift, skin artifacts, processing errors, and interpretation problems, for example:

i. Inappropriate contact of the surface electrode to the skin could distort the recording signal.
ii. Inadequate amplification of the signal could cause a recording detection problem.

iii. Selecting wrong filter parameters could efface some of the desirable information of the recorded sEMG signal.

Moreover, there are other factors such as the distance between electrodes, the electrode placement over the muscle, the skin preparation as well as the recording times used in the experiment and the type of the experiment. The device/sensors utilized in acquiring the signal must also be considered since low-level input into a recording device could affect data and yield inaccurate results.

2.3.1 sEMG Recording Concept

When skeletal muscle fibers contract by the stimulation of the nerve fiber (neural activation), they conduct electrical activity (action potentials, APs). APs can be measured by bipolar surface electrodes affixed to the surface of the skin above the belly of the muscle along its long axis. As the APs pass by the electrodes, spikes of electrical activity are observed and pulses of muscle fiber contractions are produced. Small functional groups of muscle fibers, termed motor units (MUs), contract synchronously, resulting in a motor unit action potential (MUAP). To sustain the force produced by the muscle fiber (Muscle activation force), an MU is repeatedly activated by the central nervous system several times per second. The repetition or the average of firing rate is often between 5 to 30 times per second. More details on the muscle physiology can be found in Malmivuo and Plonsey. (1995).

Figure 2.3 summarizes the concept of the sEMG signal recordings using surface electrode. The placement of the surface electrodes are based on standard recommendations. Theses alectrodes measure the potentioal differences between two points in which they produce a signal to be implemented into an amplifier resulting into the known sEMG signal.

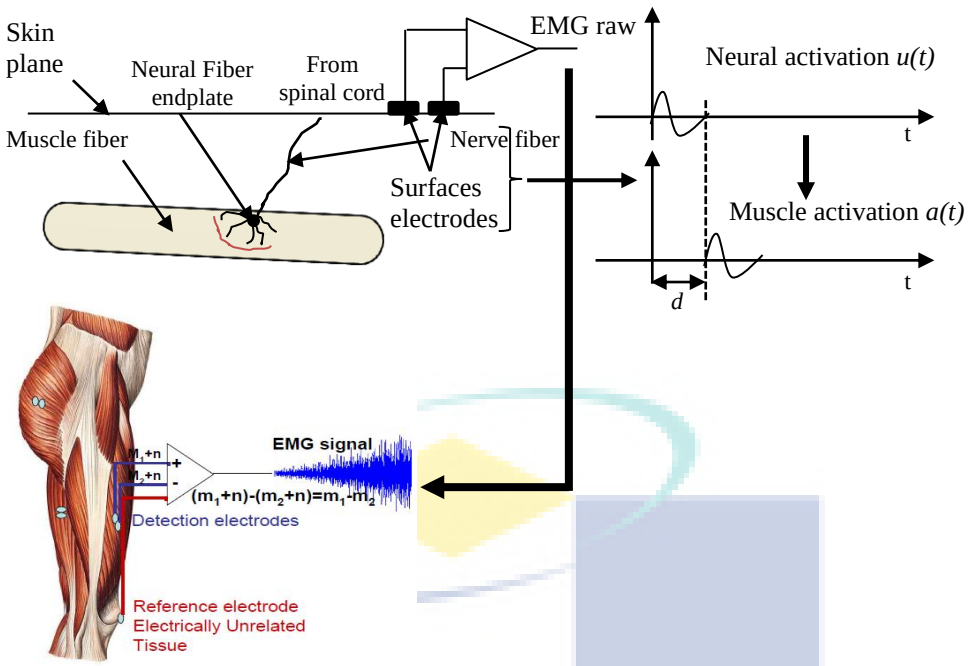

Figure 2.3. Schematic representation of the muscle fiber, the nerve fiber, the resultant activations and the concept of surface EMG recording, $\mathbf{m_1}$, $\mathbf{m_2}$ is the sEMG signal and **n** represents the noise model, *d* is the delay between neural activation and muscle activation schematically

Source Disselhorst-Klug et al. 2009

2.3.2 Crosstalk Phenomenon

For years, researchers have attempted to remove/reduce the so-called crosstalk/unwanted contaminated measurements from the sEMG signal. These measurements occur mainly when using surface electrodes over the muscle of interest. They are a mixture of signals from the neighbouring or underlying muscles caused by un-wise placing of the surface electrodes. Higher chance of the crosstalk to contaminate the signal of interest is in the dynamic contraction compared to isometric muscle contraction and other types of contractions. Indeed, the electrical potential generated by the muscle fibres propagates through the volume conductor over the placed electrodes on the targeted muscle. Obviously, this mix recording will lead to miss-interpretation of the sEMG especially when the signal intended for controlling assistive devices (Kuiken et al., 2001; Lenzi, 2012 and Khushaba et al., 2012). To obtain a signal free of crosstalk, careful efforts had been taken into consideration inline with the abovementioned suggestions and recommendations, such as selecting the appropriate electrode size, inter-

electrode distance and location of recordings over the muscle (Van Vugt and Van Dijk, 2001; Rainoldi et al., 2004; Sacco et al., 2009 and De Luca et al., 2011).

Despite all of these efforts, it is often difficult to selectively record the signal from a single muscle in practice, especially when recording signals from dynamic contractions. Thus, caution should be taken since the signal recorded from the muscle of interest may not reflect exclusively its intrinsic activity (Mezzarane et al., 2009). sEMG signals may overlapped in time with another muscle source i.e. the bursts of the targeted muscle followed by other bursts (Farina et al., 2004).

Crosstalk in sEMG has been investigated by several researchers for the purpose of providing an insight into muscle physiology, neuromuscular disease, investigation and ergonomics diagnosis (Mezzarane et al., 2009 and Kong, et al., 2010). In particular, intensive studies on the forearm to quantify the crosstalk between the muscles have been conducted because of closely located muscles (Mogk et al., 2003 and Victor et al., 2012). In contrast, the lower limb muscles have been investigated by few researchers to examine the crosstalk issue. There are two methods to reduce/detect crosstalk contamination: i) when the measurement is already recorded (offline data) and ii) before any measurement has been performed.

The most common technique used to determine the presence of crosstalk is known as blind source separation (BSS). This technique is essentially based on principal component analysis (PCA) and independent component analysis (ICA) as reported by (Farina et al., 2004 and Rubana et al., 2013), which assumes that a number of sources are separated based on the number of recordings and it is a more successful technique when these sources include different frequencies, such as ECG and MMG contaminated on sEMG signal. However, it is difficult to use ICA when attempting to separate the activities of neighbouring muscles from the signal of interest due to the similar electrical properties between muscles. Cross correlation is also a widely used tool to identify the common component between two signals (Madeleine et al., 2003 and Mogk et al., 2003). Nevertheless, this latter is only useful when the two signals are known.

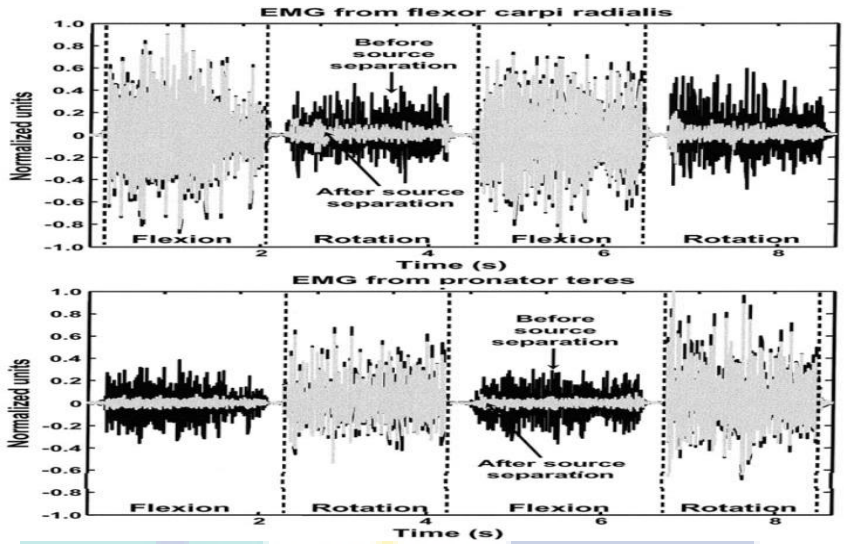

Figure 2.4. Example of mixture signal (crosstalk) adapted from Shaded area represent the crosstalk or the interfere signal (top figure), bottom figure is the corresponding force.

Source Farina et al., 2004.

As mentioned earlier, sEMG recordings are mainly based on skin-electrodes using the differential amplifier technique (differentiation process), as reported by (Merlo et al., 2010). Slight modifications at this level, i.e., skin-electrode-amplifier, could reduce the crosstalk recording. One result of this modification is presented in spatial filters that can reduce the crosstalk in sEMG signal (Van-Vugt et al., 2001 and Farina et al., 2003).

These techniques i.e. BSS and spatial filter can only reduce the level of the crosstalk in the signal of interest (Figure 2.4) and does not sufficiently reduce it until the the background noise (rest period of the muscle activity). This obviously will conceal the true determination of the onset/offset of the sEMG signal. The onset/offset detection technique is a useful parameter in sEMG to detect the rising time and the falling time of a sEMG signal bursts (Özgünen et al., 2010).

2.4 Usability of sEMG Signal in the Control of Assistive Devices

In this section, we state briefly the history of sEMG signals used as control inputs for assistive devices. The early stage of the sEMG signal implementation as control input

could be referred to the second half of the last century. The usability of the sEMG signal to control prosthesis device possibly was first implemented by Jerard (1974) to control an electro-pneumatic hand followed by the Utah artificial arm developed by Jacobson in 1982 (Figure 2.5).

As mentioned earlier, active exoskeletons were invented as early as the World War II ended, exoskeletons by then were meant only to augment the ability of human being. The use of these devices for rehabilitation purposes or as therapeutic robotic devices is a new application which requires a thorough insight on the physiology of the user in order to provide safe and close cognitive human-machine interaction.

With the new direction and purpose towards the exoskeletons, the use of sEMG signal gets its slot in controlling orthosis/exoskeletons not before 2000 (Pons, 2010).

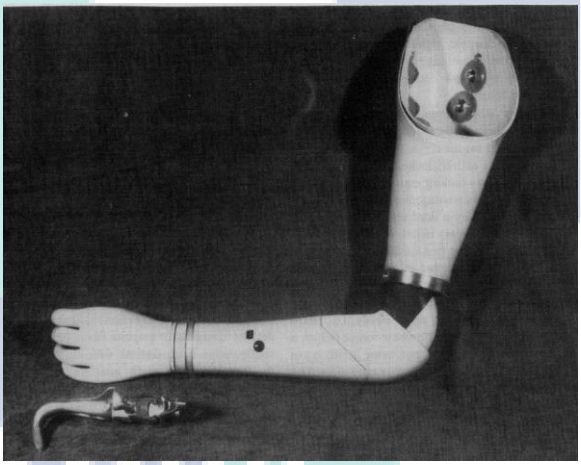

Figure 2.5. Utah prosthesis assembly

Source Jacobson 1982

Recent studies have begun to examine adaptations in electromyography and kinematics during walking with lower-limb powered assistance robots in both healthy and impaired populations (Dietz et al., 2004; Emken and Reinkensmeyer, 2005; Sawicki et al., 2005; Gordon and Ferris, 2007; Sawicki and Ferris, 2008 and Jimenez-Fabian et al., 2012).

Nowadays, a number of exoskeleton models based sEMG control exist (Rosen et al., 2001; Lucas et al., 2004 and Aguirre-Ollinger et al., 2007). The complexity of the designed exoskeleton model mainly depends on the purpose and the applications that the system is developed for. Indeed, more complex system requires more incorporation of the muscles in order to obtain smooth movement. Each of these models has limitations and qualities that require further investigation.

The exoskeleton device is mainly developed with regards to the user's need and the body segment that needs treatment; therefore, their mechanism could be one link exoskeleton and could be full suit exoskeleton. Variety models of exoskeletons have been developed for upper limb starting from hand exoskeleton, forearm exoskeleton and full upper limb exoskeletons. Similarly, for the lower limb, one can see advancement in different models from the ankle exoskeleton, knee exoskeleton and complete lower limb exoskeleton mechanisms. Yet, the DOF of these mechanisms are still very limited compared to the human limbs flexibility and number of DOF.

Our concern in this study is on the control techniques and strategies of the exoskeletons. Particularly, the use of sEMG signals as control inputs. In this review, we cover the techniques, implementation strategies and qualities of the used sEMG signals as control commands.

Saga University in Japan conducted a project on the upper limb exoskeleton for over a decade as their first work was published in 2001(Kiguchi et al., 2001). The exoskeleton was particularly designed for the elbow joint movement restricted to one degree of freedom (1DOF). Their early control strategy was detecting sEMG from two muscles named biceps and triceps group muscles. In each muscle group, two signals were extracted. The extracted feature was the waveform length (WL) for all channels with down sampling the signal by 100 samples. On the other hand, the force generated by the wrist is also introduced as a control input. Both signals (force and sEMG) were digitized at 2 kHz. These signals are then fed to fuzzy rules to estimate the impedance control equation's coefficients. This control scheme suffers from i) the down sampling of the WL which led to an unsynchronized input with generated wrist force fed to the fuzzy system. ii) Down sampling the WL signal doesn't guarantee the removal of the noises, spikes and artifacts which may be counted within the linguistic roles in the fuzzy system.

This latter then alters the control system. The graphs shown in Figure 2.6 seem to be high frequency signals in which certainly increase the computation time during the iteration. Furthermore, the WL signal, i.e. the muscle appears likely to be close to a random activation in which doesn't guarantee the repeatability of the signal pattern.

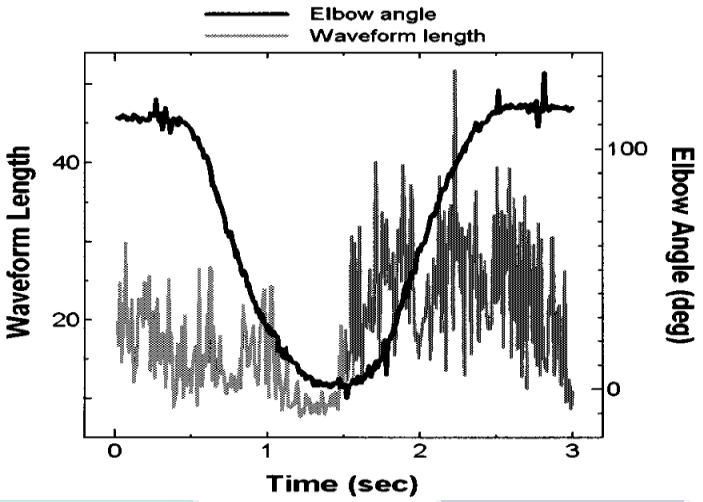

Figure 2.6. One channel of the WL with the corresponding angle

Source Kiguchi et al. 2001.

Work by Kiguchi and Hayashi (2012) from the same University describes a control strategy of an upper limb exoskeleton with slight difference compared to the 2001 work. The complexity of the system is upgraded to 7DOF upper limb exoskeleton, the number of the selected muscle channels had increased and the system seems more promising. However, the extracted feature is changed to the use of RMS feature with same sampling rate of 2 KHz. The segment to calculate the RMS was set to 400 samples. That is to say, in each iteration, the algorithm outputs one (RMS) value every 0.2s. Both, the force sensor and the sEMG signals were normalized in amplitude and compared. The higher signal in amplitude was selected as input signal for the controller. Again, this approach has no way to guarantee that the compared sEMG signal to the force signal is the pure free-noise signal. Moreover, taking 16 sEMG channels has certainly a considerable effect in delaying the execution time. Caution should be taken when comparing the muscle activities with the force as the force itself is a resultant of the muscle activity. Taking the Figure 2.7 (Figure 10 (c)) from the same article that assessed the correlation of the sEMG channel with the motion patterns shows acceptable correlation for example channel.6 with the elbow motion. In this particular motion, the

researcher could limit the inputs of the controller to one channel only since it shows good correlation.

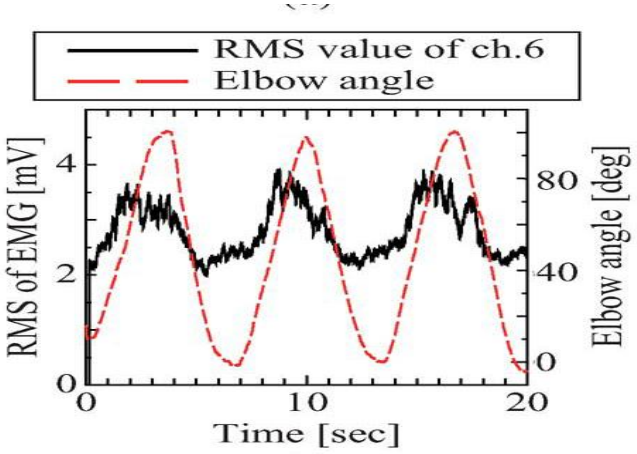

Figure 2.7. sEMG with elbow motion

Source Kiguchi et al. 2012

From the same lab at Saga University, a lower limb exoskeleton was also investigated (He and Kiguchi, 2007). The control strategy is similar to the one implemented in the upper limb exoskeleton.

In (Lenzi et al., 2012), the exoskeleton robot was used to assist the user while achieving certain upper limb movements. The device was designed to be adaptive to the sEMG recorded over the biceps and triceps muscles. This means the robot gives torque to a joint in order to reduce the efforts given by the muscle. That is to say, to keep the muscles un-fatigue even for long term exercises. This method doesn't require the estimation of the torque and moment produced by the muscles. The researcher assumes that the forces in muscles level are weighted with some factors (K_{bic} , K_{tric}) into the processed sEMG represented by linear envelope (LE) $\boldsymbol{F_{flx}}=K_{bic}*LE_{bic}$ and $\boldsymbol{f_{ex}}=LE_{tric}*K_{tric}$, (Figure 2.8).

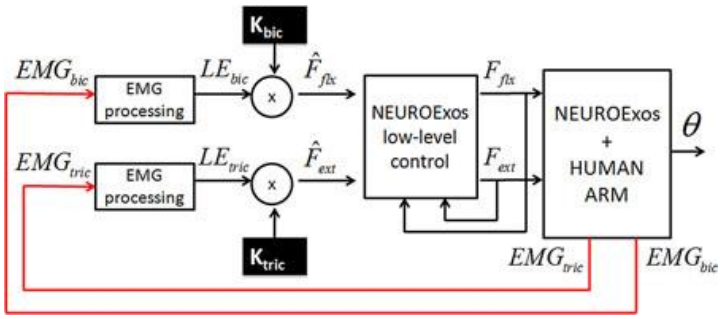

Figure 2.8. Simplified control strategy for elbow assistance

Source Lenzi et al. 2012

Furthermore, specifying only the biceps and the triceps muscles as responsible for the flexion and extension of the elbow joint might be not sufficient enough due to many muscles involve in the motion.

A more specific objective for exoskeleton model is the design of a robotic ankle exoskeleton controlled by one sEMG channel. Kinnaird and Ferris et al., (2009) had addressed the use of the medial gastrocnemius muscle activities measured by sEMG as an input control for an ankle robotic device. Their study intended to evaluate the muscle activities after the training with the powered exoskeleton. This method is similar to the method in (Lenzi et al., 2012) in which the output of the muscle was not investigated.

2.5 Butterworth Filter for sEMG Smoothing

Numerous researchers simply used moving average filter such as (Dehail et al., 2007; Song et al., 2013 and Yamamoto et al., 2014). Very few researchers used Chebychev I such as (Lu et al., 2009). However, the most acceptable filter used is the Butterworth filter due to its less ripples and fast response compared to other classical filters. Due to these advantages, it is often recommended in the biomechanics field for the purpose of data smoothing. Particularly, Butterworth filters have gained wide acceptance for sEMG filtering by several researchers.

In Table 2.2, we briefly give an overview of thirteen researchers that have used low-pass and high-pass Butterworth filter for sEMG signal smoothing. The table includes

the sampling frequency, the filter order and the cutoff frequency. The slash means they are not mentioned.

Table 2.2
Butterworth Filter usability for surface Electromyography filtering

References	**Sampling frequency**	**Filter order**	**Cutoff frequency**	
			low-pass	**high-pass**
1- Sawicki, (2007)	1200Hz	4th order	10Hz	20Hz
2- Olree, S. Kenneth (1995)	1000Hz	2nd order	3Hz	30Hz
3- Shao et al. (2009)	/	4th order	4Hz	50Hz
4- Lloyd and Besier (2003)	2000Hz	3th order	6Hz	30Hz
5- Fleisher and Hommel (2008)	1000Hz	2nd order	1.6Hz	/
6- Lenzi et al. (2012)	1000Hz	2nd order	3Hz	/
7- Kinnaird and ferris (2009)	1200Hz	2nd order	6Hz	20Hz
8- Anne K. Silveman et al. (2012)	1200Hz	4th order	4Hz	40Hz
9- Manal and Buchanan (2003)	1000Hz	/	4Hz	30Hz
10-De Luca et al. (2010)	/	2nd order	/	20Hz
11-Cappelini et al. (2010)	1000Hz	4th order	10Hz	/
12-Neptune et al.(2008)	/	4th order	10Hz	/
13-Panagiotis et al. (2008)	1000Hz	4th order	/	/

Over the past few decades, some recommendations and standards (Konrad, P., 2005) on the prior use of sEMG have been put forth to reduce low frequency noises as listed below

i. The recommendation of the international society of electromyography and kinesiology (Kadefors et al., 1980) recommended a high-pass corner frequency of 20 Hz to remove artifact.
ii. Standards for reporting EMG data (Merletti, 1999), which recommended using a high pass filter at 5Hz cutoff frequency.
iii. The requirements of the journal of electromyography and kinesiology, which requires a corner frequency of 10Hz for a report to be published.
iv. The surface EMG for non-invasive Assessment of muscles (SENIAM) recommendations (Hermens, 1998) recommends 10-20Hz for low frequency elimination.

Form the above table (Table 2.2) and the given recommendations we conclude that there is no uniform methodology to smooth the surface sEMG signal in order to obtain signals with high fidelity. Particularly, the filter parameters could significantly affect the

true information of signal. One of the effects of the low pass filter on the signal is that it overshoots/undershoots and delays and conceals the onset of the sEMG (Robertson et al., 2003 and Kerem et al., 2010)

Moreover, the use of different hardware and data acquisition systems leads to some extent to a different measurements and different embedded noises due to the difference in hardware and electronic systems, which causes thermal noises. In addition to the thermal noises, electro-chemical noises originate from the interface between the skin and the electrodes are also considered.

From the previous studies and the facts in sEMG we conclude that there are two major issues in sEMG that are not investigated carefully in order to use these signals as control input. One is the background noises in which it can mask the exact rising time of the muscle activities (onset/offset). The second issue is known as the crosstalk (unwanted recordings) which actually contaminates and overlaps in time on the signal of interest. Therefore, there is a need to analyzing the sEMG for the use as control inputs for assistive devices.

In this study, we intend to conduct a precise study on the use of sEMG in driving lower limb exoskeletons. Since bio-signals are sensitive to noise, contaminated artifact, crosstalk interference and many other noise sources, careful signal processing of the sEMG is addressed in this thesis. Standards, recommendations, experiment ethics and techniques on the way of recording sEMG signals were first accomplished prior to the experiments. Data acquisition, setting the sampling frequency recommendations with regards to the sensors frequency ranges were carefully selected due to the fact that it may distort the signals. Synchronizing the kinematics sensors with the sEMG sensors was even more important as prerequisite in order to avoid the de-correlation problem in the signals.

The assumption in this work is to detect the start and the end of the individual motion simultaneously with the sEMG recordings onset/offset detection parameter. The muscle activities that do not belong to the movement interval is categorised as crosstalk or un-expected recordings (unwanted recordings). Therefore, this latter recording needs to be determined and eliminated. Prior to this, the filtering stage in term of finding the

optimum filter parameter is conducted. An algorithm is developed to detect the onset/offset of the sEMG and the individual's motion onset/offset along with the filter to reduce the noises. The algorithm is used to detect the presence of the crosstalk in the sEMG. In order to suppress these recordings, Recursive Least Squares (RLS) method in employed.

Further process is accomplished, based on HMM; we develop a mathematical model to relate the muscles activities with knee joint moment for two protocols. The net joint moment was obtained using the inverse dynamic model of the lower limb for both experiment protocols. Whereas, the moment generated by the muscles is compared and optimized with the net moment.

2.6 Summary

In this chapter, the importance of the study in the field of rehabilitation medicine is addressed. The chapter reveals the related studies; a statement of a brief history on exoskeleton is addressed followed by the concept of muscle activities measured by means of sEMG, ways of measuring these activities along with the processing of the signals. And lastly, the chapter states the use of sEMG as input control for different types of assistive devices.

From the literature, there is no uniform methodology to filter the sEMG as the filter's parameters significantly alter the true amplitude of the signal. The issue of the overlapped and contaminated crosstalk/unwanted measurements on the signal of interest is extremely important as it certainly affect the behavior of the assistive device which leads to un-safe human-machine interaction. Two methods are considered in using sEMG as control input for the assistive device. One is sEMG based neuro-fuzzy method and the second is the sEMG driven model method. The first method is limited if the sEMG signal is not carefully processed as it alters the fuzzy logic linguistic. In this study we choose to investigate the second method.

Based on the above research gaps, we propose to clarify the effect of the filter's parameters on the sEMG smoothing and design the optimum filter. In order to determine and remove the overlapped crosstalk measurements in real time process, a pattern (sEMG-Kinematics) recording is conducted. Based on certain lower limb muscles, we propose the hill muscle model to predict the joint moment for chair rise and walking protocols.

CHAPTER 3

METHODOLOGY

3.1 Introduction

In this chapter, we first describe the processing of the sEMG signals recorded over some selected muscles of the lower limb from recording phase through data acquisition to the produced forces. The muscle forces forms an insight into the moment generated in a joint to cause a movement. To use the sEMG as signal input, there should be an output that measures the motion of an individual.

It is known fact that bio-signals are highly sensitive to noises, therefore obtaining an optimum filter is important. The use of Butterworth filter is widely accepted in biomechanics and bio-signal filtering (Erer, 2007). Pre-processing techniques of the sEMG signal is also addressed in this chapter.

The overall concept of the study is summarized in the block diagram below (Figure 3.1). The system consists of the user and the exoskeleton in which both of them interacts. The human-machine is supplied by kinematics sensor and sEMG sensors. The kinematics sensor returns the angular velocity which then can be calculated as angles and angular accelerations. During the chair-rise test, the sEMG sensors records data over the *Biceps Femoris* (BF) and *Rectus Femoris* (RF) muscles. These two signals are processed, filtered and transformed to muscle forces. These resultant forces will lead to the knee joint moment. In addition to the RF and BF muscles, two more muscles have been selected; *Solues* (Sol) and *Gastrocnemius* (Gas) in the walking case. In a similar way these muscles activation are converted to forces. These forces are then transformed into the moments in the joints (hip and knee joints). The actuator's torque are controlled

by the obtained joint moment from the muscles. The net joint moment is calculated using the inverse dynamics. An optimization method is used to optimize the estimated joint moment generated by the muscle to the measured net joint moment.

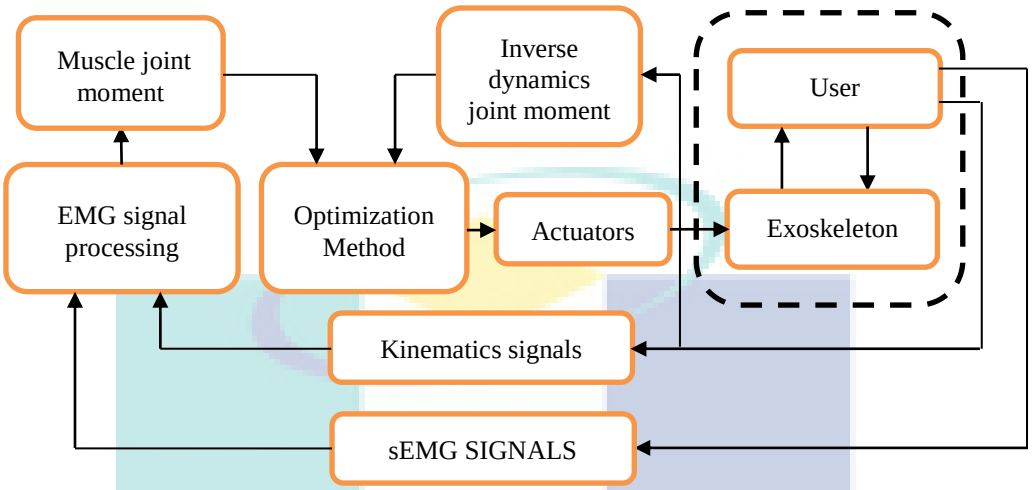

Figure 3.1. Overview block diagram of the study.

3.2 Materials

3.2.1 Software

In this study, MATRIX LABORATORY. Inc was the core software that have been used to record and analyse data. Most of the data analyses either offline or online (real time) was also done using MATLAB software. In addition, Real-term hyper-terminal software was used to capture the Bluetooth-based serial port data into MATLAB.

MATLAB

MATLAB is a strong numerical computing environment and a user friendly high-level programming language that enables researchers to perform computationally intensive tasks correctly and quickly. The name MATLAB stands for matrix laboratory. MATLAB was originally written to provide easy access to matrix software developed

UMP

3.2.2 Synchronized Biomechanics Software

Shimmer Discovery Motion (www.shimmersensing.com, Dublin, Ireland) is a company found in 2006 that develops a number of biological sensors (EMG, ECG, etc) along with motion sensors such as Gyro sensing module, accelerometer sensor. The company also provides software to record data either biological signals or movement signals. This software is limited to at most two channels at a time using MATLAB and with regards to the required channels (combination between sEMG and kinematics measurements) used in this experiment, a synchronized recording and measurement system was developed based on MATLAB. Inc. Shimmer MATLAB Instrument Driver. v1.1 which allows for six (6) channels recordings (see Appendix A).

The block diagram in Figure 3.3 represents the structure of the developed software. The physical sensors are set on the human body in order to acquire data from the muscles and the movement of the limbs. From the user interface, the user could select the number of sensors and set the sampling frequency. The communication between the sensor and the host laptop is Bluetooth based communication using the Real-term hyper terminal. Further processing is accomplished such as data calibration and filtering.

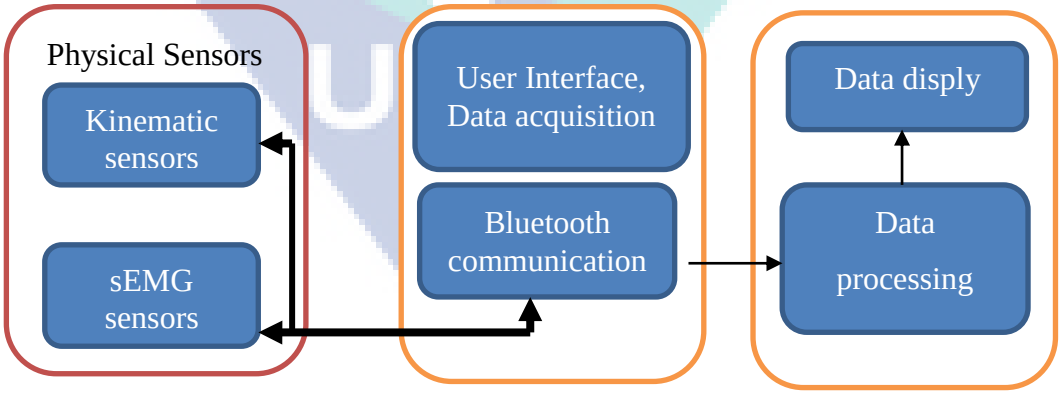

Figure 3.3 Block Diagram for the developed software

An example of one sEMG channel is given in Figure 4.3. The advantage of the software is the recording of two physical measurements (Kinematics and sEMG) in the same interface which help in correlating the two measurements.

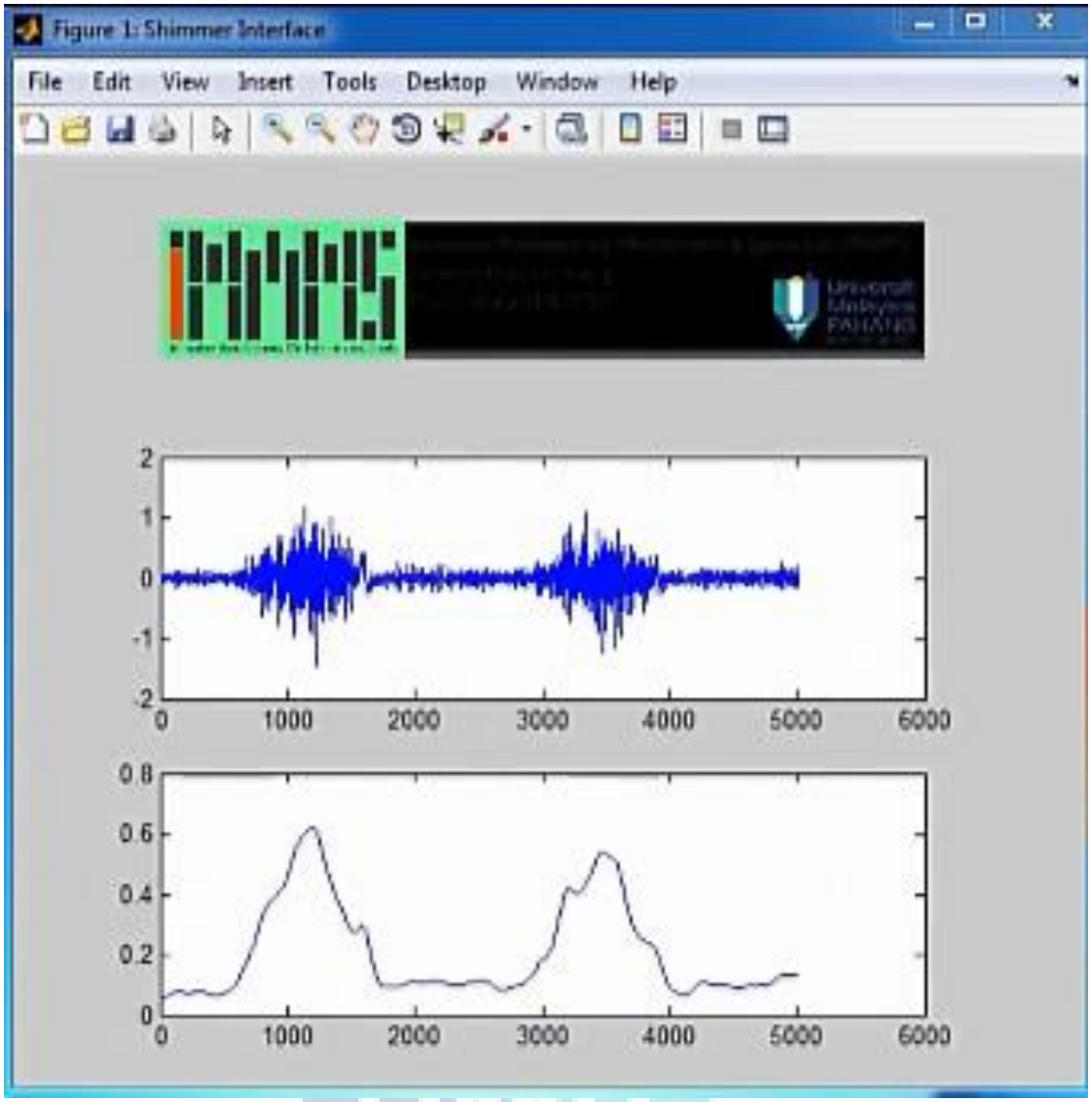

Figure 3.4. sEMG Recording user interface using MATLAB. Inc. an example of sEMG raw with the corresponding rectified-filtered signal streamed in real-time from Biceps Femoris muscle.

3.2.3 Hardware

The experimental protocol necessitates motion sensors (Gyro) and EMG based-surface electrode sensors to record the muscle activities during-chair rise and walking experiments.

EMG Sensor Specification

Electromyography (EMG) sensor is considered the centerpiece of the experiment since the main focus in this work was on analyzing the sEMG signals for the use in control schemes and strategies of assistive devices such as exoskeleton. In this research, a Shimmer EMG expansion module from Shimmer Discovery in Motion Company is used (Figure 3.5). This module is highly economical using surface electrode and Bluetooth based communication (wireless) (specification as in Table 3.1). It has three leads (positive, negative and neutral) in which each lead is connected to a disposal electrode.

Figure 3.5. Shimmer EMG sensor

Table 3.1
Shimmer EMG sensor specification

Size	53 x 32 x 23 mm
Frequency range	5-482Hz
Maximum signal range	4.4 mV
Gain	682
Max Current Drawn	180 µA

Gyroscope Sensor Specification

From the same company (Shimmer Discovery in Motion, Shimmer Technology, Dublin, Ireland), a Gyro expansion sensor is used in this work to measure the motion of the individual. It is a wireless instrument that provides three axis angular rate sensory (gyroscope). From the angular rate measurement, one can calculate the angles along with the angular accelerations.

Figure 3.6. Gyro sensor

Disposal Surface Electrodes

Disposal surface electrodes were used rather than using needle electrodes. This latter is an invasive or intramuscular technique to measure muscle activities which is maybe painful for individual. Two types of electrodes have been used in this experiment one with 3cm and 1.5cm in diameter (Figure 3.7). It has a gel part and metallic part: Ag-AgCl; manufacturer: Shenzhen Amydi-med Electronics Tech Co., Ltd.)

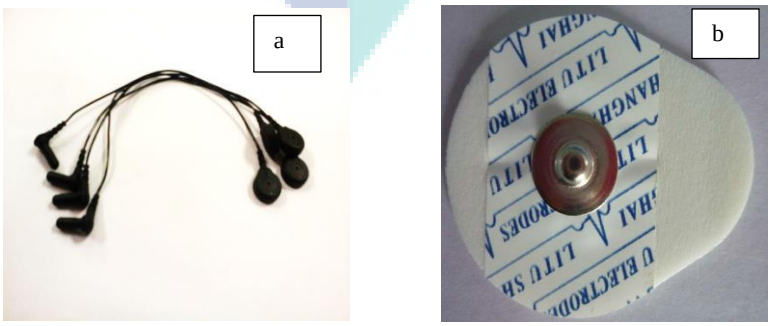

Figure 3.7. Disposal electrodes (b) and the leads (a) used to connect the sensor with surface electrodes

Arduino Uno Board

Arduino is an open source electronics platform enhanced with both software and hardware. Arduino is a programmable microcontroller based board with multi digital and analog input/output (I/O) pins (Figure 3.8). It has one USB serial port; it has access to many other peripheral boards such as the motor drive Adafruit board (see Figure 3.8). The Arduino / MatLab software/hardware together with the Adafruit motor shield were used to link the digital (I/O) system prototyped with an external actuator (one link exoskeleton) during real-time implementation.

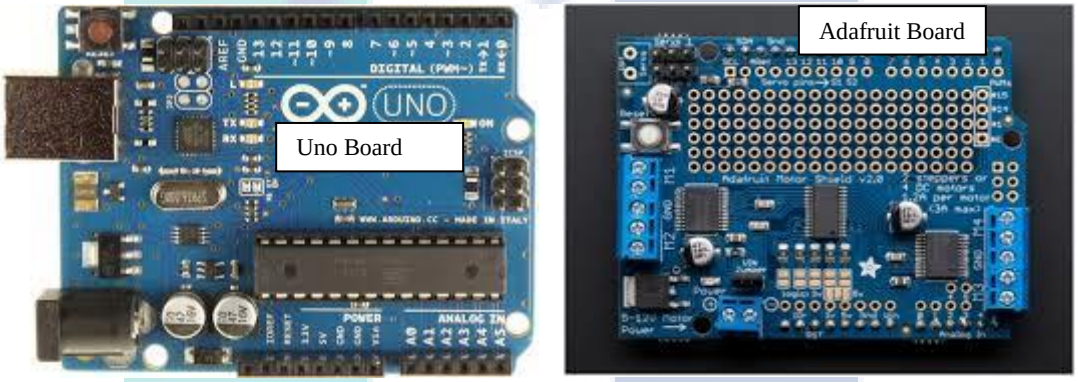

Figure 3.8. Arduino Uno and Adafruit motor shield boards

3.3 Experimental Protocol

Five healthy young adult subjects in total with (age ranging from 20 to 24 years old) volunteered in this study. The mean height of the subjects was 1.70±0.7 and the weight was 72±4 kg. Before conducting the experiment, the subjects were informed of the nature of the experiment and the purpose of the study and they have been provided with written informed consent.

Chair-rise and walking tasks are two important mobility skills in our daily life. Therefore, we choose to conduct an experiment on these tasks as it may give an insight to the movement and help in developing assistive devices for individuals with lower limb disabilities. Figure 3.9 shows the schematic representation to clarify the motion coordinates and experiment conditions. In the chair rise protocol, only the hip angle θ_2 is taken in consideration with range between 0^0 and 90^0 at chair-off and up-right

positions, respectively. In the walking experiment, the hip and the knee angles are taken into consideration.

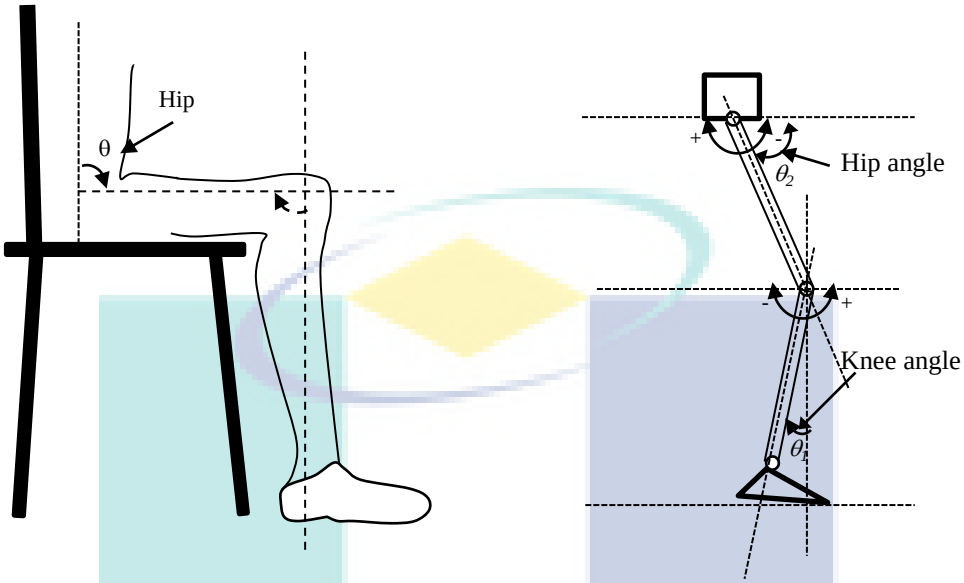

Figure 3.9. chair rising and walking protocols

Figure 3.10 presents the schematic representation of one gait cycle during walking task. It divides the the gait into two phases one is known as the stance phase and the other is known as the swing phase.

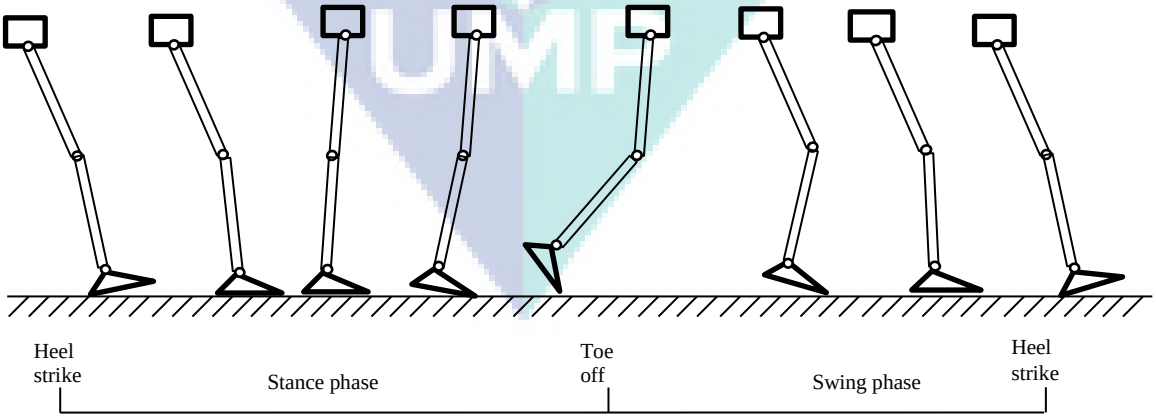

Figure 3.10. Representation scheme of human walking gait for one cycle, the gait begins and ends at heel strike.

Figure 3.11 depicts the actual set-up experiments for both chair-rise and walking experiments.

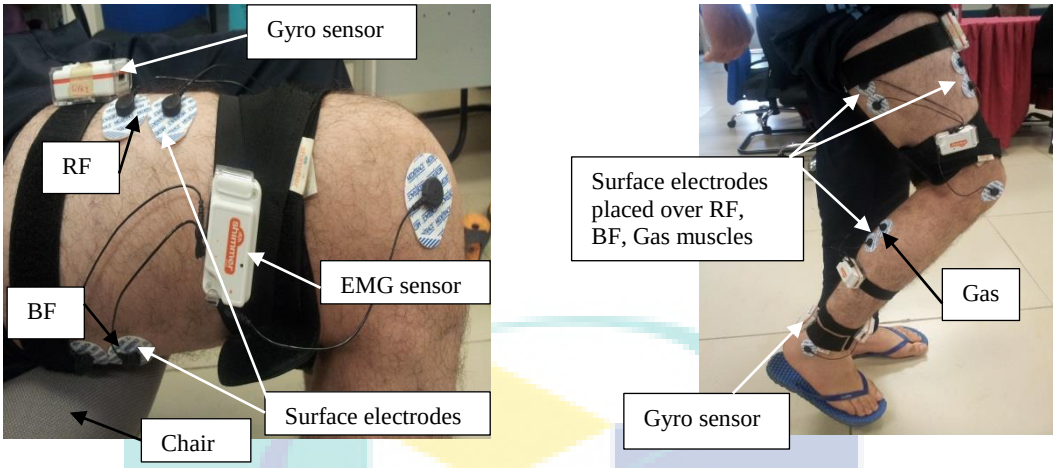

Figure 3.11. Experiment set up for chair rising and walking protocols

3.4 Data acquisition

Data acquisition is mainly the task of capturing the analog data from sEMG/kinematics sensors and encoding this data to a computer. Recording data from a sensor is often by means of analog signals or voltages that are analogous to the physical signal; its magnitude also varies through time. This is accomplished by a method called analog to digital conversion (A/D). The A/D conversion plays a crucial role in recordings, especially sEMG signal due to its high frequency nature.

A/D converter is a device that transforms a continuous time signal to a digital signal. It can be done by a series of two operations i) sampling and ii) quantization. *Sampling* is where the continuous signal converted into one that is only defined by discrete time, but whose amplitude is taken arbitrary values. The sampling operation is particularly critical if we want to avoid loss of information in the conversion. If the sampled signal could approximate closely the original signal, then the conversion from continuous to digital time is sufficient. The *Nyquist* sampling theory states that, if a signal x(t) contains no frequency components higher than original frequency of the analog signal *w* then it can be exactly reconstructed from samples taken at sampling frequency Fs >2*w*.

Quantization is in which a continuous amplitude signal is converted into a digital signal that can only take a finite set of values.

3.4.1 Sensor Placement

A number of lower limb group muscles contribute to the movement of sit to stand and stand to sit as well as walking task. For the chair rising experiment procedure, two muscles were identified as suitable to detect the sEMG signals. The two selected muscles were the BF and RF muscles, which originate at the thigh section of the human body. Whereas, in the walking experiment, the Sol and Gas muscles which originate at the leg section (refer to figure 3.11) were chosen in addition to the BF and RF. The kinematic sensors were placed on the mid-thigh of the subject for the hip joint motion measurement during chair rise task. Another kinematic sensor was placed on the back upper side of the heel in order to measure the knee joint motion during the walking task (refer to Figure 3.11).

3.4.2 Pre-Recording Data Protocol

The experiment is divided into two pairs; one is the chair rising task and the second is the walking task. For the chair rising experiment, the subjects were seated on a standard chair and were asked to rise from the chair at a self-selected speed. The initial posture of the subjects and position conditions is presented in Table 3.2. During each trial, each subject was asked to perform two times the sit to stand and stand to sit task successively.

Table 3.2
Task specification for chair rising experiment protocol.

Label	Description (sit to stand task)
S00	Sitting on a chair with 90° knee flexion
H10	Hands free, neither from the chair nor on the subject's thighs.
R20	Chair off at self-selected speed
S30	Standing upright to obtain 0° knee flexion
S40	Sitting again with normal speed to the same position (S00)

During the walking task, each subject was asked to stand upright and was encouraged initially to keep the posture at heel strike (refer to Figure 3.10) throughout the experiment for each trial. In each trial, the subject performs two strides. All subjects (five subjects) performed two trials at self-selected speed.

3.4.3 Skin Preparation and Surface Electrodes Placing

Over the selected muscles, the skin was cleaned using alcohol swab prior to the placement of the surface electrodes. The surface electrodes were carefully placed according the aforementioned recommendations in order to minimize the crosstalk measurements to reduce the movement artifact. The locations of the surface electrodes were approximately marked on the skin and pictures were taken (Figure 3.10).

3.5 Real Time Implementation

To validate the proposed methodology, a real-time prototype of an exoskeleton robot is developed (Figure 3.12). The algorithm is developed in MATLAB environment and launched into the Arduino board. The data or commands transmission between the host computer and the Arduino board are performed via a USB serial port. As the stepper motor requires a driver, the Adafruit motor shied is chosen as an I/O interface and has mounted on the Arduino board.

In this implementation, we seek to correlate the motion range of the human limb with the motion of one link exoskeleton in a natural way. On the other hand, the sEMG and the gyro sensors were positioned similar to the previous setup during recording data for both experiment protocols i.e. walking and chair rise test. As discussed earlier, both sEMG data and kinematics data were sampled at 1024 Hz. As an application in real-time processing, the down-sampling is one way to lessen the execution time. In the recording software, the reading function receives the data every 0.1s. Therefore, the hardware processing time of sEMG/Kinematic sensors is 0.1s.

However, the muscle activities require low sampling time as we set it to (1/1024 sec). This means in each 0.1 sec, a packet of data is streamed into the computer (Laptop). Referring to the sampling time and requesting time, a packet should contain about 100 samples. But, the actual packet of the data turns to do not always contain 100 samples; this is may be due Bluetooth communication and the Windows operating system. A buffer of the streamed packet's size is set to receive each packet with its size. This packet data is then processed individually i.e. removing the DC offset, high-pass filtered, fully rectified then low-pass filtered. This result is then averaged to provide one value which is the mean absolute value for the actual packet segment. As the data is streaming-in, the same process is accomplished to the following packets. The previous and the current MAV values are then compared with regards to the mean of the actual segment data and its standard deviation to detect the onset/offset time of the sEMG. Similar procedure is applied to the kinematics data. Further process is needed on the level of the obtained results from sEMG streaming data to be transformed to neural activation by implementing equation (4.34) and equation (4.36) presented in the next chapter to obtain the muscle activation. The muscle activation is used as an input to the Hill's model in order to obtain the generated force by the muscles. To this end, the force to moment model is implemented in order to obtain the joint moment.

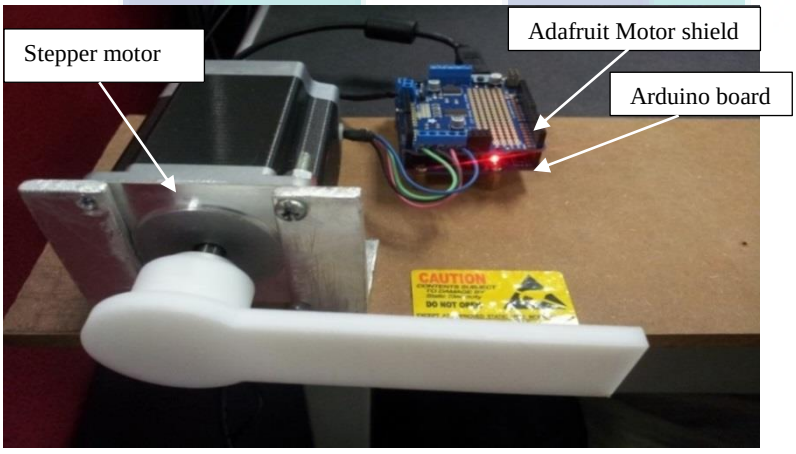

Figure 3.12. Hardware Configuration

A summary of the implementation scenario is shown in Figure 3.13. Similar experimental setup to the recording of the sEMG is accomplished, i.e. placement of the

sensors on the individual limb. A second gyro sensor is mounted on the exoskeleton link for confirmation purposes.

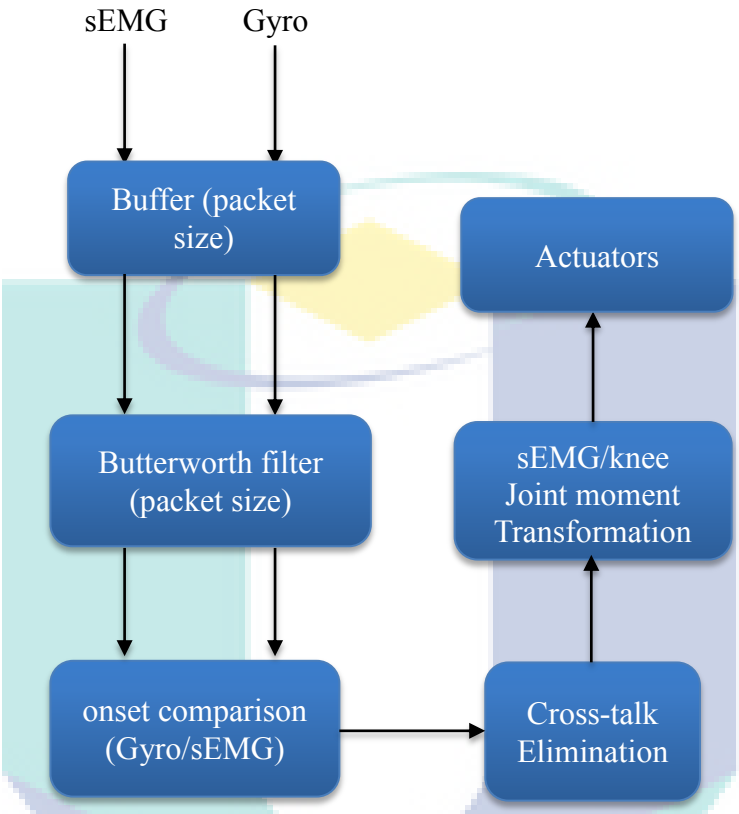

Figure 3.13. Real Time Implementation Scenario.

3.6 Summary

In order to examine muscle activities and clarify how they can be used in producing motion, we propose to divide the experiment into two folds; one is the chair-rise and the other is the walking tasks.

As summary for this chapter, to obtain a suitable sEMG signal that can be used as input control for exoskeleton robot meant for rehabilitation and/or assistance, the given recommendations to record sEMG is achieved in addition to the proposed kinematics measurement that could reduce the effect of undesirable recording in sEMG.

Software is developed in order to capture multi-channels of sEMG with accordance to the motion of the individuals. This will help in finding the true correlation between motion and the muscle activities. One link exoskeleton is prototyped to be executed in real time verification.

In the following chapter, we focus only on the sEMG signal processing part, starting from filtering stage to the force produced by muscles. The obtained forces will be further analyzed to obtain the joint moment.

UMP

CHAPTER 4

sEMG SIGNAL PROCESSING

4.1 Introduction

In this chapter, the analysis of the sEMG in term of noise filtering, crosstalk/unwanted removal, normalization of the signals in terms of amplitude and time (with accordance to the motion range of the individual's motion) is addressed.

4.2 Data Analysis Procedure

4.2.1 sEMG Normalization

To compare the activity level between muscles and between subjects, normalization of the surface EMG signal is performed. sEMG normalization is the process by which the electrical signal values of the muscle activity are expressed as a percentage of that muscle's activity during a calibrated test contraction (Lehman and McGill, 1999). Aiming to improve absolute EMG reliability and to provide an expression of relative muscle activation, the normalization of EMG data requires the use of a standardized and reliable reference value against which experimental data are measured (Burden et al., 2003). From literature review, a number of methods have been used to normalize the sEMG signal such as maximal voluntary contraction (MVC), mean value of the signal, peak value. The normalization method usually depends on the recorded sEMG nature (isometric, isokinetic or dynamic muscle actions). In this study, since the experiment protocol was on the chair-rise and walking tasks, which

resulted in dynamic muscle contractions, we have chosen the common method used in dynamic contraction. Dynamic muscle contraction is often normalized to the peak of the signal (Winter et al., 1987; Marras et al., 2001a, b; Sausa et al., 2012 and Halaki et al., 2012).

$$n_EMG(k) = EMG(k)/max(EMG) \quad (4.1)$$

where, *n_EMG (k)* is the normalized sEMG.
In real time application, the normalization is achieved by taking pre-trials i.e. recording the sEMG signal and measuring the peak values firstly.

4.2.2 Baseline Wander

Baseline wander (drift) is the effect on the zero line of the signal by shifting the amplitude up and down. This is due to the movement of electrodes and leads of the sensors. Baseline wander appears highly in bio-signals such as ECG, sEMG (Blanco-Velasco et al., 2008; De Luca et al., 2010; Pal and Mitra, 2012). The presence of the unbalanced baseline could alter and made the determination of the onset/offset of the signal difficult. There are several methods and techniques to reduce the baseline drift, one is by applying a fitting polynomial to the signal and subtracting it from the signal. The second method is known as the empirical mode decomposition (Blanco-Velasco et al., 2008) and the cubic spline method is also used to remove the baseline drift (Clifford, D.G, 2009). In this study, we used the cubic spline algorithm.

4.2.3 DC Component

DC component is the mean value of a signal or a constant that is added to a periodic waveform. It is usually undesirable as it causes signal saturation and signal distortion when for example integrating or differentiating a signal. For both kinematics and sEMG signal the zero-mean algorithm is applied. By taking the average of the signal and subtract it from the signal (zero-mean the signal), this component is removed. The average of a segment of a signal is given by the following formula

$$\overline{\mathrm{sEMG}} = \frac{1}{\mathrm{N}} \sum_{0}^{\mathrm{N}} \mathrm{sEMG} \tag{4.2}$$

$$\widetilde{\mathrm{sEMG}} = \mathrm{sEMG} - \overline{\mathrm{sEMG}} \tag{4.3}$$

where, $\widetilde{\mathrm{sEMG}}$ represent the resultant sEMG signal after DC component being removed. *N* is the segment samples.

Similarly, for kinematic data, the raw data is segmented and averaged in order to remove the DC offset.

4.2.4 sEMG Features Extraction

To obtain a better performance for sEMG application, several common features are widely used. sEMG features are classified into three classes; time domain features, frequency domain features and time-frequency features. Several researchers prove that time domain features showed better performance in control applications (Zardoshti-Kermani et al., 1995, Phinyomark et al., 2009 and Rubana et al., 2013). Among these features are the integrated EMG (IEMG), mean absolute value (MAV), Modified mean absolute value1 (MMAV1), Modified mean absolute value 2 (MMAV2), simple square integral (SSI), Variance (VAR) and root mean squares (RMS). Table 4.1 summarizes the mathematics formulas for each of the above-mentioned features and a brief description on the features. From the mathematical expressions of the sEMG features, it is clear that most of these features are related to each other and therefore the extracted EMG feature preserves the waveform of the signal. For further validation, we used the cross correlation to quantify the relationship between the extracted features.

Table 4.1

Brief description and the mathematical equations for some of sEMG applicable features.

Extracted Feature	**Mathematical formula**
- Integrated EMG (IEMG) is a method to measure the total muscular effort. IEMG is important for quantitative EMG relationships (EMG vs work, EMG vs force). IEMG is obtained by calculating the summation of the absolute values of the EMG raw.	$$IEMG = \sum_{i=1}^{N} \lvert x_i \rvert$$
- Mean Absolute Value (MAV): is the moving average of full-wave rectified EMG signal.	$$MAV = \frac{1}{N} \sum_{i=1}^{N} \lvert x_i \rvert$$
- Modified Mean Absolute Value (MMAV1): Is an extension of the MAV with slight modification in the weight segment of the EMG.	$$MMAV1 = \frac{1}{N} \sum_{i=1}^{N} w_n \lvert x_i \rvert$$ $$w_n = \begin{cases} 1 & \text{if } 0.25N \le n \le 0.75N \\ 0.5 & \text{otherwise} \end{cases}$$
- Modified Mean Absolute Value (MMAV2): similar to the MMAV1, with the continuous weighting segment function w_n is improved.	$$MMAV1 = \frac{1}{N} \sum_{i=1}^{N} w_n \lvert x_i \rvert$$ $$w_n = \begin{cases} 1 & \text{if } 0.25N \le n \le 0.75N \\ \frac{4n}{N} & \text{if } 0.25N > n \\ \frac{4(n-N)}{N} & \text{if } 0.75 < n \end{cases}$$
- Simple Square Integral (SSI): Is the energy or the power of the sEMG.	$$SSI = \sum_{i=1}^{N} \lvert x_i \rvert^2$$
- Root Mean Squares (RMS) is obtained by calculating the mean value of the square of all values of the EMG signal and dividing it by the length of the vector N and then the root of this result is calculated.	$$RMS = \sqrt{\frac{1}{N} \sum_{i=1}^{N} x_i^2}$$
- Variance (VAR) is the mean value of the square of the deviation.	$$VAR = \frac{1}{N-1} \sum_{i=1}^{N} (x_i)^2$$

Cross-Correlation

In order to quantify the linear relationship between sEMG features, one of the most widely used technique, is the cross-correlation defined by the following equation.

$$R_{x,y} = \frac{\text{cov}(x, y)}{\sigma_x \sigma_y} \tag{4.4}$$

where, cov is the covariance, σ_x and σ_y are the variance of the x and y features of the sEMG signal. In this study, we extracted the sEMG features and we quantify them using cross-correlation technique. Table 4.2 illustrate that there is a strong correlation between the IEMG and other features. Therefore, we have chosen to use the MAV feature for further analysis and in the implementation of the system in real time.

Table 4.2
Correlation between sEMG features.

EMG Features	**R^2**
Integrated EMG *vs* Mean Absolute Value	1.0000
Integrated EMG *vs* Root Mean squared EMG	0.9971
Integrated EMG *vs* Simple square Integral (SSI)	0.9227
Integrated EMG *vs* Modified Mean Absolute Value1	0.9996
Integrated EMG *vs* Modified Mean Absolute Value2	1.0000
Integrated EMG *vs* Variance	0.8764

4.2.5 High Pass Filtering

Low frequency artifacts induced with the sEMG could be removed using high pass filter with a cutoff frequency between 2Hz to 20Hz. One of the low frequency signals is the cardiography signal (ECG).

Many methods have been proposed to reduce the effect of the heart beat (ECG) signal on the sEMG signal. One of the methods is known as the independent component analysis (ICA) in which it separates the original source from additional noises (Chritiaan et al., 2015). Other techniques such as wavelet de-noising method, hybrid wavelet-neural network are also widely used. Q-R-S (ECG complexes) detection method is an alternative method used to determine these complexes. As ECG is a low frequency signal, the frequency corner of a filter is highly concerned. Redfern et al. (1993) investigated the influence of adjusting the cutoff frequency of a high-pass filter and suggested that a cutoff frequency of approximately 30Hz seemed optimal in balancing ECG removal with excessive sEMG degradation (Redfern et al., 1993). In this study, we apply Redfern's method using a high pass-third order Butterworth filter with a cutoff frequency of 30Hz.

4.2.6 Low Pass Filter

Digital low-pass filter is an essential procedure for noisy signals such as sEMG. Low pass filter for sEMG is considered the closest representation for the muscle activity and leads to the correct force produced by the muscles group in which they provide the required moment to the joint. Therefore, unwise choice of the filter and its parameters may thwart the anticipated results.

Two types of filters are used in this work to ensure free sEMG distortion and reduced noises, one is the Butterworth filter and the second is the wavelet filter. A comparison between the two filters is accomplished. The mathematical recursive model of a low-pass digital filter is described by the following difference equation

$$a_1.y(n) = b_1.x(n) + b_2.x(n-1) + ... + b_{n_b+1}.x(n-n_b) - a_2.y(n-1) - ... - a_{n_a+1}.y(n-n_a) \quad (4.5)$$

where, $a_1=1$, *x(n)* the actual sEMG at sample time *n*, a's and b's terms are constant coefficients, y(*n*) is the output of the filter.

Based on the recursive equation of a second-order Butterworth digital filter developed by Roberson and Dowling (2003), and after performing many tests using MATLAB. Inc., software, the *b's* term of the filter coefficients from order *N* to order *N+1* follow Pascal's triangle, as illustrated in Figure 4.1

2nd order	b_0 $2b_0$ b_0
3rd order	b_0 $3b_0$ $3b_0$ b_0
4th order	b_0 $4b_0$ $6b_0$ $4b_0$ b_0
5th order	b_0 $5b_0$ $10b_0$ $10b_0$ $5b_0$ b_0

Figure 4.1. Determination of Butterworth coefficients

As a result, a third-order recursive Butterworth digital filter could be defined as follows:

$$y_n = b_0(x_n + 3x_{n-1} + 3x_{n-2} + x_{n-3}) - a_1y_{n-1} - a_2y_{n-2} - a_3y_{n-3} \quad (4.6)$$

The term y_n refers to the current filtered data point, which is determined by the preceding three points (y_{n-1} y_{n-2} y_{n-3}), *n* is the sample index. The coefficients of the Butterworth filter are a function of the frequency corner, and their number depends on the filter order.

The angular cut-off frequency can be modelled as reported by Roberson and Dowling, (2003) $w_c = \tan(\frac{\pi f_c}{2 f_s})$ where, f_c and f_s are the cut-off frequency and the sampling frequency, respectively.

In most cases, the bilinear transform is used to translate an IIR filter from the s plane to the z plane (Lam, 1979). The bilinear transformation operator is defined as

$$z = \frac{1+s}{1-s}.$$

To obtain a zero-lag filter, filtering forward and backward was achieved.

A third-order system for a digital filter can be represented in the z domain by the following:

$$G(z) = \frac{b_0 + 3b_0z^1 + 3b_0z^2 + b_0z^3}{1 + a_1z^1 + a_2z^2 + a_3z^3} \tag{4.7}$$

Frequency Response

The behavior of a filter can be summarized by the so-called frequency response function, H_c. The frequency response function of the Butterworth low-pass filter has the following formula

$$|H_c(jw)|^2 = \frac{1}{1+(\frac{f_c}{f_s})^{2N}} \tag{4.8}$$

For low-pass filter, the inequality $f_s > f_c$ has to be satisfied. where, f_s, f_c are the sampling frequency and the cutoff frequency respectively. Let;

$$w = \frac{f_c}{f_s}$$

$$\begin{cases} \text{if } w \to 0 \to H_c = 1 \\ \text{if } w \to \infty \to H_c = 0 \end{cases} \tag{4.9}$$

when, H_c =1, the filter will pass all the signal frequency component and if H_c= 0 doesn't pass any frequency components. Corresponding to the normalized Nyquist frequency, the ratio $\frac{f_c}{f_s}$ should be within the range of 0 to 1.

Wavelet Approach for Filters

The de-noising algorithm based wavelet for sEMG filtering has been investigated by many researchers (Conforto et al., 1999; Khezri and Jahed, 2008 and Phinyomark et al., 2009). In this work, the wavelet approach for filter is used as comparative and validation tool with the abovementioned Butterworth filter.

Classical Fourier analysis has some limitations compared to wavelet analysis which unfolds a time series system not only in frequency but also in time; this is more adequate when the signal is high frequency which may be difficult to model it using Fourier transform.

The wavelet analysis block transforms the signal into different time-frequency scales. The wavelet transform(WT) uses the wavelet function and scaling function to perform simultaneously the multiresolution analysis (MRA) decomposition and reconstruction of the measured signal.

The scaled wavelet by λ and shifted by *a* could be written as the following

$$\Psi_{\lambda,a}(t) = \Psi.\frac{(t-a)}{\lambda} \tag{4.10}$$

where, ψ(t) is the Daubechies3 mother wavelet (the waveform is presented in Appendix C. Fig.C.1) .

Similar, to the Fourier concept, wavelet could be considered as special case from the Fourier transform by taking a scaling function. The coefficients can be estimated as follow,

$$c_{\lambda,a} = \sum x(t).\psi_{\lambda,a}(t) \tag{4.11}$$

and the signal can be reconstructed by the formula

$$x(t) = \sum_{\lambda}\sum_{a} c_{\lambda,a}(t).\psi_{\lambda,a}(t) \tag{4.12}$$

The signal at level N can be expressed by the following formula

$$x(t) = A_N(t) + D_{N-1}(t) + D_{N-2}(t) + ... + D_1(t) \quad (4.13)$$

where, A_N is called the approximation at level N, and D_1, D_2, ..., D_N are the details of the wavelet.

Signal to Noise Ratio

Signal to noise ratio (SNR) is a quality measure used in science and engineering to characterize the strength of the signal to the noise. SNR can be calculated in term of different physical measurements such as the power, voltage (Root Mean Squares), the variance and the peak level. In this study, we choose to quantify the variance between the de-noised and actual sEMG signal. The sEMG is defined as the combination of the clean signal $sEMG_c$ and the noise model $sEMG_n$ i.e.

$$sEMG(k) = sEMG_c(k) + sEMG_n(k) \quad (4.14)$$

with *k* is the signal's sample.

The filtered $sEMG_c$ is defined as the difference between the input to the filter and the output of the filter. However, the filter used herein is the Butterworth filter.

The signal to noise ratio is defined by the following formula,

$$SNR = 10 * \log_{10}\left[\frac{var(sEMG_c)}{var(sEMG_n)}\right] \quad (4.15)$$

where, *var* is the variance operator.

4.3 Onset/Offset of sEMG (Offline Detection)

In this section, the recorded data from the selected muscles are analysed offline. The absolute values of the recorded sEMG were used to indicate the muscle activities for all selected muscles in this study. We first considered a recorded raw EMG signal as $x(n)$ signal (rectified and low-passed filtered). The onset/offset algorithm takes the average between two points a and b before the first sEMG burst and an average between two other points $\boldsymbol{c}$ and d later after the first sEMG burst i.e. at the baseline level. These averages result into two points, which are defined by the following equations and are considered as the references or threshold points for the detection of the *onset* and *offset*, respectively:

$$\bar{x}_{a,b} = \frac{1}{N_{ab}} \sum_{0}^{N} (x_b - x_a) \tag{4.16}$$

$$\bar{x}_{c,d} = \frac{1}{N_{cd}} \sum_{0}^{N} (x_c - x_d) \tag{4.17}$$

where, x_a , x_b x_c and x_d are the sEMG values at points (a, b, c and d), N_{ab} and N_{cd} is the number of samples of the [a, b] and the [c, d] segments, respectively (Figure 4.2). This is also done when one wants to detect the *onset/offset* of the second, third, and so forth bursts of the sEMG. The following equations search for the index points (the sample index) of the onset/ offset along the rectified-filtered sEMG signal.

$$\begin{cases} \text{if } x_{(ind_1, amp_1)} > 2 * \bar{x}_{a,b} & \text{onset} \\ \text{if } x_{(ind_2, amp_2)} < 2 * \bar{x}_{c,d} & \text{offset} \end{cases} \tag{4.18}$$

where, ind_1 , amp_1 and ind_2, amp_2 are the coordinates of the sEMG signal. If the current point of the EMG is greater than twice the average of the set segment, then this point is counted as an onset point. Contrary, with offset detection, if the current value of the signal is less than twice the segment [c,d], then the this point is an offset.

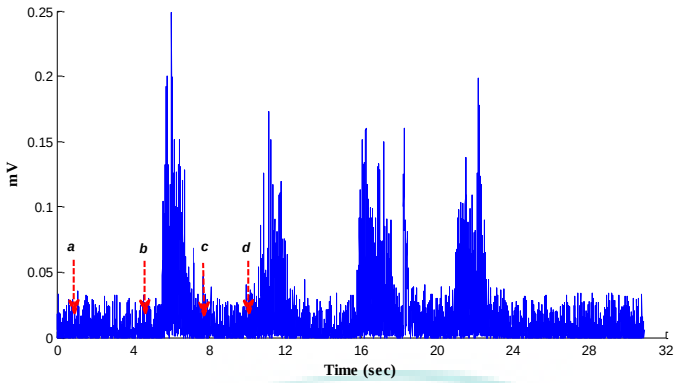

Figure 4.2. Example of Onset/Offset of sEMG (Offline Detection)

However, the baseline of the kinematics recording data is usually centred approximately on the zero line after filtering and removing the DC offset. In this study, we consider an angular velocity point of 7^0/s (standard deviation) as a threshold point to detect the individual beginning of the movement.

4.4 Modified Butterworth Filter for crosstalk/unwanted Measurements Removal

As mentioned earlier, the sEMG may exhibit additional interference measurements in which the discussed Butterworth filter fails to overcome this problem, nor the wavelet for filter. Correlating the kinematics data with the sEMG might give an insight on when the muscle should be activated. Since the onset/offset of the sEMG and the kinematic data are detected, one can compare both results to define the crosstalk measurements.

Figure 4.3 shows a block diagram of the stages taken for the application of the adaptive filter. The first step involves streaming the sEMG/kinematics data to be filtered using a 3rd order Butterworth filter with cutoff frequency of 6Hz. The smoothed data is then employed into a system that detects when the sEMG is at rest and when it is bursting along with kinematics data onset/offset detection. These index points (onset/offset of both sEMG and kinematics raw data) are then compared. If the sEMG burst corresponds to a movement, the raw data is smoothed using a conventional 3rd order Butterworth filter at cutoff frequency of 6Hz. However, if the sEMG

onsets/offsets do not correspond to any movement represented by the kinematic sensor, the Butterworth filter adaptively decreases its cut-off corner to eliminate this contaminated burst.

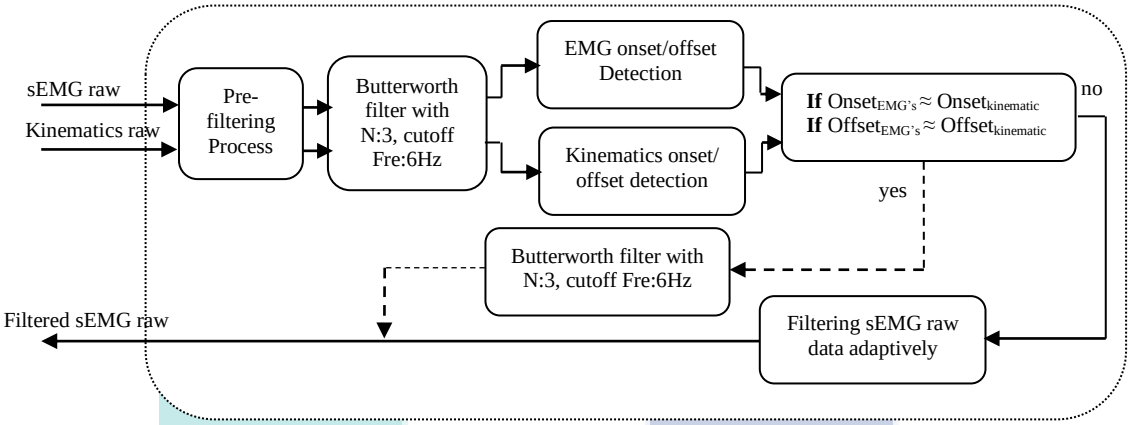

Figure 4. 3. Adaptive Butterworth filter stages.

4.4.1 Recursive Least Squares

The recursive least squares algorithm minimizes the sum of the squares of the error at each index point along the sEMG signal. The general model is given by

$$\hat{y}(n) = w^T X(n) \tag{4.19}$$

where w^T is the weight vector, which contains the *a's* and *b's* terms of the previously defined Butterworth digital filter. Because the selected filer was a third-order filter, the weight vector *w* is modelled by the following vector form:

$$w^T = [b_0 \quad 3b_0 \quad 3b_0 \quad b_0 \quad a_1 \quad a_2 \quad a_3]^T \tag{4.20}$$

The regression vector was defined as

$X(n)=[x_n \; x_{n-1} \; x_{n-2} \; x_{n-3} \; \hat{y}_{n-1} \; \hat{y}_{n-2} \; \hat{y}_{n-3}]$, and the error vector was defined as

$\sum e(n) = \sum d(n) - \hat{y}(n) = \sum d(n) - w^T X(n)$, where $d(n)$ is the desired baseline vector which is defined in this study as the previous filtered baseline of the sEMG signal.

The sum of the squares of the errors is then

$$w^T = [b_0 \quad 3b_0 \quad 3b_0 \quad b_0 \quad a_1 \quad a_2 \quad a_3]^T \tag{4.21}$$

$$\sum e(n)^2 = \sum (d(n) - w^T X(n))^2 \tag{4.22}$$

$$\sum e(n)^2 = \sum (d(n)^2 + w\, X(n) X(n)^T w^T) - 2\sum (d(n).\, w^T X(n) \tag{4.23}$$

The introduction of a factor λ to reduce the effect of the previous data, $0 << \lambda < 1$, called the "forgetting factor" to the above sum of the squares of the errors led to the following:

$$\sum \lambda\, e(n)^2 = \sum \lambda\, (d(n)^2 + w\, X(n) X(n)^T w^T) - 2\sum \lambda\, (d(n).\, w^T X(n) \tag{4.24}$$

To minimize the error, setting the derivatives of the $\sum \lambda\, e(n)^2$ term with respect to the weight w to zero,

$$\frac{\partial e(n)}{\partial w(n)} = \sum \lambda w(n) X(n) X^T(n) - 2\sum \lambda X(n) d(n) = 0 \tag{4.25}$$

$$\sum \lambda w(n) X(n) X^T(n) = 2\sum \lambda X(n) d(n) \tag{4.26}$$

The following terms were then defined: $R(n) = \sum \lambda X(n) X^T(n)$ and $R(n) = 2\sum \lambda X(n) d(n)$

This leads to $R(n)w(n) = P(n)$, which generates the optimal coefficients

$$w(n) = R^{-1}(n) P(n) \tag{4.27}$$

The weight vector w is updated recursively based on the recursive $R^{-1}(n)$ and $P(n)$. The matrix $P(n)$ could be defined recursively as

$$P(n+1) = \lambda\, P(n) + X(n+1)d(n+1). \tag{4.28}$$

In contrast, the inverse matrix of $R(n)$ is recursively updated based on the *lemma* inversion reported by Rowell (2008), which is given by

$$R^{-1}(n+1) = \lambda^{-1}\left[R^{-1}(n) - \frac{R^{-1}(n)X(n+1)X^{T}(n+1)R^{T}(n)}{\lambda + X^{T}(n+1)R^{-1}(n)X(n+1)} \right] \tag{4.29}$$

To further abstract the above equation, the so-called *Kalman gains* is defined by

$$\mathrm{k}(\mathrm{n}+1) = \frac{\mathrm{R}^{-1}(\mathrm{n})\mathrm{X}(\mathrm{n}+1)}{\lambda + \mathrm{X}^{\mathrm{T}}(\mathrm{n}+1)\mathrm{R}^{-1}(\mathrm{n})\mathrm{X}(\mathrm{n}+1)} \tag{4.30}$$

Equation (4.29) can then be re-expressed as

$$\mathrm{R}^{-1}(\mathrm{n}+1) = \lambda^{-1}\left[\mathrm{R}^{-1}(\mathrm{n}) - \mathrm{k}(\mathrm{n}+1)\mathrm{X}^{\mathrm{T}}(\mathrm{n}+1)\mathrm{R}^{-1}(\mathrm{n})\right] \tag{4.31}$$

The updated weight w can then be expressed as $w(n+1) = R^{-1}(n+1)P(n+1)$ by substituting equation (4.31) and equation (4.28) into equation (4.27). With further calculation, the updated weight can be defined as

$$\mathrm{w}(\mathrm{n}+1) = \mathrm{w}(\mathrm{n}) + \mathrm{k}(\mathrm{n}+1)\left[\mathrm{d}(\mathrm{n}+1) - \mathrm{X}(\mathrm{n}+1)\,\mathrm{w}(\mathrm{n})\right] \tag{4.32}$$

Another factor, δ may be introduced for the initialization of the matrix $R^{-1}(n)$ to avoid the risk of singularity. This factor is usually defined by $R^{-1}(0) = \delta\mathbf{I}$, where I is the identity matrix.

The cutoff frequency could be then relatively easy to compute based on the updated weight w,

$$b_0 = \frac{f_c^3}{1 + 2f_c + 2f_c^2 + f_c^3} \tag{4.33}$$

4.5 sEMG Signal to Muscle Activation Model

When a muscle contracts, the result of this contractions will produce the so-called muscle force. However, the generated force usually is delayed by about 10ms to 100ms (Buchanan et al., 2004).

A recorded raw sEMG signal is a voltage that is both positive and negative, whereas muscle activation is expressed as a number between 0 and 1; the zero value refers to a deactivated muscle, while 1 refers to a full activated muscle. The muscle activation needs a well smoothed or filtered to be accounted for the way that sEMG is related to force.

As mentioned earlier, there exists a time delay *d* for the muscle to be activated; this process is called "muscle activation dynamics" (Zajac, 1989). Figure 4.4 illustrates the process of the sEMG being transformed to a force generated by a specific muscle.

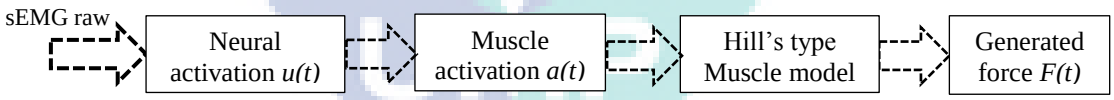

Figure 4.4. Schematic representation of the steps involved to transform sEMG signal to the muscle force.

The neural activation has the following recursive model

$$u(k) = \alpha.\, e\,(k - d) - \beta_1.u(k\text{-}1) - \beta_2.u(k\text{-}2) \tag{4.34}$$

u(k) is the neural activation, d is the electromechanical delay which usually taken as d=40ms (Lloyd and Besier, 2003 and Han et al., 2015), $e(k)$ is the normalized-rectified-filtered sEMG signal.

β_1 , β_2 and α are coefficients defining the second order dynamics. To ensure the stability of the above equation, a set of constraints were implemented.

$$\beta_1 = \Upsilon_1 + \Upsilon_2 , \beta_2 = \Upsilon_1 . \Upsilon_2 \text{ and } \alpha - \beta_1 - \beta_2 = 1 \quad (4.35)$$

with, $|\Upsilon_1| < 1$, $|\Upsilon_2| < 1$.

The arithmetic model that relate the neural activation with muscle activation is proposed by (Buahanan et al., 2004)

$$a(k) = \frac{e^{A.u(k)} - 1}{e^{A} - 1} \quad (4.36)$$

where, A is a factor between -3 and 0. Having A= -3, the muscle force activation is highly exponential with the neural activation. When A=0, the relationship between the neural activation $u(k)$ and the force activation $a(k)$ is closely to a linear relationship (Figure 4.5) (Shao et al., 2009 and Manal et al., 2003).

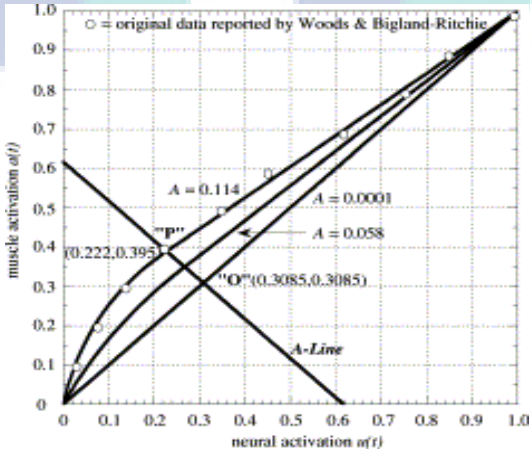

Figure 4.5. A-model: neural activation to muscle activation

Source Manal et al. 2003

In the following section; we present the hill's model that simulates the muscle force from the muscle activation.

4.6 Hill's Muscle Model

The common models used in biomechanics to represent the muscle forces during various movements are the Hill's type models (Hill, 1938). These models have the ability to predict the muscle force on the level of the muscle organ. The output of the Hill type model is a one dimension force which is applied to a skeletal model. However the inputs to the model are muscle length, or more precisely muscle–tendon-complex (MTC) length, MTC contraction velocity and neural muscle stimulation, (Figure 4.6) (Zajac, 1989; Van Soest and Bobbert, 1993; Winters, 1995; Günther and Ruder, 2003; Kistemaker et al., 2006 and Haeufle et al., 2014).

Hills muscle type model consists of two main elements, one is the contractile element (CE) used to produce the active muscle force (F_A^m). Whereas, the second element which is connected in parallel with the contractile element, is a passive elastic element (PE) used to produce passive force (F_P^m).

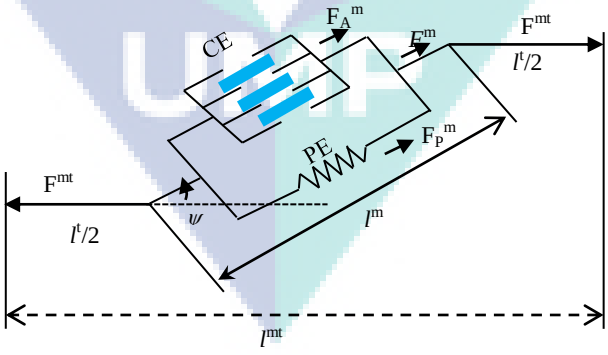

Figure 4.6. Hill's muscle type model

It is assumed that the total muscle force is the sum of the active and passive forces.

$$F^m = F_A^m + F_P^m \tag{4.37}$$

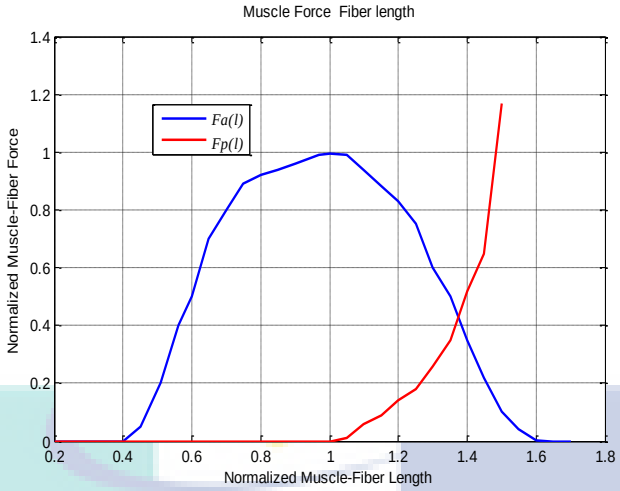

Figure 4.7. Relationship between the muscle forces to the fiber length

Source Lloyd et al., 2003

The tendon is modeled in series with muscle fiber (Figure. 4.6). It is noted from Figure 4.6 that the total muscle-tendon force can be expressed as

$$F^{mt} = F^{m} .cos\,(\psi) \tag{4.38}$$

and the muscle-tendon length can be calculated as

$$l^{mt} = l^{t} + l^{m} .cos(\psi) \tag{4.39}$$

where, ψ is the pennation angle at which the muscle fiber connect to the tendon, i.e the angle between the muscle fiber and the tendon. Zajac (1989) results showed that the pennation angle has less effect on the produced force if it is less than 20 degrees (Table 4.3), therefore in this study we choose to neglect the pennation angle for the selected muscles. l^{t} is the total length of the tendon.

The active muscle force and the passive force can be described as

$$F_A{}^{m} = f_A\,(l).\, f_v\,(v).\, a(k).\, F_0{}^{m} \tag{4.40}$$

$$F_P^m = f_P(l).\ F_0^m \tag{4.41}$$

where, $f_A(l)$, $f_v(v)$ and $f_P(l)$ represent the normalized active force-length relationship, force-velocity relationship and the passive elastic force-length relationship respectively (Figure 4.3).

The resulted muscle-tendon force F^m is then modeled as

$$F_i^m = [f_A(l).\ f_v(v).\ a(k) + f_P(l)]\ .\ F_0^m \tag{4.42}$$

F_0^m is the maximum isometric muscle force, l is the normalized muscle fiber length and v is the normalized muscle fiber velocity during muscle contraction and i denotes a specific muscle.

The coupling between the muscle activation and the optimal fiber length is given by

$$l_0^m(k) = l_0^m(\eta(1 - a(k)) + 1) \tag{4.43}$$

where, η is the percentage change in the optimal fiber length, it was calibrated at 15% according to Lloyd et al., 2003. $l^m{}_o$ is the optimal fiber length at maximum activation. $l^m{}_o(k)$ is the optimal fiber at sample time k with muscle activation $a(k)$.

With some simplification on the level of $f_A(l)$, $f(v)$ and $f_P(l)$ proposed in the literature review we have

$$\begin{aligned} f_A(l) &= C_0 + C_1.l + C_2.l^2, \quad 0.5 \le l \le 1.5 \\ f_A(l) &= 0. \qquad\qquad \text{otherwise} \\ f_P(l) &= e^{10.l\,-15} \\ f_v(l) &= 1. \end{aligned} \tag{4.44}$$

where, l is the normalized muscle fiber length, C_0, C_1 and C_2 are constants.

Substituting equation (4.43) into (4.44) gives

$$\begin{aligned} f_A(l) &= C_0 + C_1.\ l_0^m(\eta(1 - a(k)) + 1) + C_2.\ l_0^m(\eta(1 - a(k)) + 1)^2, \quad 0.5 \le l \le 1.5 \\ f_A(l) &= 0. \qquad\qquad \text{otherwise} \\ f_P(l) &= e^{10.l_0^m(\eta(1 - a(k)) + 1)\,-15} \\ f_v(l) &= 1. \end{aligned} \tag{4.45}$$

Recent study (Ward et al., 2009) on lower limb muscles architecture reveals the following fiber length, muscle length and pennation angle for the RF, BF and Gas muscles. In table 4.3, the optimal length and the maximum forces for the selected muscles obtained from (Raasch et al., 1997)

Table 4.3
Properties of the selected muscles (*Ward et al., 2009 and Raasch et al.,* 1997)

Muscle	**Muscle length l^m (*cm*)**	**Fiber length *l*(*cm*)**	**Pennation angle (^{0})**	**Max force*(N)***	**Optimal length $l^m{}_0$ (*cm*)**
RF	36.28±4.73	7.95±1.28	13.9±3.5	974	8.400
BF	34.73±3.65	9.76±2.62	11.06±5.5	1312	10.09
Gas	26.94±4.65	5.10±0.98	9.9±4.4	2225	4.500
Sol	40.54±8.32	4.40±0.99	28.3±10.1	3529	3.000

Once the parameters $l^m{}_0$, $F_0{}^m$ are given, one can calculate the active force. The initial values of the coefficients C_0, C_1 and C_2 are also given to fit a piecewise parabola (Qichuan et al., 2011), C_0=-2.06, C_1=6.16 and C_2 = -3.13. Substituting equation (4.44) into (4.42) will form the total force generated by a specific muscle

$$F_i^m = [(\mathrm{C}_0 + \mathrm{C}_1 l_0^m(\eta(1-a(k)+1)) + \mathrm{C}_2 l_0^m(\eta(1-a(k)+1))^2).a(k) + \mathrm{e}^{10 l_0^m(\eta(1-a(k)+1)-15}].F_0^m \quad (4.46)$$

Let the general equation of the muscle force as the following

$$F_i^m(k) = F_0^m[\mathrm{K}_{1i}a_i(k) + \mathrm{K}_{2i}a_i{}^2(k) + \mathrm{K}_{3i}\,a_i{}^3(k) + \mathrm{K}_{4i}\mathrm{e}^{\mathrm{K}_{5i}a_i(k)}] \quad (4.47)$$

where, K_{1i}, K_{2i} , $\mathrm{K}_{3i,}$ K_{4i} and K_{5i} are constants. K_{3i}, K_{4i} , and K_{5i} can initially calculated since l_0^m and η are known see (Table 4.3). The subscript *i* refers to a specific muscle. The coefficients K_{4i} seem to be very close to zero (0). Therefore, we ignore the exponential term in the above equation.

Further simplification and expansion of the coefficients can be found in Appendix B.

On the other hand, a study done by Visser et al. (1990) proposed that the length of a muscle (tendon-muscle length) is related to the knee and hip angles by a second order polynomial.

$$l^{mt}=A_0+A_1\theta_j + A_2(\theta_j)^2 \quad (4.48)$$

where, A_0, A_1 *and* A_2 are constant. j =1, 2 and θ_j is the hip and the knee angles. The experiment was conducted on five human cadavers.

The moment arms is calculated by the derivation of the muscle tendon length

$$M.A_i = A_1 + 2.\, A_2\,(\theta_j) \quad (4.49)$$

In this study, we use the estimated coefficients in (Visser et al., 1990) for the BF, RF and Gas muscles as illustrated in Table 4.4.

Table 4.4
Estimated coefficients of the equation (4.45)

		Constants		
Joint	**Muscle**	A_0	A_1	A_2
Knee	RF	-0.02346	0.24222	-0.00059
Hip	RF	-0.01966	-0.15041	0.00044
Knee	BF	0.19826	-0.04600	0.00000
Hip	BF	0.16644	0.31078	0.00061
Knee	Gas	-0.08268	-0.08028	-0.00013

The joint moment is estimated by the sum of the forces generated by a group of muscles given by

$$M_J=\sum M.A_i \text{ x } F_i^m \quad (4.50)$$

where, J =1,2 is denoting the knee and hip joints, i denotes a specific muscle.

As we have used two muscles for the chair-rise experiment, two terms of the force for both BF and RF is addressed in a matrix form (eq. 4.51). This means the total joint moment can be expressed by two variables which are the sEMG for BF and sEMG for RF.

$$\begin{bmatrix} \mathrm{M}_K \\ 0 \end{bmatrix} = \begin{bmatrix} F_{BF}^{m}(k) & F_{RF}^{m}(k) \\ 0 & 0 \end{bmatrix} \begin{bmatrix} F_{0BF}^{m}.\mathrm{M.A}_{\mathrm{iBF}} \\ F_{0RF}^{m}.\mathrm{M.A}_{\mathrm{iRF}} \end{bmatrix} \tag{4.51}$$

Similarly for the walking task, the Gas muscle force is introduced; this yield to to the following matrix form which obtains the knee joint moment,

$$\begin{bmatrix} \mathrm{M}_K \\ 0 \\ 0 \end{bmatrix} = \begin{bmatrix} F_{BF}^{m}(k) & F_{RF}^{m}(k) & F_{Gas}^{m}(k) \\ 0 & 0 & 0 \\ 0 & 0 & 0 \end{bmatrix} \begin{bmatrix} F_{0BF}^{m}.\mathrm{M.A}_{\mathrm{iBF}} \\ F_{0RF}^{m}.\mathrm{M.A}_{\mathrm{iRF}} \\ F_{0\mathrm{Gas}}^{m}.\mathrm{M.A}_{\mathrm{iGas}} \end{bmatrix} \tag{4.52}$$

where, $F_{BF}^{m}(k)$ $F_{BF}^{m}(k)$ and $F_{Gas}^{m}(k)$ are the forces of the BF, RF and Gas muscles respectively. The equations of these forces are further explained in appendix B. F_{0BF}^{m}, F_{0RF}^{m} and $F_{0\mathrm{Gas}}^{m}$ are the maximum forces of the BF, RF and Gas muscles summarized previously in Table 4.3.

4.7 Inverse Dynamics Method

Inverse dynamics is a method that calculates the moment or the joint from the dynamic equation of motion. In this study, the positions of the limbs are measured using a gyroscope sensor that returns the angular velocity. The angular velocity is then used to obtain the angles and the angular accelerations. Inverse dynamics requires the masses, moment of inertia and the length of each link segment i.e. the hip and the knee joints.
During chair rise task, we consider the movement about the knee joint only in order to lift the whole body. We assume also that the lower leg is fixed at vertical posture. Initially, we assume that the knee angle was 0^0 and the hip was 45^0. For more definition of the variables on each joint segment, a schematic model is presented in Figure 4.8. Moments of inertia, centre of gravities were calculated according to the anthropometric data given by (Winter D. A., 2009). Using Lagrangian formalism, the joint moment is calculated from

$$M_J^{inv} = \frac{d}{dt}\left(\frac{\partial \mathrm{L}}{\partial \dot{\theta}_J}\right) - \frac{\partial \mathrm{L}}{\partial \theta_J} \tag{4.53}$$

where, θ_J, $\dot{\theta}_J$ are the joint angle and is the angular velocity respectively, and $L = E_k - E_p$ with E_k and E_p are the kinetic and the potential energies, respectively.

The general equation of motion is given by the following;

$$M_J^{inv} = D_J(\theta_J)\ddot{\theta}_J + C(\theta_J, \dot{\theta}_J) + G(\theta_J) \tag{4.54}$$

where, D is the inertia matrix, C is the Coriolis vector and G is the gravity vector; θ_J, $\dot{\theta}_J$, $\ddot{\theta}_J$ are the angles, angular velocities and angular accelerations, respectively. J =1, 2 refers to the hip and the knee joints.

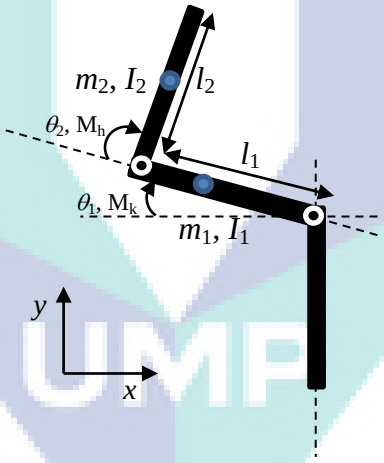

Figure 4.8. Segmental model of the chair-rise, the movement is about the knee joint.

The hip angle is modelled as a function of the knee angle by the following

$$\theta_2 = -3\theta_1/2 + 3\pi/2.$$

where, m_1, m_2, I_1, I_2, l_1, l_2 are the masses, the moments of inertia and the lengths of the upper leg (thigh) and the trunk segments, respectively. M_k and M_h, are the net knee and hip joint moments.

Segment 1: the thigh segment

Let d_1=0.567 a percentage from the total length to represent the CoG of segment 1 and d_2 = 0.903 is percentage from the total length to represent the CoG of segment 2.

$$E_{k,1} = \frac{1}{2} m_1 (d_1)^2 l_1^2 \dot{\theta}_1^2 + \frac{1}{2} I_1 \dot{\theta}_1^2 \quad E_{p,1} = -m_1 g (d_1) l_1 \cos(\theta_1) \tag{4.55}$$

Segment 2: the hip segment

$$\begin{aligned} E_{k,2} &= \frac{1}{2} m_2 v^2 + \frac{1}{2} I_2 (\dot{\theta}_1 + \dot{\theta}_2)^2 \\ E_{p,2} &= -m_2 g (l_1 \cos(\theta_1) + d_2 . l_2 \cos(\theta_1 + \theta_2)) \end{aligned} \tag{4.56}$$

where, $v^2 = \dot{x}^2 + \dot{y}^2$, with x and y the CoG of the hip segment coordinate.

$$x = l_1 \sin(\theta_1) + d_2 \, l_2 \sin(\theta_1 + \theta_2) \tag{4.57}$$

$$y = l_1 \cos(\theta_1) + d_2 \, l_2 \cos(\theta_1 + \theta_2) \tag{4.58}$$

Substituting (4.57), (4.58), into (4.56) and (4.55) into (4.54), the knee joint moment can be derived as

$$\begin{aligned} M_k^{inv} = \ddot{\theta}_1 (& m_2 d_2^2 l_2^2 + m_1 d_1^2 l_1^2 + 2 m_2 l_1^2 + m_2 l_1 l_2 d_2 \sin((3/2)\theta_1) + I_1 + \frac{1}{4} I_2) \\ & + m_2 l_1 l_2 d_2 \cos((3/2)\theta_1) \dot{\theta}_1^2 + m_1 g d_1 \, l_1 \sin(\theta_1) + m_2 g \, l_1 \sin(\theta_1) \\ & - \frac{1}{2} m_2 g d_2 \, l_2 \sin(\frac{1}{2}\theta_1) \end{aligned} \tag{4.59}$$

Similarly, using the Lagrangian method for the walking task gives the following dynamics system for the knee joint moment. The two segments herein are the leg and the thigh with d_0 = 0.433 is the CoG of the leg segment.

$$M_k^{inv} = (\frac{1}{2} m_1 d_0^2 l_1^2 + I_1)\ddot{\theta}_1 + \frac{1}{2} I_2(\ddot{\theta}_1 + \ddot{\theta}_2) + m_2(2l_1^2\ddot{\theta}_1 + 2d_1^2 l_2^2(\ddot{\theta}_1 + \ddot{\theta}_2) + d_1 l_1 l_2(2\ddot{\theta}_1 + \ddot{\theta}_2)\cos\theta_2 - d_1 l_1 l_2(2\dot{\theta}_1\dot{\theta}_2 + \dot{\theta}_1^2)\sin\theta_2) + m_1 g d_0 l_1 \cos(\theta_1) + m_2 g l_1 \cos(\theta_1) + m_2 g d_1 l_2 \cos(\theta_1 + \theta_2) \quad (4.60)$$

In this study, we emphasize to optimize only the knee joint moment variables i.e. the moment obtained from the inverse dynamic and the moment obtained from the muscles.

To optimize the knee joint moment by the muscles M_k, we used LS (Least Squares) optimization method that minimizes the sum of the squared errors between the M_k and M_k^{inv} (Rogers et al., 2007).

$$\min \sum (M_J - M_k^{inv})^2 \quad (4.61)$$

This leads to the estimation of the coefficients (C_0, C_1, C_2) presented in equation (4.46).

From the dynamics of human gait addressed in (Vaughan, et al., 1999, pages 20-25), some of the individual's anthropometry parameters can be predicted from basic data such as the segment's length and the circumference of the limb with the total weight of the body. Since the equation of motion requires the mass and the moment inertia, we have calculated these two parameters for one subject.

The following table (Table 4.5) includes some of the parameters in order to calculate the moment in a joint.

Table 4.5
Anthropometric data of one subject with weight of 71*kg*

Segment	**Mass (kg)**	**Length (m)**	**Moment of inertia (kg.m^2)**
Thigh	7.1	0.460	0.138
Leg	3.3	0.430	0.049
HAT	48.15	0.297	1.14

4.8 Summary

The chapter discussed the sequence of the sEMG signal processing. It includes the pre-filtering part by analysing the DC offset in sEMG, the baseline wander, low frequency noises filtering. As it is known that the true muscle activities could be represented by the output of the low pass filter, it was essential to search for the optimum digital low pass filter that guarantees signal free distortion and free noise. The onset/offset of the sEMG was essential to detect the rising and the falling time of the sEMG signal. To this end, implementing the algorithm of the detection of the onset/offset for both sEMG and kinematic measurements could determine the cross-talk recordings. A discussion on how to remove these additional measurements (cross talk) is stated. We propose to integrate the Hill Muscle Model in order to obtain the force generated by a muscle. From the latter generated force, one can calculate the moment provided to the joint by a specific muscle. Since one or two moments generated by specific muscles cannot achieve full motion, we implement the inverse dynamic for optimization purposes. In the next chapter, we present the all the findings of the research.

CHAPTER 5

RESULTS AND DISCUSSION

5.1 Introduction

This chapter presents the findings of the study; it clarifies the behavior of the sEMG signal of lower limb with accordance to certain daily life tasks. The analysis of the data includes the pre-processing part which addressed the DC offset effect, the baseline wander, low frequency noises such as ECG signal.

The filter parameters influences on the amplitude of the sEMG is presented and discussed in details. This led to a search for the optimal parameters of the filter by comparing two types of filters. To scale the sEMG signals to a uniform scale, the data were normalized to the peak and the standard deviation. To check the correlation of the EMG patterns with the movement, all the data were normalized to the motion range of the individual. The crosstalk phenomena are also addressed in this chapter. Then the transformation of the muscle activity to the generated force based on Hill's model is presented. The summation of all muscle forces output is then used to predict the moment in a joint. In the last subsection, we present the predicted moment generated by the muscle to achieve a complete task.

5.2 Pre-Processing

In this section, a summary of the pre-processing results i.e. treating the DC offset component, the baseline wander, designing the optimum filter is presented.

Figure 4.1 presents an example of sEMG signal recoded during performing a chair rise experiment.

Initially the recorded sEMG raw was not centered at the zero line axis as shown in Figure 5.1 (blue). Similarly, the kinematics data was also zero-mean.

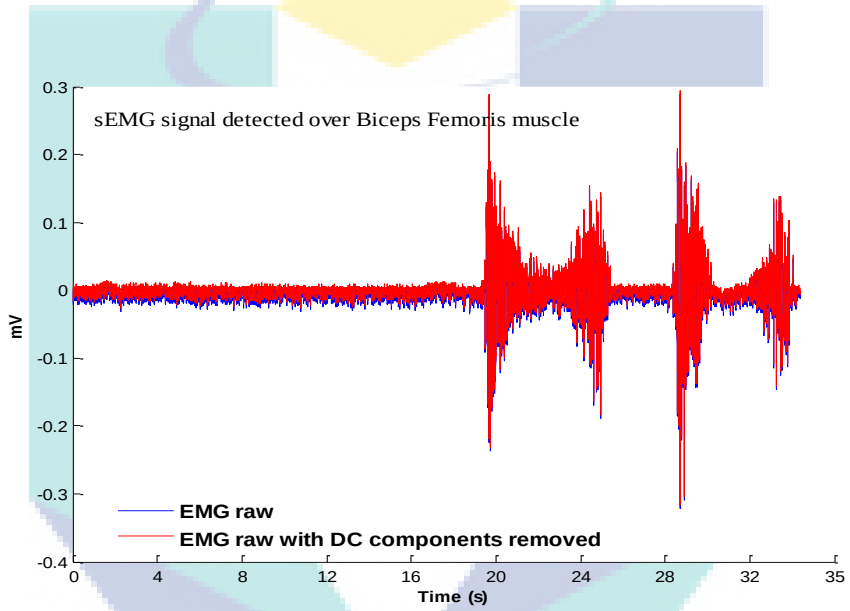

Figure 5.1. Example of a sEMG raw with DC component being removed. (blue) is the original sEMG raw, (red) is the sEMG raw with DC being removed.

Ideally, the gyroscope should output a zero angular velocity when there is no movement. But the Gyro output measurement tends to give values sporadically near zero (Figure 5.2, blue line). This bias directly affects the resulted angle by drifting its values. Many researchers choose to calibrate the Gyro by recording data at rest then taking the mean of this recording to be used as threshold point in the experiment. Similarly, to the sEMG procedure, in this study, we subtract the mean values (baseline segment) from the actual angular velocity (Figure 5.2, black line). Figure 5.3 shows one example of the resulting angle from angular velocity measurements achieved during performing a chair rise task for two trials. It is clear that the range of the motion is approximately from 0^0 while sitting until 80^0 at the up-right posture.

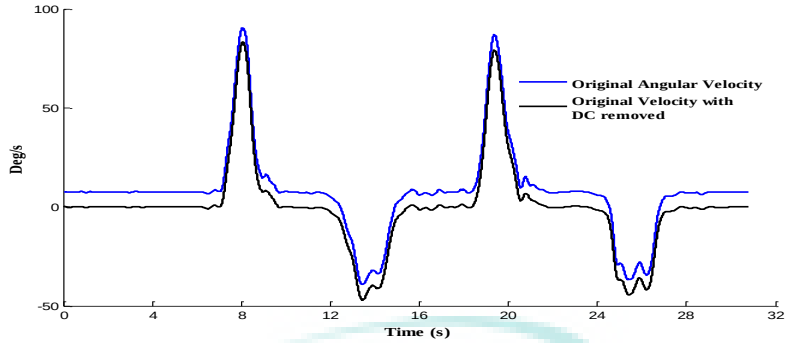

Figure 5.2. Example of a measured angular velocity achieved during chair rise task for two trials, (blue) is the original angular velocity, (black) is the angular velocity with DC bias being removed.

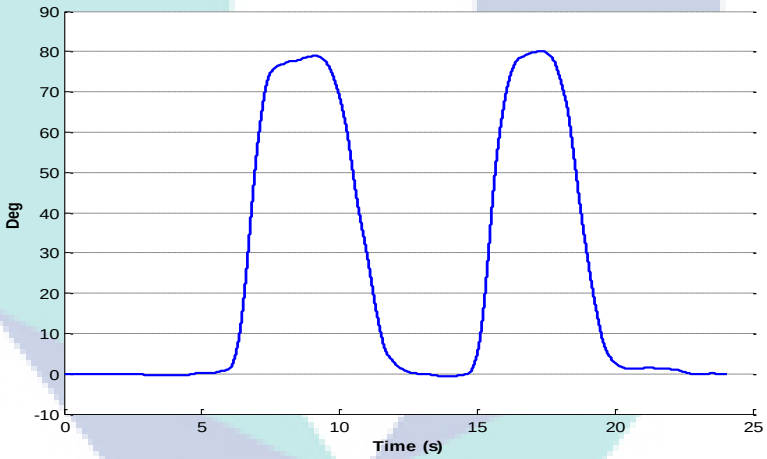

Figure 5.3. Example of a resulted hip angle during chair rise task for two trials.

Figure 5.4 depicts an example of an original sEMG raw recorded over the BF and RF during chair-rise experiments for two trials. Prior to any processing, the signals contain positive and negative values which reflect the positive and negative leads of the sensor. Visual inspection may approximately determine the onset/offset of the signal (presented in red and black arrow respectively), but the accuracy would be suspicious.

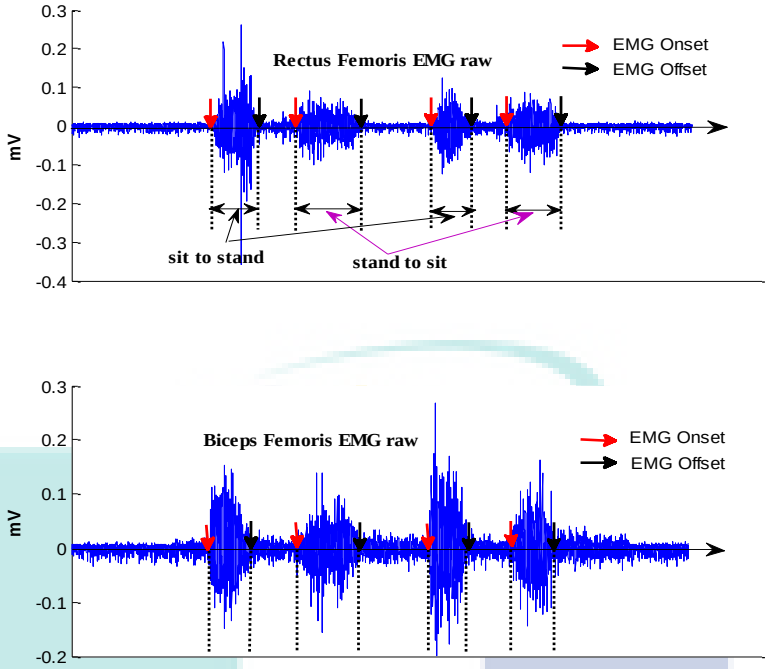

Figure 5.4. Example of sEMG raw over RF (top Figure) and BF (bottom Figure) muscles during chiar rise protocol for two trials. Red arrows represent the onset timing of the sEMG and black arrows represent offset timing the sEMG.

5.3 Butterworth Filter Performance

In this section, the effect of the cutoff frequency on the sEMG is presented. An example of raw sEMG recorded from one volunteer over the Biceps Femoris muscle during sit to stand task is processed. Note that in all the following results, we applied zero-lag Butterworth filter. For simplicity, we showed only the results of the Butterworth filter at the following selected cut-off frequencies [2, 5, 6, 8] Hz respectively at filter's order varies from 1 to 7.

Figure 5.5 shows the rectified filtered sEMG using the Butterworth filter at a cut-off frequency of 2Hz with the filter's orders varies from 1 to 7. By enlarging the first and the third bursts of the signal, it is clear that the Butterworth filter undershoots the data with all filter's order except the first order. Emphasizing on the first order output, the result shows that the filter maybe is responding earlier than the original signal which may lead to a false interpretation in determining the rising time of the burst (onset time). It is also noticeable that the amplitude of the signal varies significantly between all the

outputs of the Butterworth filter. However, the falling time (offset time) show agreement with all filter's orders.

Figure 5.6 compares the outputs of the Butterworth filter at cut-off frequency of 5Hz with the same filter's order mentioned above. Apart from the output of the first order filter which shows considerable ripples, all other outputs are in strong correlation with less undershooting of the data in the first burst. However, in the second burst, the 5^{th}, 6^{th} and the 7^{th} order filter outputs showed slight undershoot in the data below zero line (Figure 5.6 (c)). These results might not be suitable and applicable for further investigation.

Figure 5.7 depicts the Butterworth filter outputs at cut-off frequency of 6Hz with different filter's order. Similarly, the outputs of the filter shows no difference between them with close similarity in amplitude apart from the first order output in which the result appears in a rippled waveform. It is clear from Figures 5.7 (b) and (c) that the undershoot level in this case is very minor compare to the previous cases.

Figure 5.8 presents the output of the Butterworth filter at different filter's order with a cutoff frequency of 8Hz. With 8Hz cutoff frequency, it seems that the Butterworth filter outputs the same results with significant ripples at the 1^{st} order. However, all other outputs tend to be ripples also compared with the above cutoff setting.

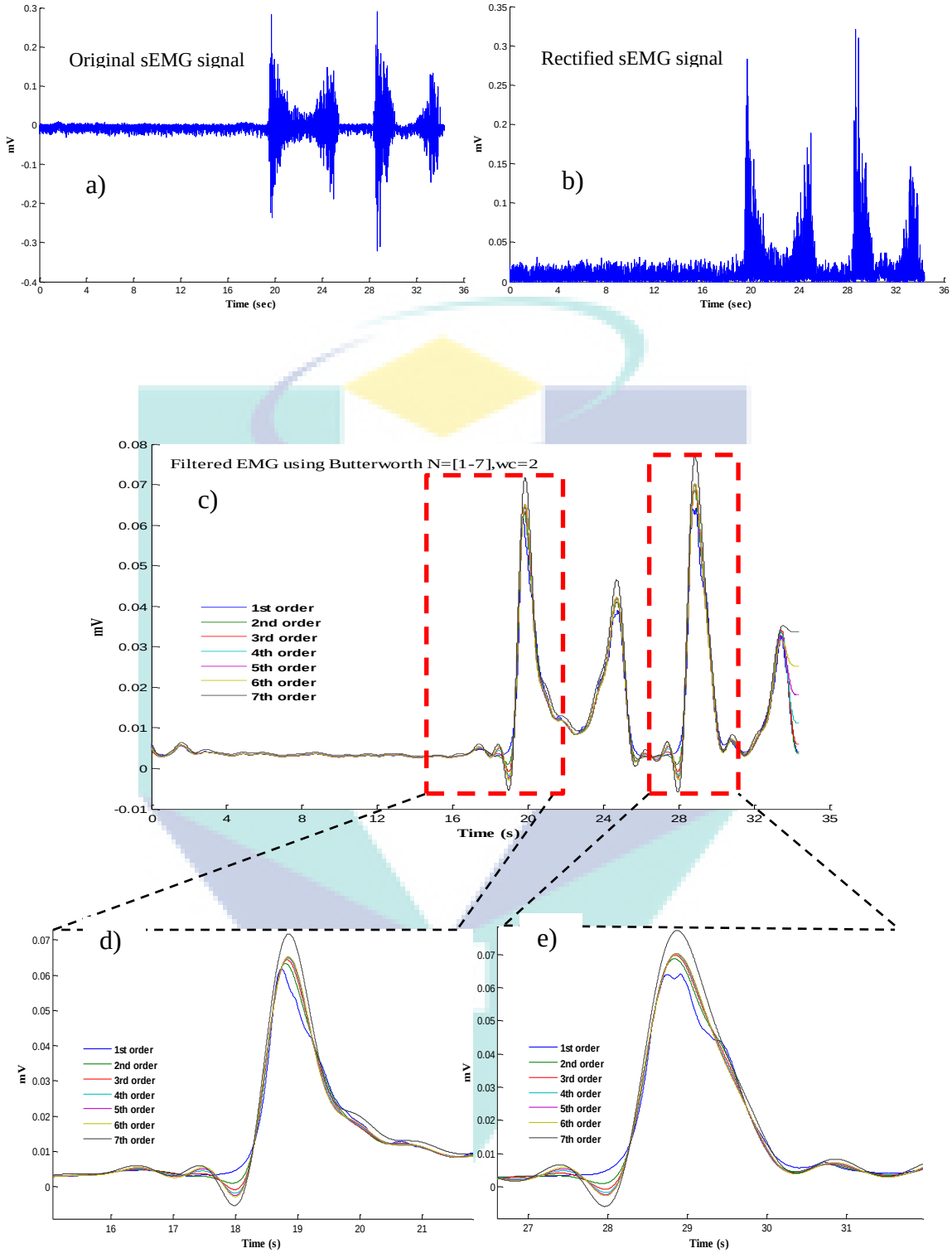

Figure 5.5. Butterworth Filter Performance at w_c = 2Hz. a) and b) are the original and the rectified sEMG raw. Example of a filtered sEMG raw using Butterworth filter at different orders with cut-off frequency w_c = 2Hz (c)). (d) and (e) enlargement of the first and the third bursts of the sEMG raw where they show a remarkable undershoot of the signal at certain orders.

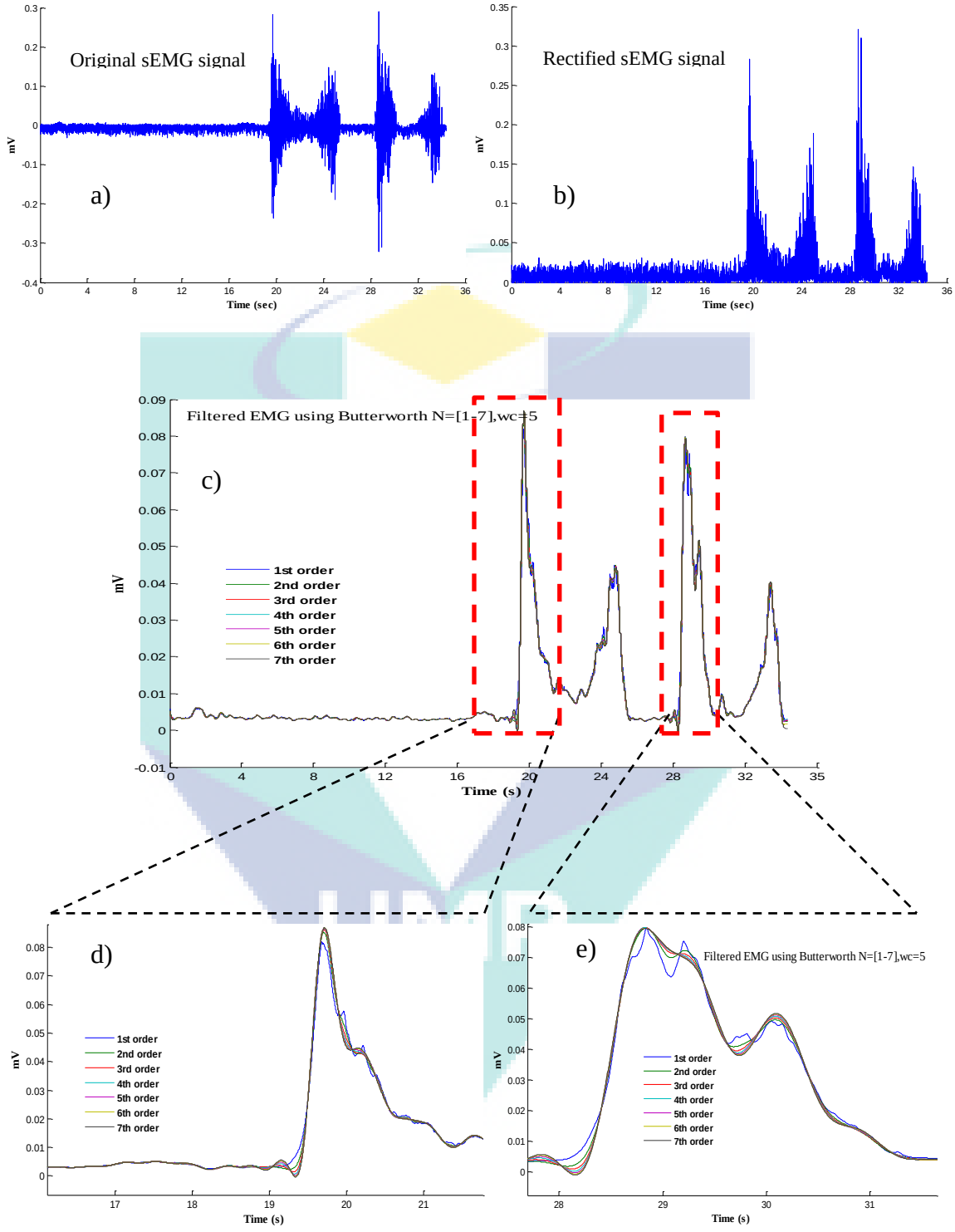

Figure 5.6. Butterworth Filter Performance at w_c = 5Hz. a) and b) are the original and the rectified sEMG raw. Example of a filtered sEMG raw using Butterworth filter at different orders with cut-off frequency w_c = 5Hz (figure (c)). (d) and (e) enlargement of the first and the third bursts of the sEMG raw.

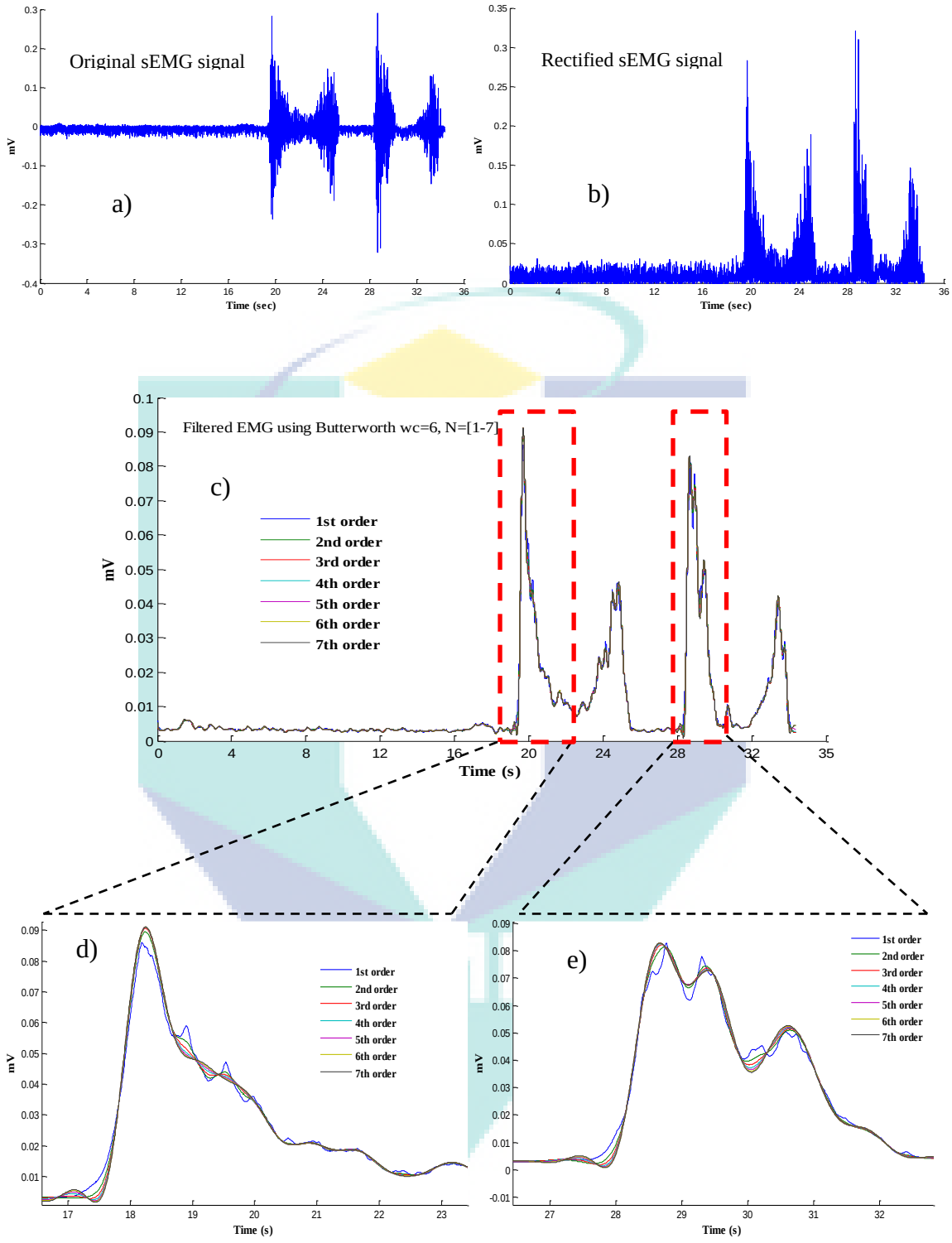

Figure 5.7. Butterworth Filter Performance at w_c = 6Hz. a) and b) are the original and the rectified sEMG raw. Example of a filtered sEMG raw using Butterworth filter at different orders with cut-off frequency w_c = 6Hz (figure (c)). (d) and (e) enlargement of the first and the third bursts of the sEMG raw.

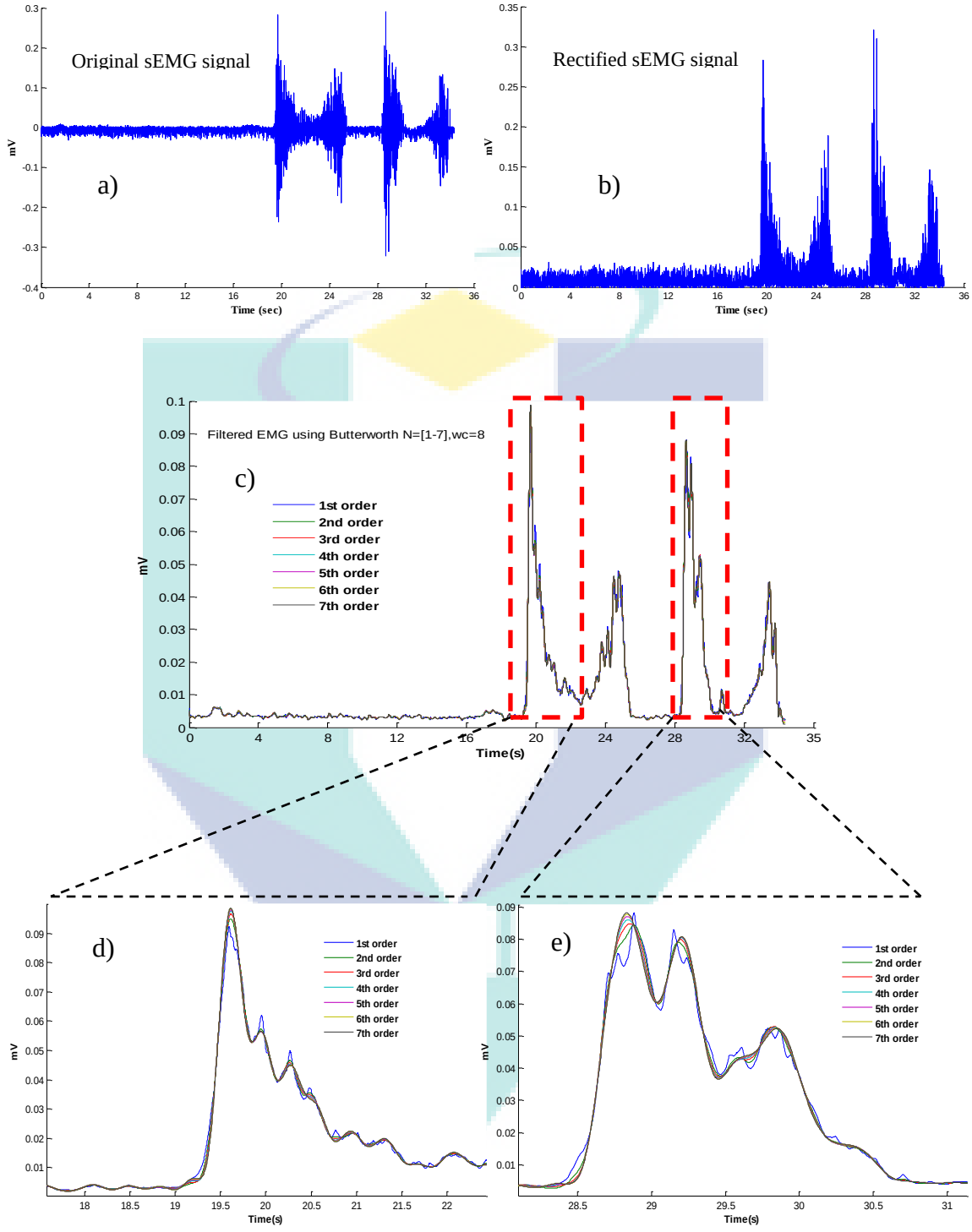

Figure 5.8. Butterworth Filter Performance at w_c = 8Hz. a) and b) are the original and the rectified sEMG raw. Example of a rectified-filtered sEMG raw using Butterworth filter at different orders with cut-off frequency w_c = 8Hz (figure (c)). (d) and (e) enlargement of the first and the third bursts of the sEMG

We conclude from the above results of the effects of the filter parameters on the sEMG smoothing that caution should be taken when filtering sEMG. For instance, when using a cutoff frequency of 2Hz, the filter order should not be greater than the first order. In the 5Hz cutoff frequency example, the accepted filter orders are maybe only the 1st, 2nd and 3rd orders. When choosing a 6Hz cutoff frequency, the 1st order should be excluded and the 3rd order filter could be the best as it shows almost the average of the remaining filter outputs. Lastly, the 8Hz cutoff frequency shows a number of ripples in all selected filter orders compare to the 6Hz example.

Table 5.1 clarifies the differences in the peaks of the filtered sEMG at the aforementioned cutoff frequencies with filter order varies 1 to 7. It shows that the change in amplitudes with regards to the filter order at the cutoff frequency wc=5Hz and wc=6Hz is very minor compare to the amplitudes at wc=2Hz. At cutoff frequency wc=8Hz, the change also is very minor, but from the above graph, the results shows ripples.

Table 5.1
Maximum values of the filtered sEMG

		Peaks						
	Order	N=1	N=2	N=3	N=4	N=5	N=6	N=7
Cutoff Freq(Hz)	2	0.0642	0.0687	0.0698	0.0701	0.0703	0.0703	0.0772
	5	0.0819	0.0853	0.0862	0.0867	0.0866	0.0868	0.0869
	6	0.0861	0.0895	0.0906	0.0909	0.0910	0.0910	0.0910
	8	0.0923	0.0949	0.0967	0.0976	0.0981	0.0984	0.0984

Further confirmation/validation of filtering the sEMG signal have been made by comparing the wavelet outputs at different level with the Butterworth filter outputs.

5.3.1 Optimum Filter Order

To determine the optimum filter order, we fixed the cutoff frequency and simultaneously vary the Butterworth filter order from 1 to 8; meanwhile we compute the correlations with regards to the wavelet filter at different scales from 4 to 8 (see Table. 5.2). The main finding from Table 5.2 shows that wavelet approach at scale six (6) possesses the best correlation with all selected orders of the Butterworth filter (more details on correlation results can be found in appendix C). Referring again to table 5.2

(column correspond to the sixth level), the highest correlation point (0.9879) corresponds to the third filter order. For a clearer view, the highlighted column in Table 5.1 is plotted in Figure 5.9. Third filter order is then maybe the optimum order that the Butterworth filter outputs can produce. Third order inhere also shows agreement with the previous results at cutoff frequency of 6Hz.

Table 5.2
Wavelet output correlation with Butterworth filter

Butterworth filter order		Wavelet scales				
		4	5	6	7	8
1	Correlation	0.948	0.9851	0.9847	0.9657	0.9393
2		0.9352	0.9862	0.9878	0.9624	0.9339
3		0.9298	0.9847	0.9879	0.9601	0.9315
4		0.9267	0.983	0.9874	0.9587	0.9302
5		0.925	0.982	0.9872	0.958	0.9295
6		0.9237	0.9812	0.9868	0.9575	0.929
7		0.9229	0.9805	0.9866	0.9571	0.9286
8		0.9222	0.9801	0.9864	0.9568	0.9283

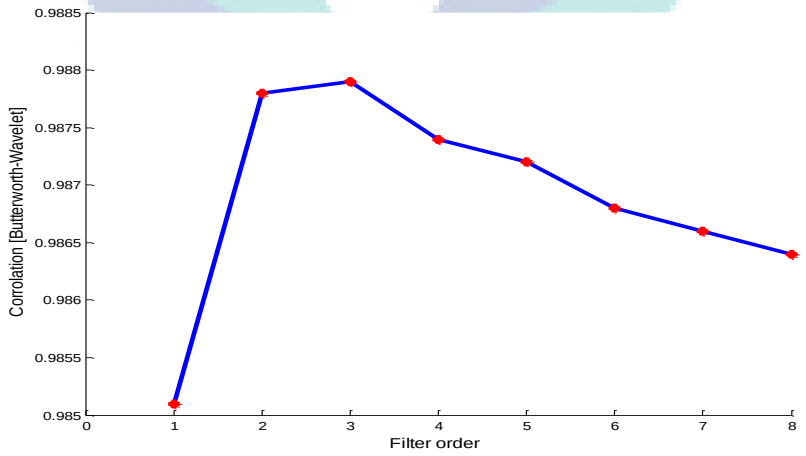

Figure 5.9. Correlation between the wavelet output at level six and the outputs of the Butterworth filter at different order.

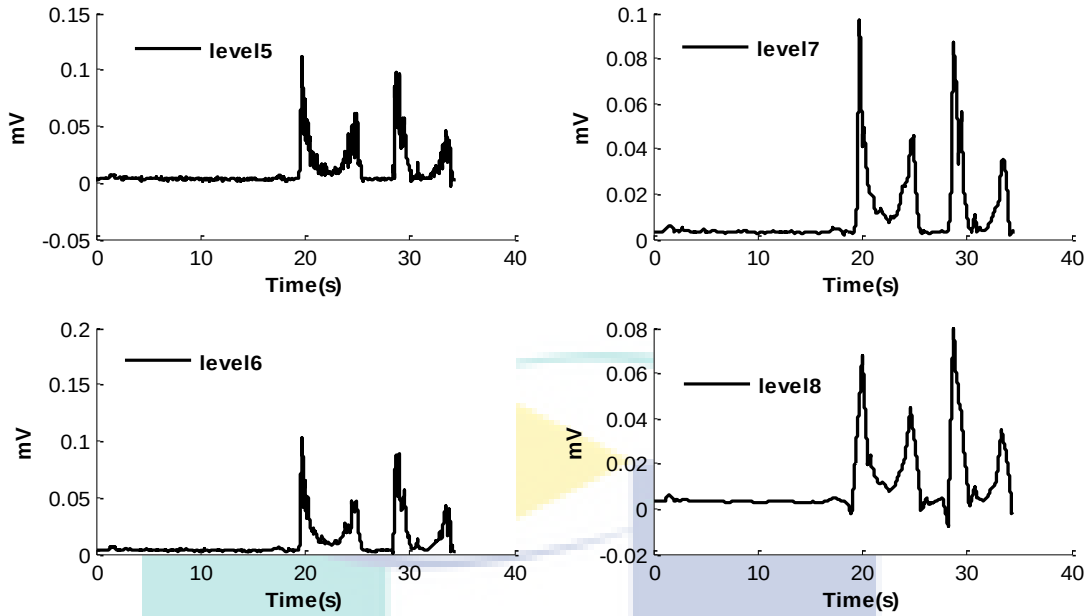

Figure 5.10. Example of the wavelet outputs at scales 5, 6, 7 and 8.

It is clear from Figure 5.10 that the wavelet output at level 5 is considered as not clean as anticipated. On the other hand, the wavelet output at level 8 has shown an undershoot in the 1st and the 3rd bursts of the filtered sEMG signal. The most suitable outputs of the wavelet outputs could be level 6 or level 7.

5.3.2 Optimum Cutoff Frequency

Once the optimum filter order is selected, an appropriate cutoff frequency has to be determined for the filter. The correlations of the original signal (rectified signal in this case) and the filtered signal at different cutoff frequency is computed and graphed along with the correlations of the original signal to the wavelet filter at different scales as illustrated in Figure 5.11. The cross point (B= 6) between the two curves is selected as the best optimum cutoff frequency as well as it is the best scale for the wavelet that the sEMG signal could be reconstructed on. Selecting a filter order above the point B, the sEMG signal is getting noisier. In contrast, when selecting a filter order below the point B, the signal will get more distorted. On the other hand, wavelet is performing the opposite idea of the Butterworth filter. When selecting a scale above the point B, the signal is more distorted and when selecting a scale below the point B the signal is noisy.

As discussed earlier in the previous chapter, from the recursive equation of the Butterworth filter, the signal output is one dimension. However, for the wavelet outputs to obtain for example a level 6 output, the computation is a multi-dimensioned process (6 dimensions). This lead to a longer computation time compared to the Butterworth computation time (Table 5.3). Therefore, using the Butterworth filter is recommended.

Table 5.3
Computation time difference between wavelet and Butterworth

Butterworth Computation Time	Wavelet Computation Time
0.002784s	0.036473s

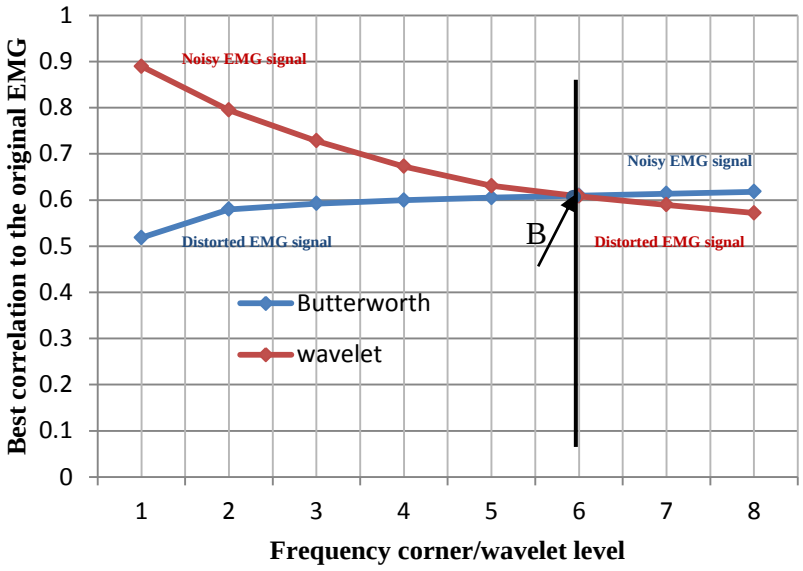

Figure 5.11. Filters output correlation with the original signal. Correlations of the original signal to both Butterworth (blue) and wavelet (red) with regards to the filter cut-off frequency and wavelet levels.

5.4 Lower Limb Muscle Activities Normalization to Motion Range

In this section, a summary of the normalized results for the selected lower limb muscles to the range of motion is presented. There are two components in the normalization procedure based on the conducted experiments: the first component is the chair protocol which is divided into two parts; one is the sit-to-stand task and the second is the stand-to-sit task. The second component is the walking task. In this section, we

present the motion of five subjects for each task, i.e., the sit-to-stand, stand-to-sit and the walking tasks. In the chair rise protocol, the RF and BF muscle activities represented by sEMG is normalized to the hip angle motion range from approximately [0-90] and [90-0] during the sit-to-stand and stand-to-sit tasks, respectively. Additional results on the normalization procedure for validation are presented in Appendix F.

During the sit-to-stand task, the subjects took shorter time (2.37s) than the stand-to-sit (2.54s) task (Table 5.3). The initial posture (hip-angle) of the subjects at chair-off was close to zero (1.2 ± 2.38^0) while at upright posture, the angle was about (86.5 ± 4.83^0) as presented in Table 5.4.

Table 5.4
Hip angles range and movement time during chair rise task.

Hip angle (Deg± SD)		**Movement time (s ± SD)**	
At chair-off	At upright posture	Sit-to-stand	Stand-to-sit
1.2 ± 2.38	86.5 ± 4.83	2.37 ± 0.0354	2.54 ± 0.0432

Throughout the following results, the sEMG signals are presented in a filtered waveform using 3rd order Butterworth filter at w_c = 6Hz. They are normalized in term of amplitude to the peak of the filtered sEMG signal with the standard deviation as mentioned before.

5.4.1 Sit to Stand Results

Sit-to-stand sEMG raw for both RF and BF muscles are normalized to the travelling distance from chair-off to stand upright is presented in this sub-suction. The subjects movements presented by the hip angle shows agreement between the five subjects with an angle travelling from approximately 0^0 (sitting on the chair) to 90^0 (standing upright posture) as shown in Figure 5.12 (left). The standard deviation error contour (shadowed area) along with the average of all angles indicates that movement is repetitive (Figure 5.12 (right)) with all subject.

The normalized RF muscle activities versus the motion range during sit to stand is presented in Figure 5.13. It is noticeable that the RF muscle activities appears to burst

prior to the starting time of the individual movement and decays in short time after the burst. The peak point of the averaged signal (0.6 mV) corresponds to about 15% from the total range of the movement. This result is consistent with the result presented in (Gross et al., 1998).

In Figure 5.14, the BF sEMG signal is normalized to the motion range; again, the muscle activity bursts before the motion of the individual starts. The peak level of the BF occurs at about 10% of the total movement range. This means that these muscles might not be contributing only to flexion and extension of the knee joint movement but also to the adduction and abduction movements.

Figure 5.15 shows the schematic representation of both RF and BF muscles activities and their maximal burst occurrence during the sit to stand range of motion. The activation of RF muscle preceded the BF activation. However, in both muscles the average of onset time is approximately ended together, but before the motion had ended.

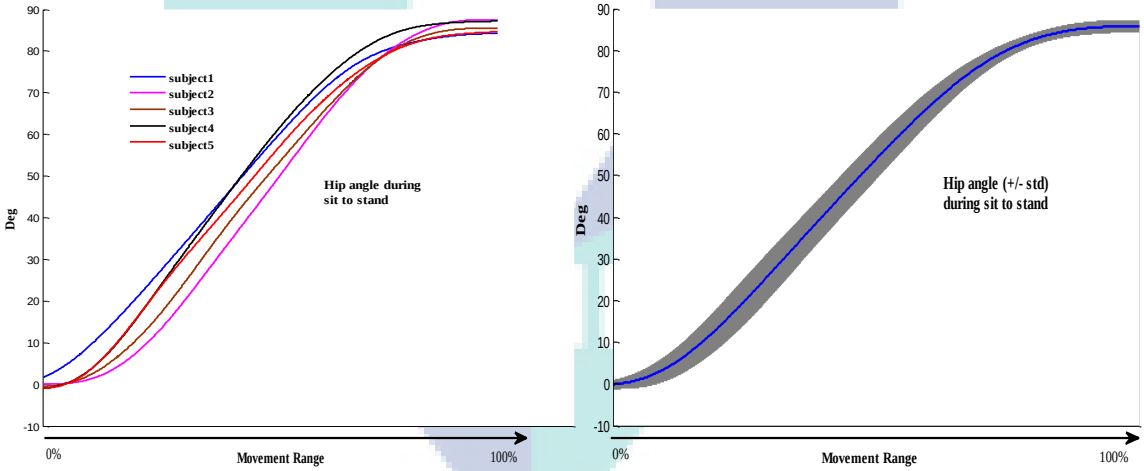

Figure 5.12. Hip angles of five subjects during performing sit to stand task (left), the thick curve is the average of the five subjects during sit to stand task and the (+/-) standard deviation error contour is presented in grey area (right).

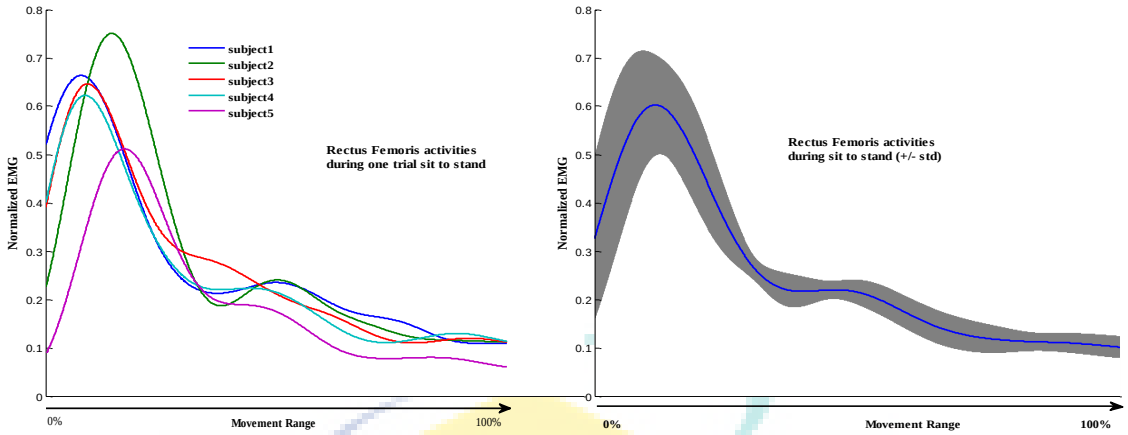

Figure 5.13. RF muscle activity of five subjects during performing sit to stand task, the thick curve is the average and the (+/-) standard deviation presented in grey area.

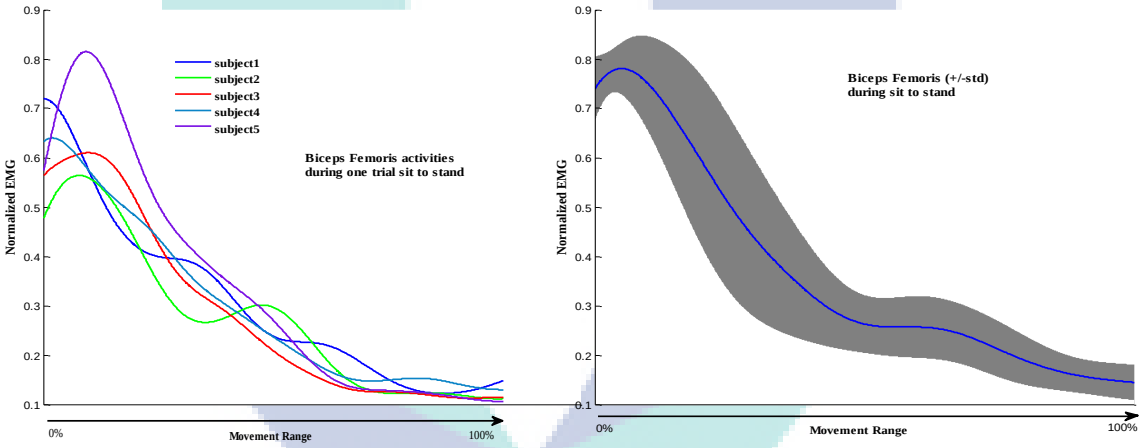

Figure 5.14. BF muscle activity of five subjects during performing sit to stand, the average and the (+/-) standard deviation presented in grey area.

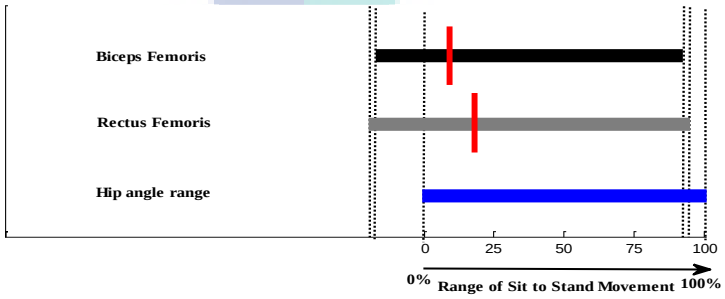

Figure 5.15. Schematic representation of the BF and RF muscle activities onset time range (Black and grey, respectively) with regards to the motion range during sit to stand task. The red vertical mark represents the maximal burst (peak) of the sEMG. The blue horizontal bar represents the hip angle movement range in percentage.

Table 5.5 details the standard deviation (STD) of the sit to stand task for the five subjects. The table shows the the STD of the sEMG with accordance to the movement range.

Table 5.5
STD during sit to stand task

Muscle	STD (0%)	STD (50%)	STD (100%)
RF	0.12	0.07	0.04
BF	0.1	0.14	0.05

5.4.2 Stand to Sit Results

In the following, we present the results of the experiment of chair rise protocol, particularly, the stand to sit task. In Figure 5.16 (a), the hip angles are presented for five subjects during performing the task of stand to sit. It is clear that the movements shows agreement between the five subjects with an angle travelling from approximately 90^0 (standing upright posture) to 0^0 (sitting on the chair). Figure 5.16 (b) shows the average of the hip angles and the (+/-) standard deviation contour of movement (shaded).

In the stand to sit task, the muscles activities i.e. the onset time is found to be within the range of the individual's motion. As presented in Figures 5.17 and 5.18, the activation of the RF and the BF muscles starts at nearly the same time with the movement of the individual. This means that there was no delay between the muscle activity and the movement time. However, the decaying time of both muscles occurred nearly at 70% form the total range of the motion.

Figure 5.19 shows a schematic representation of both RF and BF muscles activities and their maximal burst occurrence during the stand to sit with accordance to the range of motion. Both RF and BF muscles activation burst on time or in accordance to the starting point of the movement. The peak point of the the BF happened at about 45% from the range of the motion, whereas, the RF maximal point occurred later at about 55% from the total motion range. However, the onset time latency of the BF decays faster than the onset time of the RF muscle with regard to the movement.

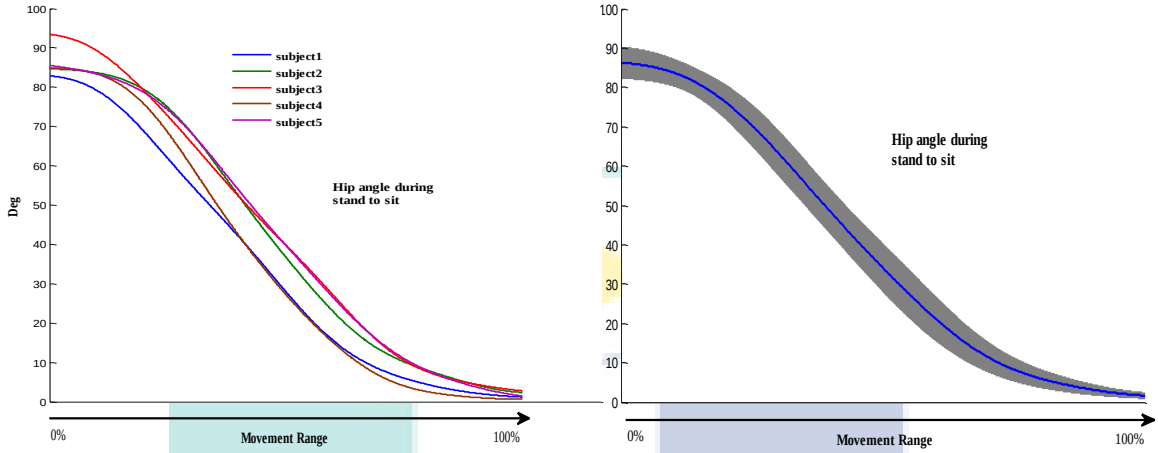

Figure 5.16. Hip angles during stand to sit. Hip angle of five subjects during stand to sit protocol (left), the average and the (+/-) standard deviation of the hip angle presented in grey area.

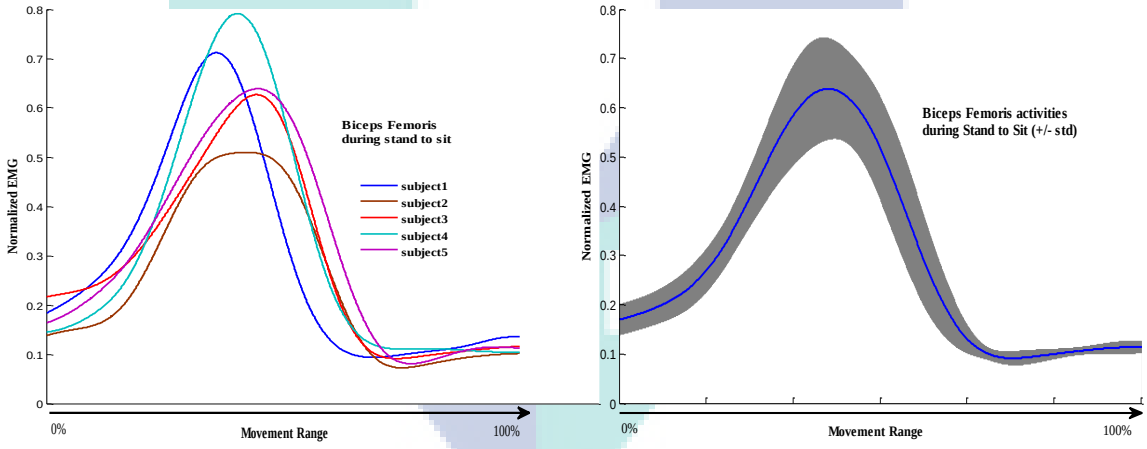

Figure 5.17. BF muscle activities normalized to the stand to sit motion range. BF muscle activity of five subjects during performing stand to sit (left), the BF activity average and the (+/-) standard deviation presented in grey area (right).

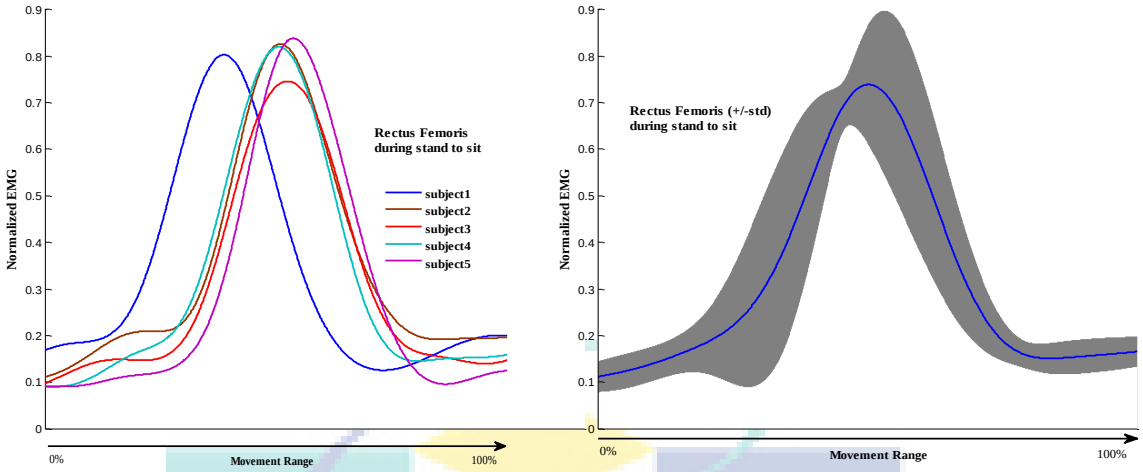

Figure 5.18. RF muscle activities normalized to the stand to sit motion range. RF muscle activity of five subjects during performing stand to sit (left figure), the RF activity average and the (+/-) standard deviation presented in grey area (right figure).

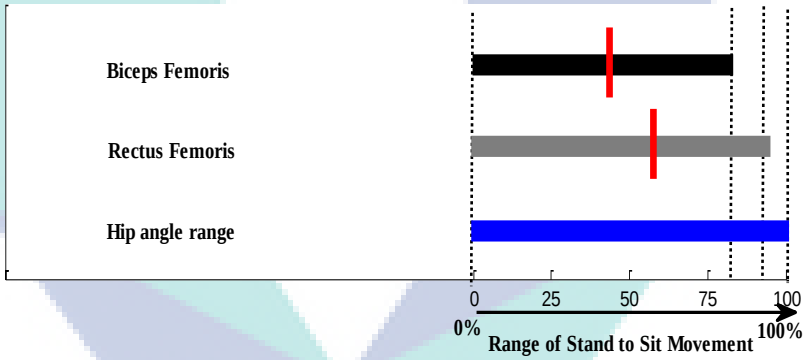

Figure 5.19. Schematic representation of the BF and RF muscle activities onset range (Black and grey, respectively) during stand to sit task. The red vertical mark represents the maximal burst of the EMG. The blue horizontal bar represents the hip angle movement range in percentage.

Table 5.6 details the standard deviation (STD) of the stand to sit task for the five subjects. The table shows the the STD of the sEMG with accordance to the movement range.

Table 5.6
STD during stand to sit task

Muscle	**STD (0%)**	**STD (50%)**	**STD (100%)**
BF	0.04	0.08	0.04
RF	0.02	0.06	0.02

5.4.3 Walking Results

In walking protocol as we discussed in the previous chapter, we have placed the surface electrodes over four muscles of the lower limb to record the sEMG. For kinematics data recordings, we have positioned two Gyro sensors, one over the hamstring muscle (the mid-thigh) and the other on the back heel side. Therefore, in the following we will presents four sEMG signals with two kinematics signals that record the angular velocity and then progressed to angles. All the following results of the four muscles are normalized in amplitude to the peak of the signal plus its standard deviation and in time as a function of the gait cycle.

Figure 5.20 shows the hip angle for one cycle for five subjects (right), an average over the over five subjects and its standard deviation is presented in the left side of Figure 5.20. Because the starting point of the movement was at the heel strike, the angle appears to begin with negative values. The range of the hip angle is summarized in Table 5.5. Same explanations and information for the knee angle presented in Figure 5.21 could be given. The motion results show excellent agreement with the literature review (Veneman et al., 2007; Sawicki, 2007 and Buchanan et al., 2005). During the stance phase the knee angle shows small variation, while in the swing phase, the angle sloped faster during toe-off to heel strike movement.

Table 5.7
Motion range and movement time during walking for one stride.

Hip angle		**Knee angle**		**Movement time (s)**
Min	**Max**	**Min**	**Max**	**One gait cycle**
-24.72±2.81	14.32±2.67	-69.82±2.69	1.03±2.18	3.27 ± 0.46

The RF muscle activities of five subjects are shown in Figure 5.22 during walking for one stride. The waveform of the RF muscle shows different behaves compare to the chair rise experiment. Consistent with the literature (Olree et al., 1996), the RF activities were the least variation (identical results). In Figure 5.23, the BF activities for five subjects were presented along with the standard deviation contour. Most variation appears to be similar in BF activity compared to the results presented by (Olree et al., 1996 and Veneman et al., 2007). The Gas muscle activities that are presented in Figure 5.24 show good agreement with literature review (Olree et al., 1996;

Veneman et al., 2007 and Sawicki, 2007). Lastly, the Sol muscle seems to contribute more in the stance phase rather than the swing phase. This is due to the fact the Sol is directly related to the ankle movement i.e. when the toe is off there is no movement in the ankle level.

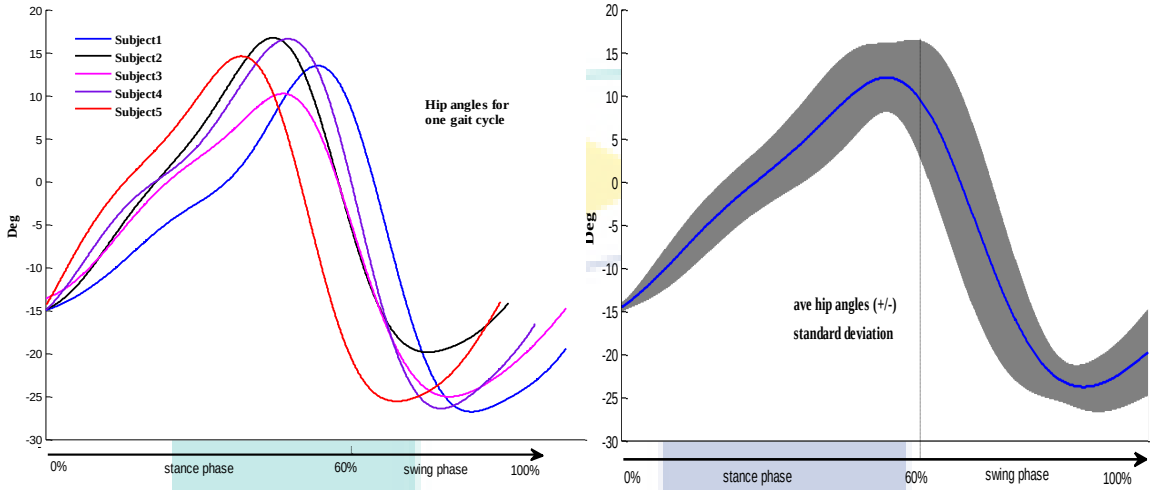

Figure 5.20. Hip angle of five subjects during walking for one stride (left), the average and the (+/-) standard deviation presented in grey area. The movement starts at heel strike of the gait and ends at heel strike.

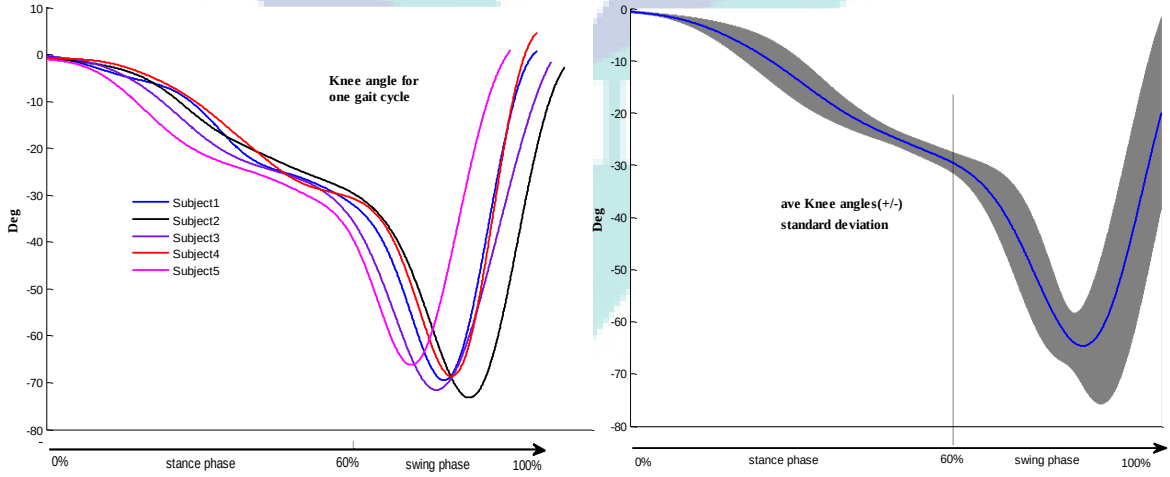

Figure 5.21. Knee angles during walking. Knee angle of five subjects during walking for one stride (left), the average and the (+/-) standard deviation presented in grey area.

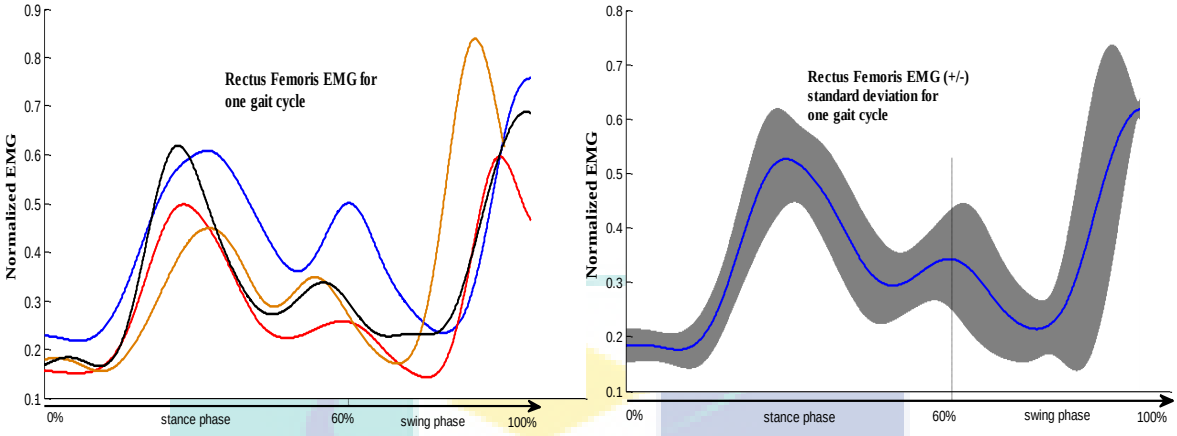

Figure 5.22. RF muscle activities normalized to one gait cycle. RF muscle activity of five subjects during walking for one gait cycle (left), the RF activity average and the (+/-) standard deviation presented in grey area (right).

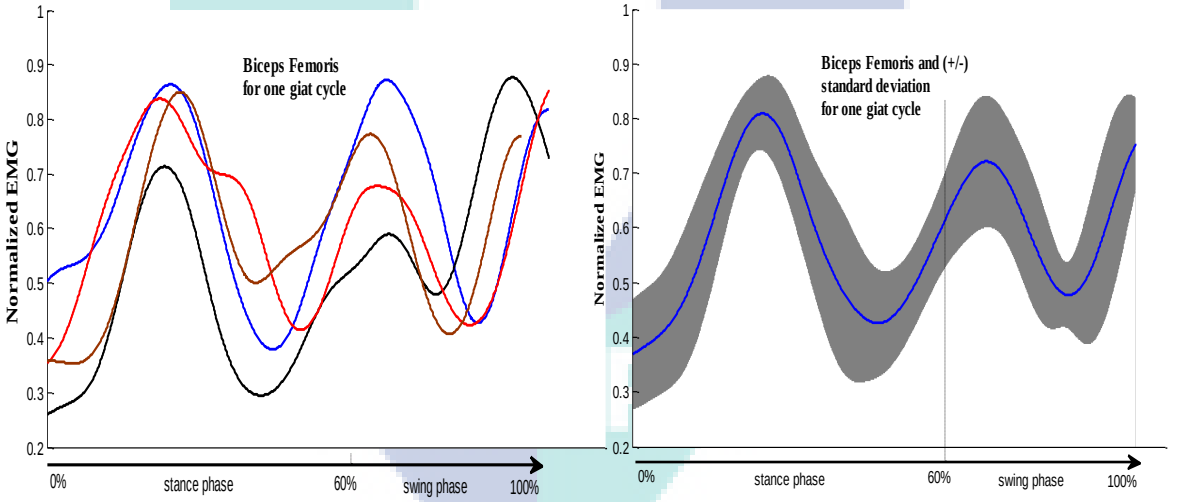

Figure 5.23. BF muscle activities normalized to one gait cycle. BF muscle activity of five subjects during walking for one gait cycle (left), the BF activity average and the (+/-) standard deviation presented in grey area (right).

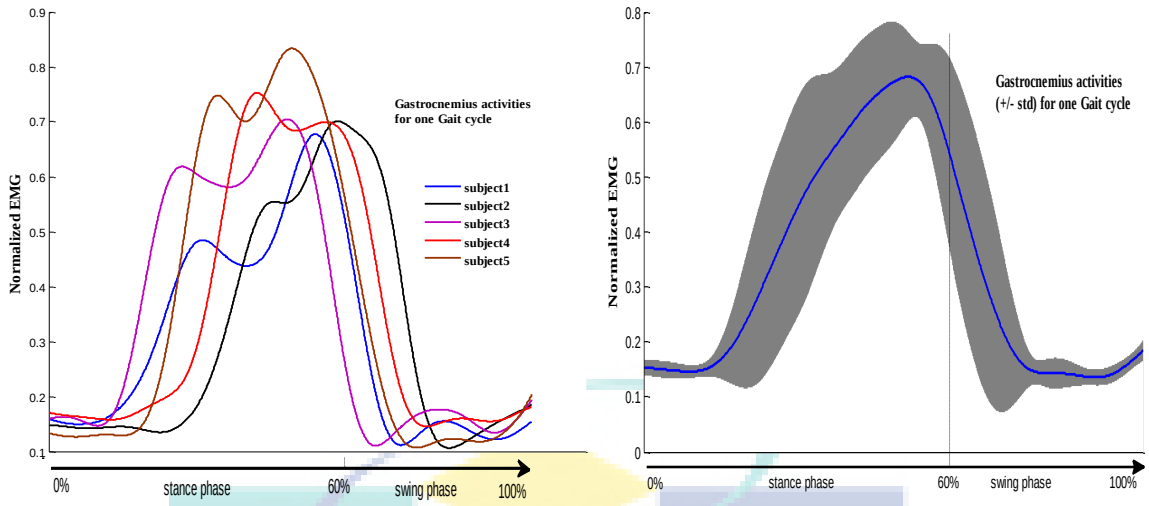

Figure 5.24. Gastrocnemius muscle activities normalized to one gait cycle. Gas muscle activity of five subjects during walking for one gait cycle (left), the Gas activity average and the (+/-) standard deviation presented in grey area (right).

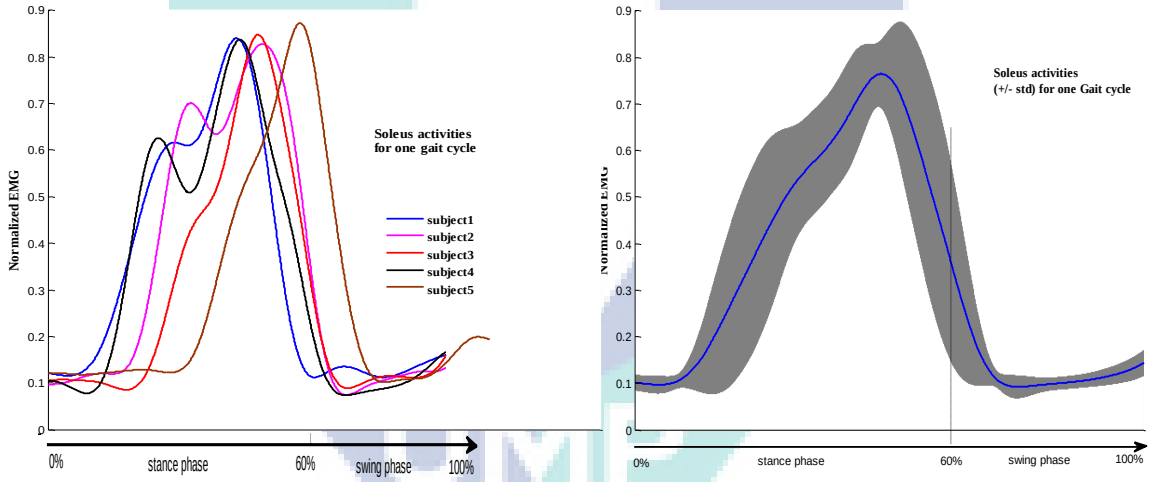

Figure 5.25. Soleus muscle activities normalized to one gait cycle. Soleus muscle activity of five subjects during walking for one gait cycle (left), the Soleus activity average and the (+/-) standard deviation presented in grey area (right).

5.5 Crosstalk /Unwanted Recordings Removal

In this section, we present the results of the modified Butterworth filter to suppress the presence of the crosstalk/unwanted measurements. Three examples are addressed, but we have abstracted the explanation only on the first example due to similar explanation in all other examples. In each example, the original signal, the filtered signal with conventional Butterworth, the filtered signal with the modified filter and also the cutoff frequency adaptation are presented.

The recorded measurements over the RF and BF muscles along with the kinematics recordings are presented in Figure 5.26. The RF recordings show six (6) bursts while the BF recordings display four (4) which corresponds to the motion of the subject during sit to stand. For more clarification, the signals could be divided into four sub-bands. The 1st and 3rd bursts in BF tend to the 1st and 2nd risings from the chair-off to upright position, whereas the 2nd and 4th bursts tend to 1st and 2nd standing to sitting on the chair position. On the other hand, in the RF recordings, the 1st and 4th correspond to the 1st and 2nd risings from the chair-off to upright position, whereas the 3nd and 6th bursts tend to 1st and 2nd standing to sitting on the chair position, while the remaining two bursts are categorized as crosstalk recordings. These activities associated with the signal of interest may lead to a miss interpretation of the signal or miss-use of the signal if it is used to control for example a prosthesis device.

From Figure 5.26, the presence of the cross-talk started after the first burst of the RF muscle when the subject achieved the first chair-off task at time about 8.4s and ended at about 12s and it was associated with the signal of interest after the second rising from the chair exhibiting in an interval time [20s to 24s]. At these periods there was no recording on the level of angular velocity (standing upright without movement). On the other hand, the BF EMG recording was at rest with accordance to the individual motion. Applying a 3rd order Butterworth filter at 6Hz cutoff frequency shows a well-smoothed output within the BF, RF and gyro signals (Figures 5.27) but it does not eliminate the crosstalk recordings contaminating on the RF muscle. When the BF is at rest and the gyro corresponds to no movement, it is of interest to bring the RF signal at this period to rest (baseline). Thus, the already smoothed baseline signal of the relevant muscle was proposed to be the desired signal at this interval for two reasons: 1) to have the same magnitude of the signal with the baseline and 2) to avoid a sharp drop from the point where the crosstalk recordings start to the baseline reference. Point A1 (Figure 5.27(a)), which is the point where the crosstalk on the RF recording starts to become activated, is projected to B1. Hence, the desired signal is the reflected signal from B1 back through the baseline within the range of the *start/end* points of the crosstalk recording as highlighted in red rectangular Figure 5.27(a). For more clear view the reader can refer to Figure 5.27(b and c).

During the two intervals when the RF exhibited extra means of recordings (crosstalk recordings), this appears to change the behaviour of the Butterworth filter. That is to vary the cutoff frequency in order to decrease the crosstalk activities adaptively leading this segment of the signal to the baseline reference (see Figure 5.28(b), black solid line). The 3rd order adaptive Butterworth filter shows agreement to drive the signal to the baseline even when the peaks of the crosstalk activities almost matching the peaks of the actual sEMG signal at time 9.5s and 20.5s with magnitudes of 0.08mV and 0.07mV, respectively. It is noticeable from Figure 5.28(b) (black solid line) that there still a spike in the second burst, this can be removed using spikes removal algorithm. Figure 5.28 (e) presents the cutoff frequency which adaptively decreases whenever applicable i.e. when the crosstalk activities contaminated the signal of interest. The cutoff frequency dropped considerably whenever the magnitude of the crosstalk is higher than the base line amplitude of the signal.

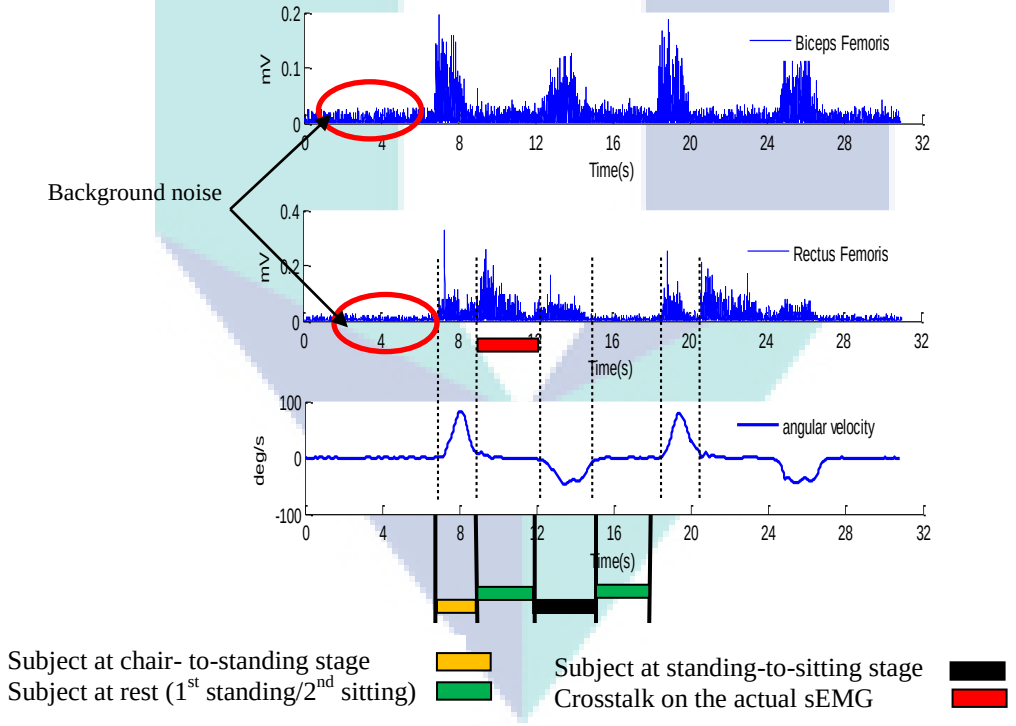

Figure 5.26. BF and RF sEMG recording with the corresponding angular velocity. (a) and (b) Example of sEMG recordings obtained from the Biceps Femoris and Rectus Femoris muscle of the volunteer during sit to stand task for two trials. (c) Angular velocity during sit to stand (The gyro was placed on the mid-thigh of the subject)

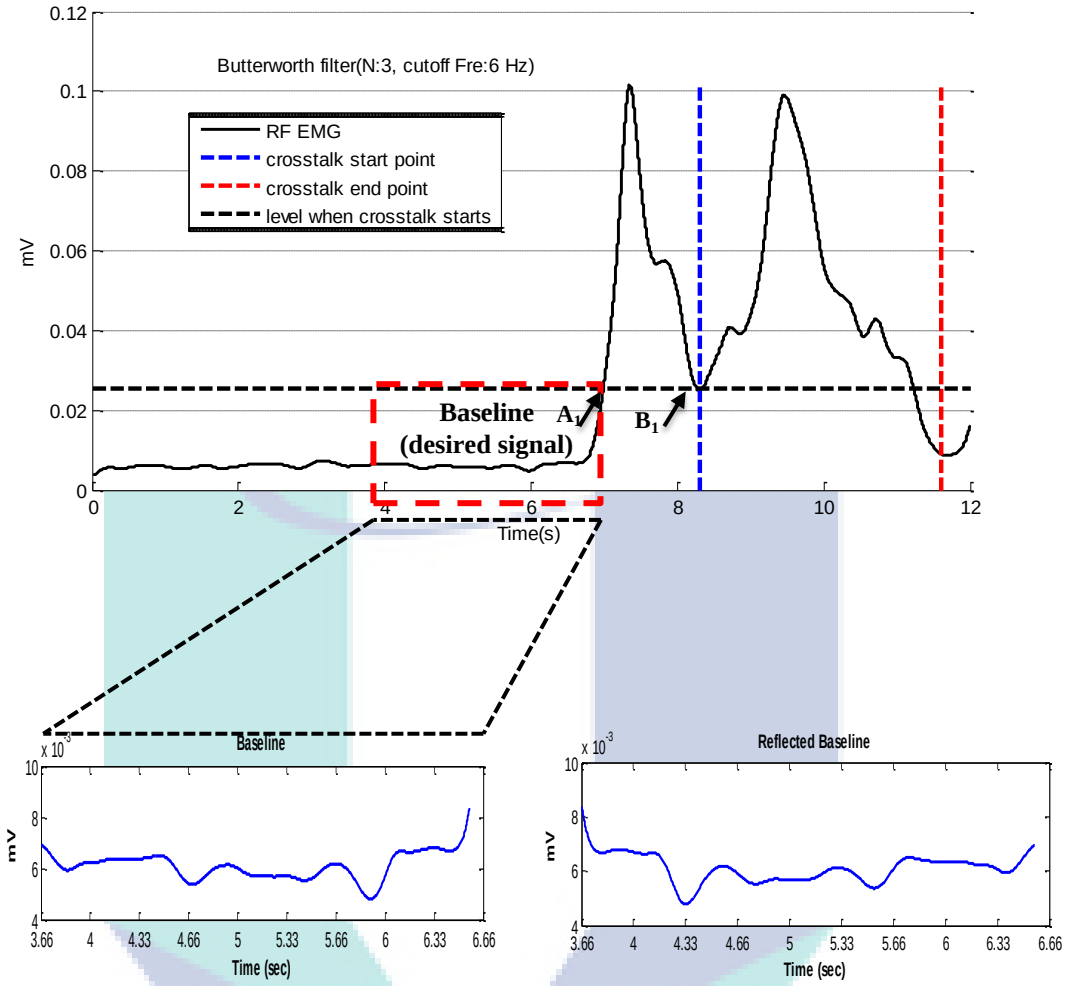

Figure 5.27. (a) Smoothed sEMG of RF muscle using 3rd order Butterworth filter and determining the crosstalk interval (approximately 8.2s -11.7s), the rectangular defined the desired baseline, the blue/red vertical lines present the start point/end point of the crosstalk recordings respectively. (b) The selected desired baseline signal expanded from (a). (c) The reflected signal in (b) to be attained by the RLS algorithm.

Further examples on the crosstalk phenomena are illustrated in Figure 29 and Figure 30. The crosstalk contamination occurred at approximately 16th second after the third burst of the RF during sit to stand task (Figure 29). Similarly, a 3rd order Butterworth filter with adaptive cut-off frequency was applied to eliminate the additional signal. It is noticeable that the latter signal is less amplitude and therefore the drop in the cutoff frequency was less accordingly from 6Hz to 5.4Hz (Figure 29 (e)). Figure 30 presents another example of the crosstalk signal contaminated on the signal of interest. In this example the additional signal tends to occur after the first burst of the muscle (8th seconds during the sit to stand task). The adaptive filter was applied and successfully suppresses the contaminated signal.

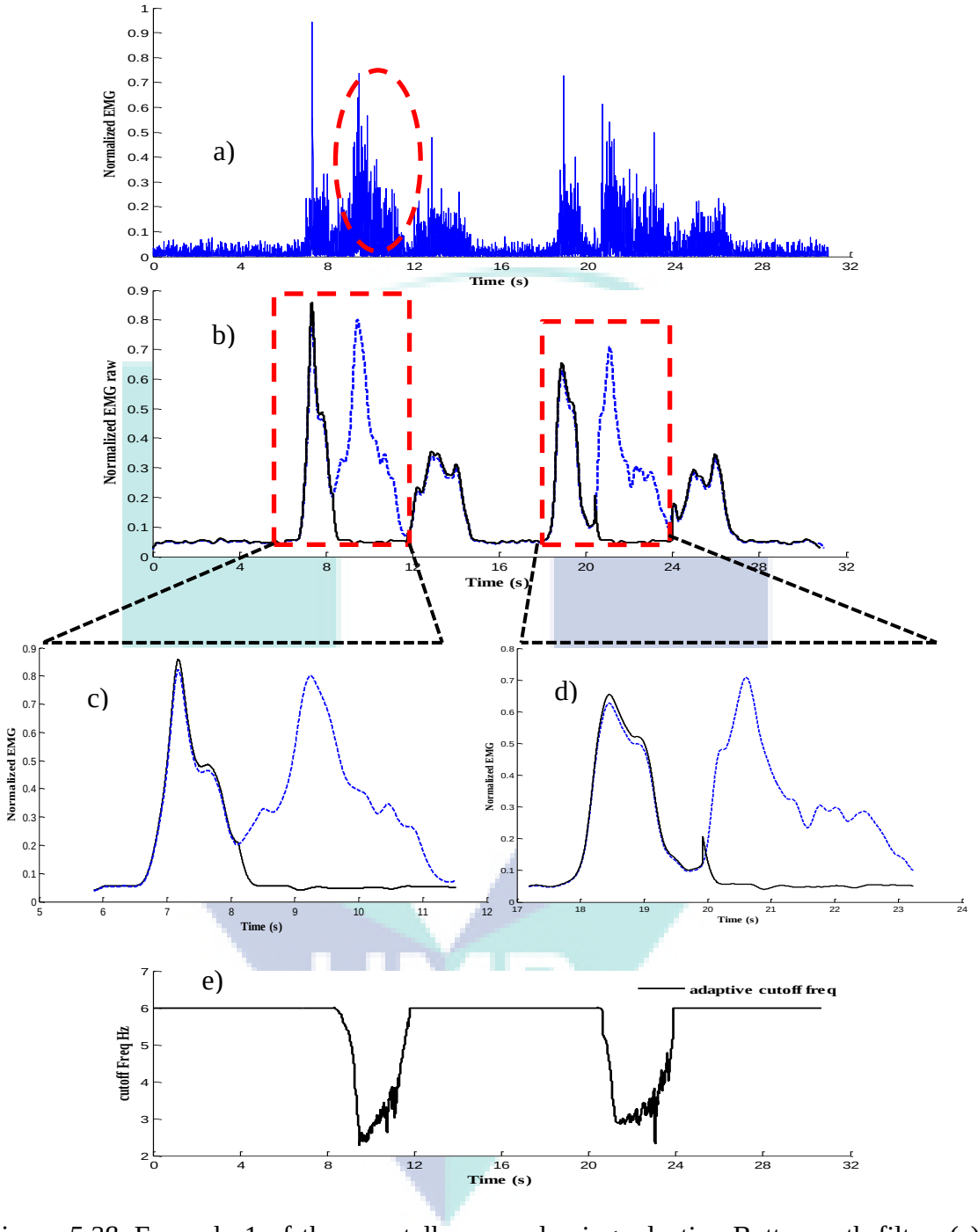

Figure 5.28. Example 1 of the crosstalk removal using adaptive Butterworth filter. (a) Cleaned sEMG of RF muscle 3rd order Butterworth filter with a cutoff frequency at 6 Hz (blue dashed line) and cleaned sEMG with crosstalk removal using adaptive Butterworth filter(black solid line). b) and c) expansions of the same recordings from (b). (d) Adaptive cut-off frequency. The frequency is fixed at 6Hz and decreases only when the crosstalk recordings presented in e).

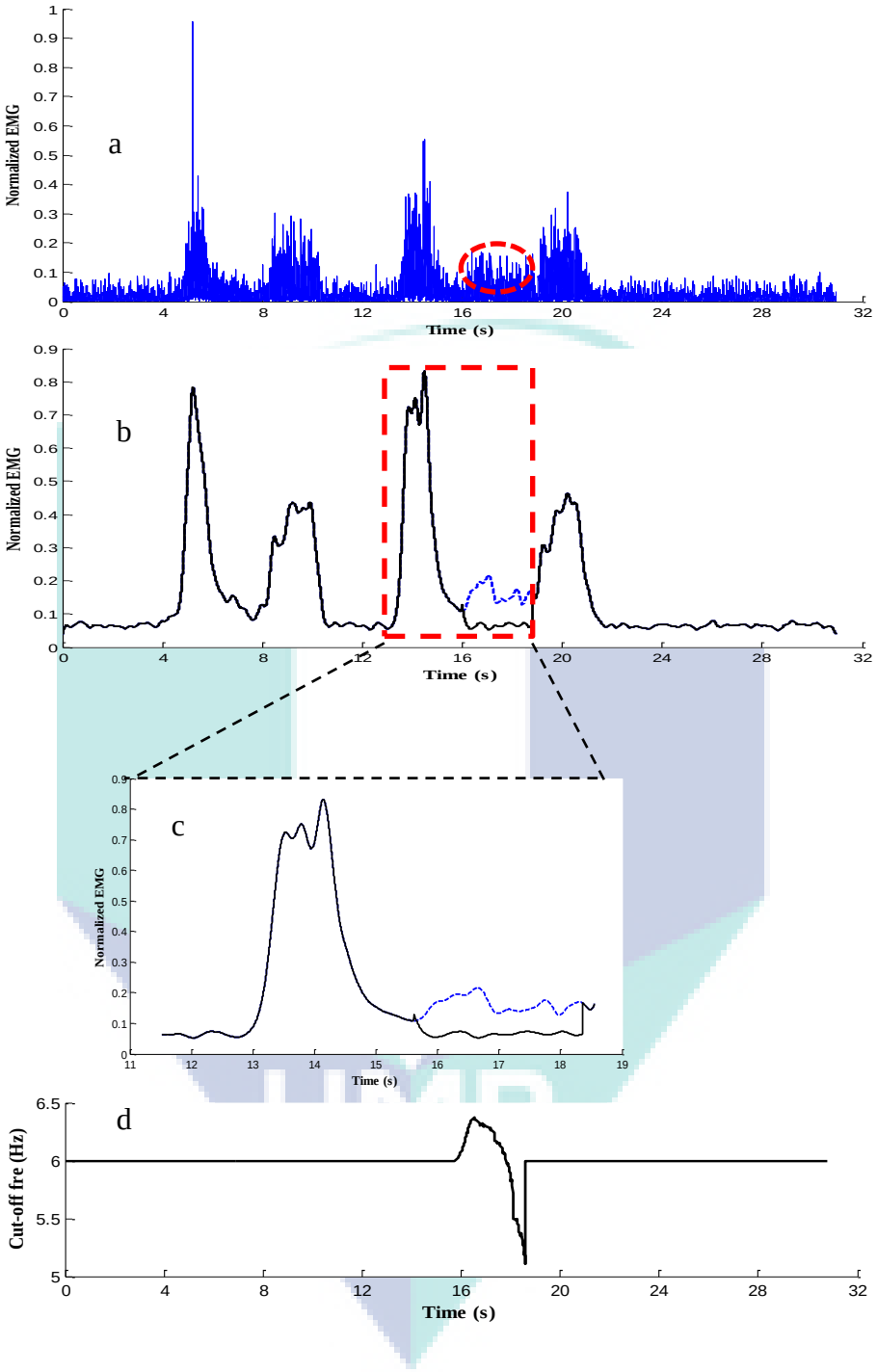

Figure 5.29. Example 2 of the crosstalk removal using adaptive Butterworth filter. (a) Cleaned sEMG of RF muscle 3rd order Butterworth filter with a cut-off frequency at 6 Hz (blue dashed line) and cleaned sEMG with crosstalk removal using adaptive Butterworth filter(black solid line). (b and c) expansions of the same recordings from (b). (d) Adaptive cut-off frequency. The frequency is fixed at 6Hz and decreases only when the crosstalk recordings presented.

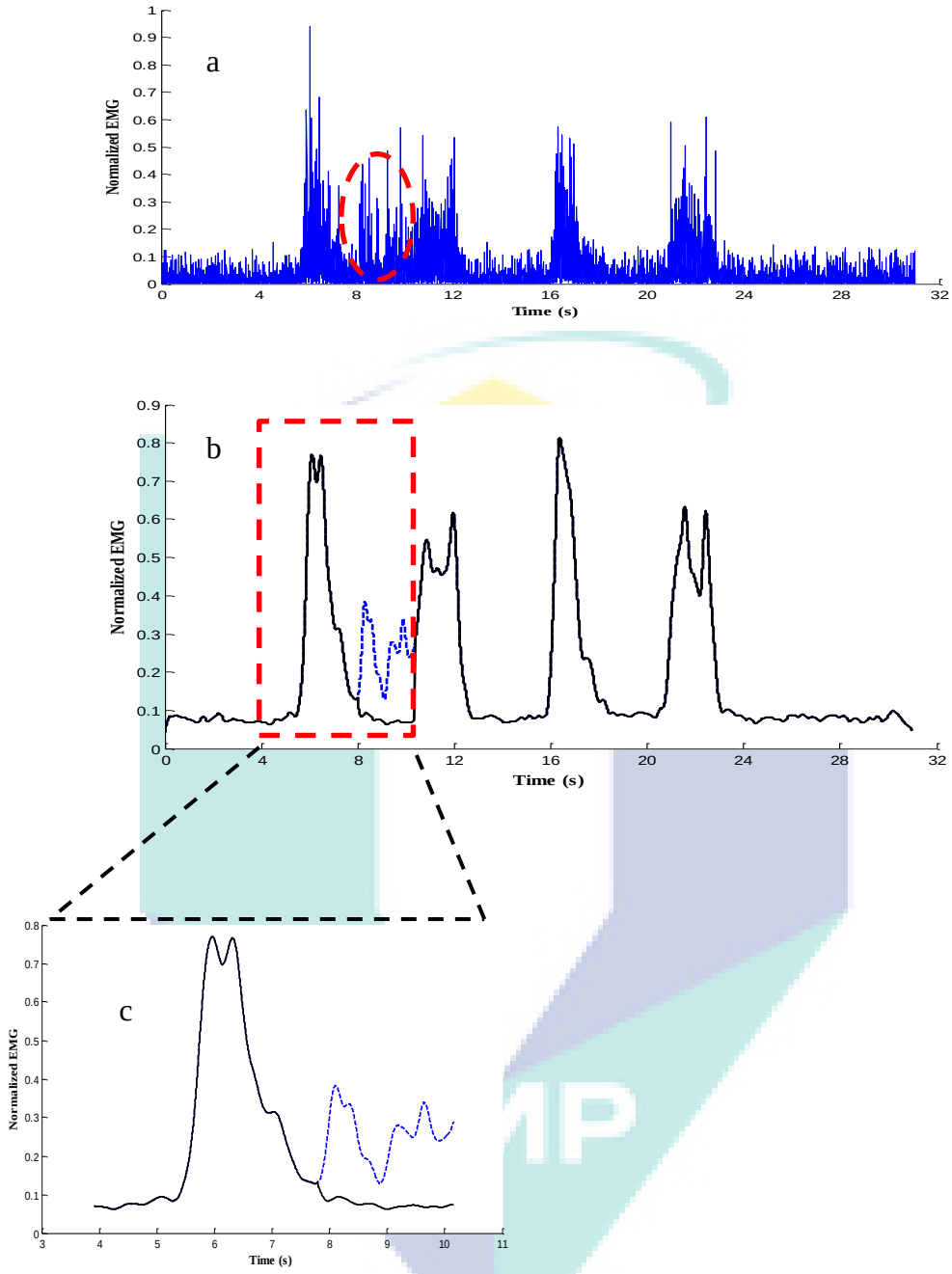

Figure 5.30. Example 3 of the crosstalk removal using adaptive Butterworth filter. (a) Cleaned sEMG of RF muscle 3rd order Butterworth filter with a cutoff frequency at 6 Hz (blue dashed line) and cleaned sEMG with crosstalk removal using adaptive Butterworth filter(black solid line). (b and c) expansions of the same recordings from (b).

From Figures 5.28, 5.29 and 5.30, it is concluded that the modified Butterworth filter successfully eliminates the un-expected recordings (crosstalk) contaminated on the sEMG signal of interest. This method is applicable in real-time procedure compare to Blind Separation Source (BSS) in which it requires offline data.

5.6 Muscle Activation Dynamics

Figure 5.31 shows an example of sEMG signal (processed until the normalization in amplitude) presented with $e(k)$ recorded over the BF during sit to stand being transformed to firstly to the neural activation $u(k)$. It can be seen that the resultant $u(k)$ almost matching the $e(k)$ with a delay time d as mentioned in equation (4.34). The $u(k)$ was then transformed to the muscle activation $a(k)$, which shows higher amplitude with slightly change in the waveform of the signal due to the nonlinearity in equation (4.36). This result is comparable with the results presented by Buchanan et al. (2004).

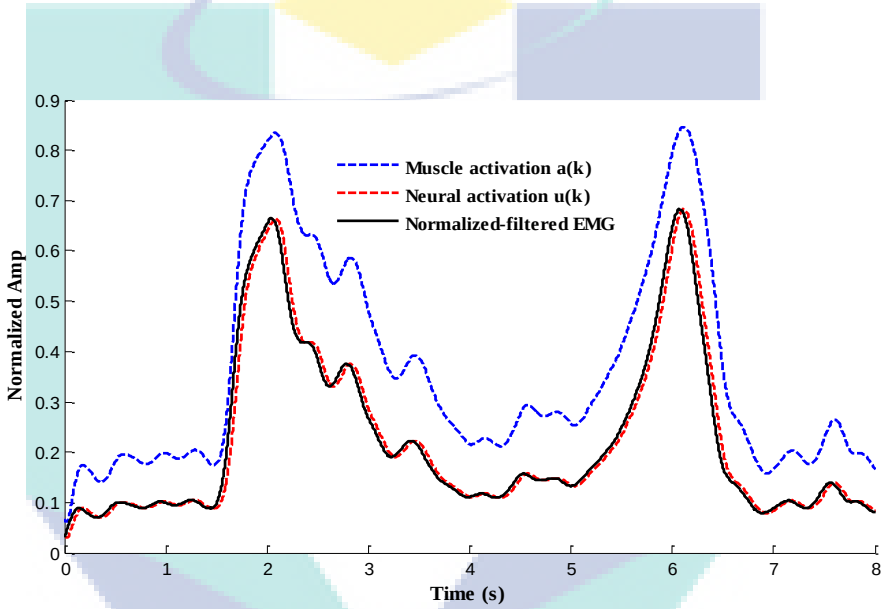

Figure 5.31. Example of the transformation of the sEMG (e(k)) to the muscle activation ($a(k)$).

In the following, we present the results of the hill's model i.e. the force generated by a specific muscle. As mentioned before, the inputs to the hill's model were 1) neural activation $a(k)$; 2) the muscle fiber length.

5.7 Hill's Model Output

The hill's force for the selected muscles is presented in this section. In the chair-rise experiment, the BF and RF are selected and the sums of the two resultant forces are used to estimate the moment in the knee joint. However, in the walking experiment, three muscles are selected we exclude the soleus muscle because this muscle contributes more to the ankle joint motion.

Figure 5.32 shows the forces during sit to stand for the BF and the RF muscles. The BF force was higher than the RF force. Initially the BF force was about 1000N while the RF force was about 500N and in short time the forces reach their maximum points (750N at about 0.4s and 1050N at about 0.3s for the RF and BF respectively). This can be explained that when the subject at chair off, he/she requires high push up forces in order to lift the whole body. The forces decay faster as the individual travels this range of motion. This means, the RF and BF muscles contribute more at the beginning of the motion.

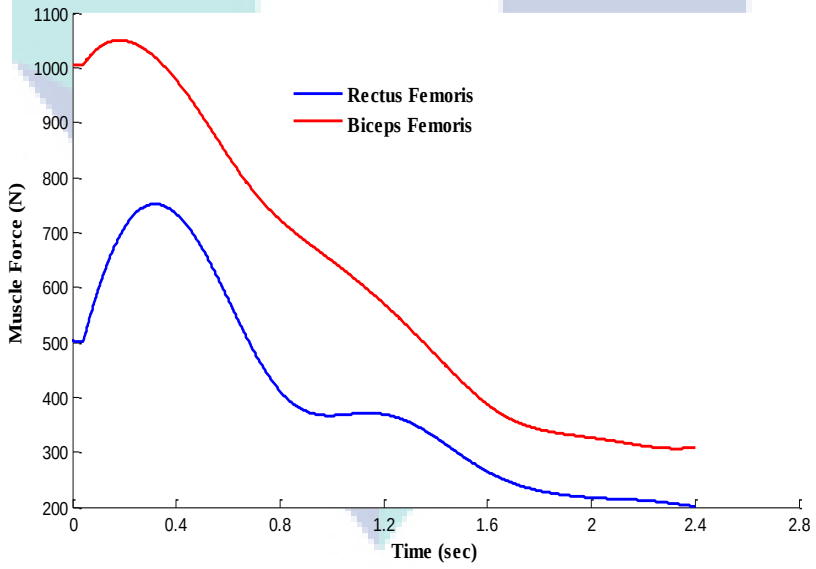

Figure 5.32. Example of the transformation of the sEMG (*e*(k)) to the muscle Force (F*a*(*k*)).

Figure 5.33 present the knee joint moment generated by the BF and RF for the sit to stand and stand to sit tasks. It is noticeable from Figure 5.33 that the maximum joint moment was about 125N.m at about 0.35s (chair-off). Whereas, in the stand to sit

task, the maximum knee joint moment (140N.m) was late at time 1.45s, this means that the muscle activities were less at the first stage of the motion and more activated when the individual almost reached the sitting position.

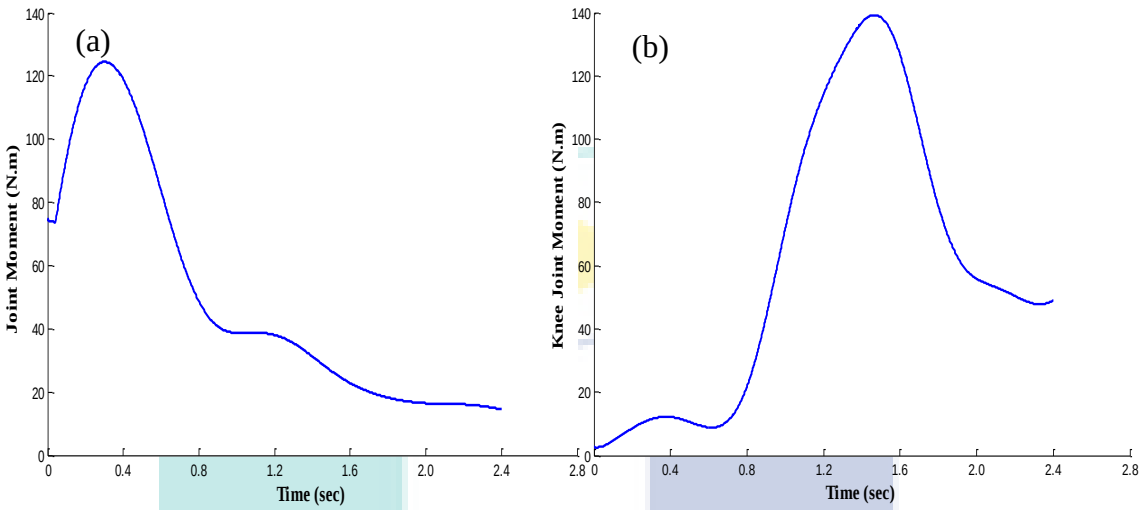

Figure 5.33. Knee joint moment generated by the RF and BF muscle during chair-rise task. (a), sit to stand (b) stand to sit.

Figure 5.34 represent the knee joint moment produced by the BF, RF and Gas muscles during one gait cycle.

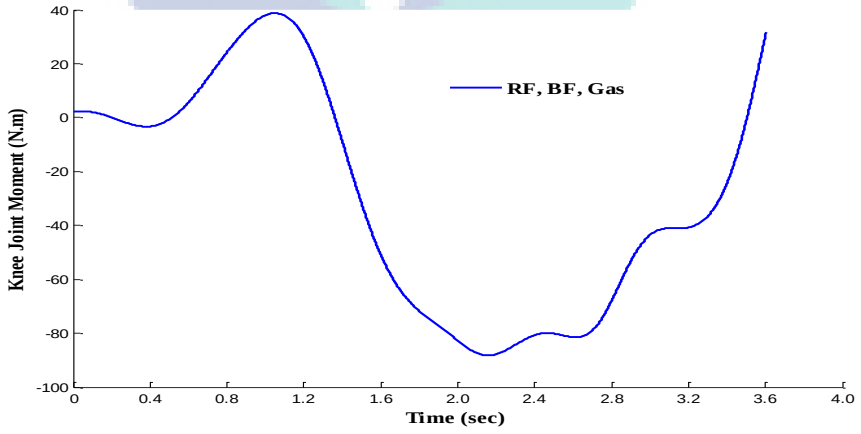

Figure 5.34. Net joint moment obtained from the BF, RF and Gas muscles during walking task for one gait cycle.

5.8 Inverse Dynamics Results

As mentioned earlier, one of the methods to calculate the net moment in a joint is to use the inverse dynamics. That is to find the joint moment based on the measured position, angular velocity and angular acceleration. From the anthropometrics data given in Table 4.5 and with the use of equations 4.47 and 4.49, the joint moment is calculated.

Figure 5.35 shows the net knee joint moment measured by the inverse dynamics and the moment produced by the RF and BF muscles activation. The measured moment form BF and RF maximum point was about 150 N.m while the moment obtained from the inverse dynamics was about 200 N.m at the beginning of the movement. This could be explained as the individual is at chair-off stage; he/she requires higher moment to lift-up the body and therefore involves more effort from the muscles. Moreover, this gives an insight understanding that the BF and RF muscles contribute more at the beginning of the motion. Noting that poor agreement in amplitude between the two moments along the sit to stand motion range and then they converge to about about 5 N.m. However, both moments possessed almost the same waveform during the motion. This is clearly indicate that taking the generated moment from the BF and RF muscles only is not sufficient to produce a full joint moment. On the other hand, during the stand to sit task (Figure 5.35 (b)), the produced moment by the BF and RF begun with minor moment (1N.m), similarly to the inverse dynamics moment where it began at about -5N.m. As the individual moved to sit down, the two moments slightly started to diverge. At sit on the chair posture, the inverse dynamics ended at maximum point of about 200N.m whereas, the muscles moment tends to decay to about 50N.m. Again this means the two muscles cannot provide the sufficient moment in order to achieve and complete the task as many other muscles are involved. One can notice also that the moment during sit to stand is opposite to the moment during the stand to sit.

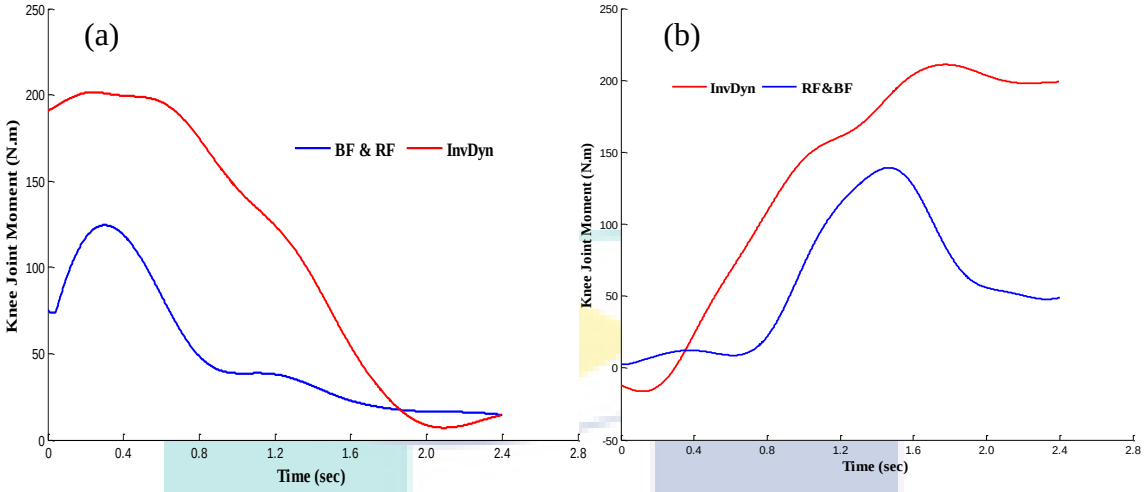

Figure 5.35. Inverse dynamic of the knee joint moment and the moment produced by the BF and RF muscles during chair-rise: (a) sit to stand, (b) sit to stand task.

Figure 5.36 presents the knee joint moment calculated through the inverse dynamics method and the moment obtained from the selected muscles during walking for one stride. The inverse dynamic moment level initially was about 55 N.m which maybe resulted from the reaction forces acting on the knee joint during the stance phase. In the swing phase and while the knee joint is flexing, the moment has dropped faster and back to increase while the knee begun to extent. On the other hand, the knee joint moment resulted from the selected muscles (BF, RF and Gas) shows different waveform from the inverse dynamic joint moment. It begun almost at 2 N.m as the muscles were not activated and then a maximum point occurred (40 N.m) during the single limb support. While the knee flexed, the muscles moment experienced negative values with maximum point (90N.m), however during the swing phase, the knee joint moment increased.

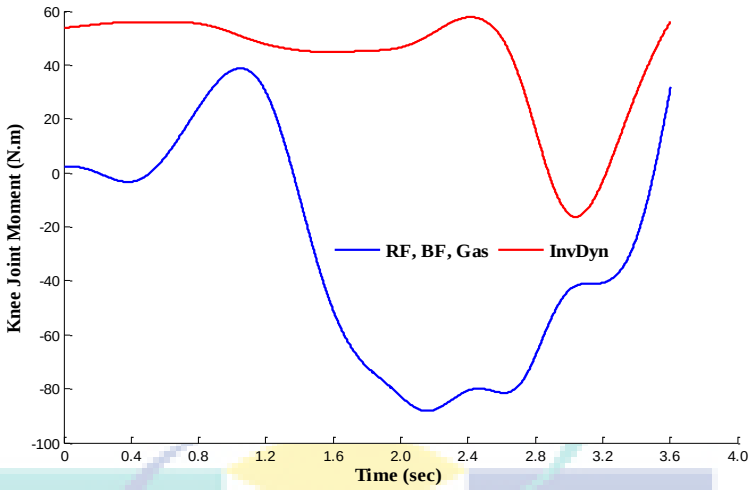

Figure 5.36. Inverse dynamic joint moment and the selected muscles during walking task for one gait cycle.

5.8.1 Predicted Joint Moment

As mentioned earlier, the LS based Levenbarg-Marquart algorithm is used to optimize the moment generated by the muscle to the net joint moment estimated by the inverse dynamics.

The root mean square difference and the correlation coefficients are used to quantify the accuracy of optimized joint moment.

$$RMSE = \sqrt{\frac{(M_k^{inv} - \hat{M}_k)^T (M_k^{inv} - \hat{M}_k)}{N}}\ ,$$

$$R^2 = \frac{cov(M_k^{inv}, \hat{M}_k)}{\sigma_{M_k^{inv}} \sigma_{\hat{M}_k}} \qquad (5.1)$$

where, M_k^{inv} and $\hat{M}_k$ are N x 1 vectors with their entries represented by the net joint moment obtained from the inverse dynamics and the estimated moment from the muscles.

Figure 5.37 (a) and (b) depicts the modeled moment obtained from the muscles and the measured using the inverse dynamic (i.e. measured). The model shows good agreement with the calculated moment during the chair-rise. The optimized model

during the walking task for one gait cycle shows less matching with the moment using the inverse dynamics method (Figure 5.38). This might be because the walking task incorporates many muscles.

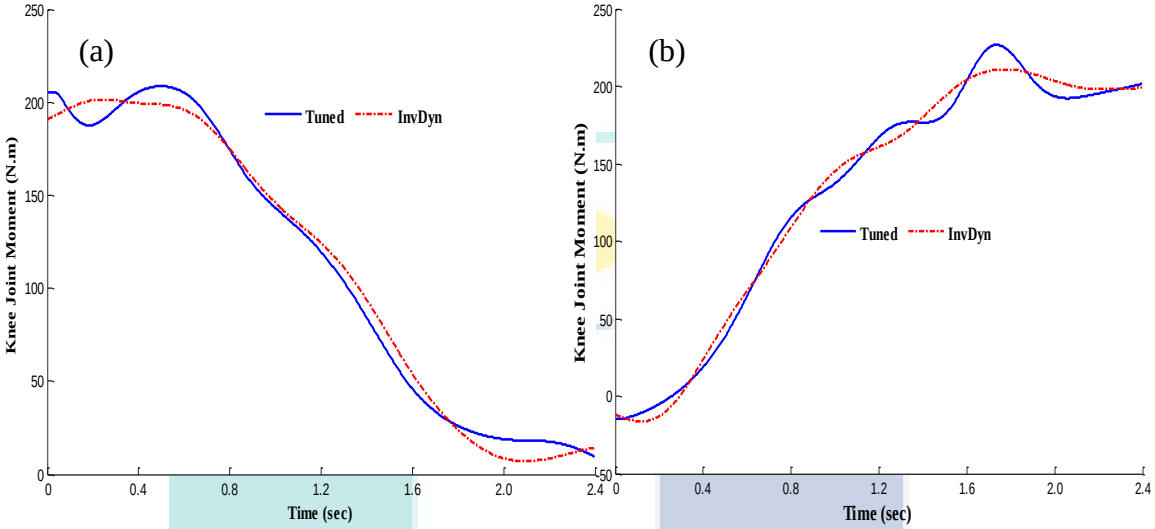

Figure 5.37. Inverse dynamic net joint moment and the tuned joint moment during chair-rise. (a) Sit to stand, (b) stand to sit task

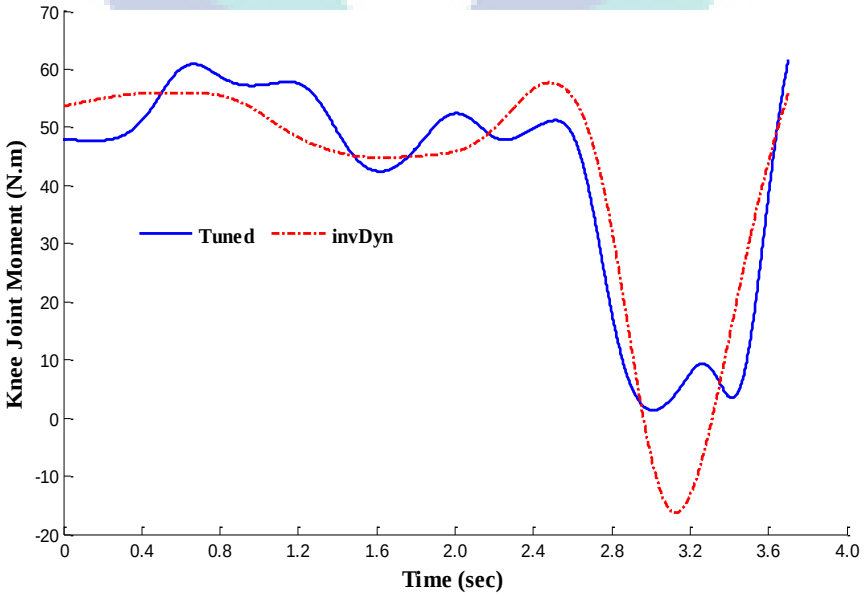

Figure 5.38. Inverse dynamic net joint moment and the tuned joint moment during walking for one gait cycle.

Table 5.8 listed the estimated coefficients of the forces generated by the BF, RF and Gas muscles. As mentioned in the previous chapter, K_3—K_5 are calculated from the data listed in table 4.3 based on literature review. The remaining coefficients are $K_1$and K_2, which includes the constants C_0, C_1 and C_2 (see appendix B) of the equation 4.46.
It is noticeable from Table 5.8 that during the chair-rise task (sit to stand and stand to sit), the coefficients K_1 and K_2 are close to each other for both the BF and the RF muscles. Therefore, one can select only one coefficient rather than two coefficients.

Table 5.8
Identified Parameters based LS method

Coeffs / Tasks	Biceps Femoris Muscle				
	K_1	**K_2**	**K_3**	**K_4**	**K_5**
Sit To Stand	-1.6456	4.2437	0.3018	0.0013	-0.1514
Stand To Sit	-1.5589	2.9722	0.3018	0.0013	-0.1514
Walking	17.2398	-21.7598	0.3018	0.0013	-0.1514

Coeff / Tasks	Rectus Femoris Muscle				
	K_1	**K_2**	**K_3**	**K_4**	**K_5**
Sit To Stand	-11.3109	19.6632	0.1496	$7.6.10^{-4}$	-0.126
Stand To Sit	-10.9754	16.9391	0.1496	$7.6.10^{-4}$	-0.126
Walking	6.0555	-11.5828	0.1496	$7.6.10^{-4}$	-0.126

Coeff / Task	Gastrocnemius Muscle				
	K_1	**K_2**	**K_3**	**K_4**	**K_5**
Walking	-1.5940	1.7187	0.10	0.001	-0.0675

Table 5.9 presents the accuracy of the predicted model for both experiments in term of correlation and root mean squared error (RMSE).

For the sit to stand and the stand to sit experiment, the optimized model showed good agreement with the inverse dynamic model (R^2 varies from 0.9952-0.9963). The RMSE were relatively low varying between a minimum of 6.7763 and a maximum of

7.4161. However, during the walking task, the predicted model showed less agreement with the inverse dynamic model with R^2 of 0.9139 and an RSME of 8.3172.

Table 5.9
R^2 *and RMSE values*

Accuracy / Task	R^2	RMSE
Sit To stand	0.9952	7.4165
Stand To Sit	0.9963	6.7763
Walking	0.9139	8.3172

5.8.2 Real Time Implementation

As mentioned in chapter 3, a real time system was developed in order to validate the proposed method. Figure 5.39 illustrates the open loop model output (angle scenario) during chair rise task. A validation of the model was made by using a gyro sensor to measure the angle of a one link exoskeleton and the actual movement of the individual. Results shows good matching at the beginning of the motion, slight difference occurs when the individual at about the upright posture. This is because the model is an open loop system. Yet the exoskeleton motion could track the individual movement sufficiently.

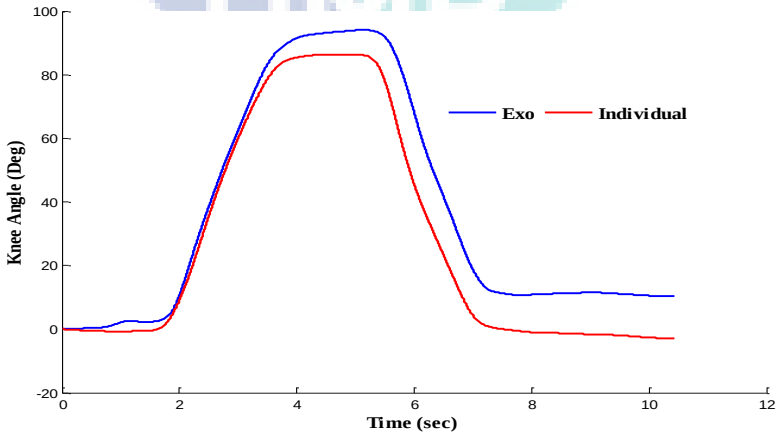

Figure 5.39. Knee angles of the individual compared with angle of the exoskeleton during chair-rise task.

5.9 Summary

To summarize this chapter, the results of the proposed methodology are presented. The recorded sEMG and the kinematics data were first presented in order to clarify the signals defect and the amount of the noises in them. It was important to remove the DC offset in both signals as it certainly conceal the rising and falling time in sEMG and it results in un-correct if further processing of the kinematics data is performed. The second important concern was to analyze the effect of the Butterworth filter on the amplitude of the sEMG signal as the rising/falling time of the signal. The presence of the overlapped crosstalk/unwanted measurements was determined using the onset/offset time of both the sEMG and the kinematics data. Modified Butterworth filter based RLS algorithm was developed to eliminate the existed crosstalk/unwanted measurements. To better understand the contribution of a muscle to the individual's motion, the sEMG signals were normalized with the regards to the motion range in both experiments (chair-rise and walking). Hill's muscle model was implemented to obtain the forces generated by the muscles. Further process was to calculate the joint moments produced by the muscle forces and compare these results with the obtained from the inverse dynamics. Lastly, the real time implementation results were presented in order to validate the proposed method.

CHAPTER 6

CONCLUSIONS AND FUTURE WORK

6.1 Introduction

The overall purpose of this thesis was to examine some of the lower limb group muscles activities measured by means of the surface electromyography in order to be full in use for exoskeleton sEMG-based control.

Capturing sEMG signals along with motion data was the core of the experiments. The sEMG data were acquired from two muscles of the lower limb during chair-rise task while in the walking task, four muscles were acquired. Gyroscopes sensors were used to capture the motion of the heel (knee flexion) and the hip motion during walking. Even though, the experiments setup i.e. acquiring the sEMG signals were according to some of the standard and recommendations, these signals were not guaranteed for the use in controlling assistive devices in order to obtain safe human machine interaction.

6.2 Summary of the Research

Four objectives were identified in this study as the following:

i. To design an optimum digital filter that cleans the noises in surface electromyography signals. Results showed that unwise selecting the filter's

parameters (i.e. the filter order and the cutoff frequency) undershoot the signal and may delay the onset time of the signal. For instance, taking a cutoff frequency of 2Hz with the filter's order from [1-7] undershoot the signal with all orders expect the 1st order in which it delayed the onset time of the signal. Whereas, when taking a cutoff of 6Hz, the outputs of the filter showed no difference between them with close similarity in amplitude apart from the first order output in which the result appears in a rippled waveform. The 3rd order with cutoff frequency of 6Hz appeared to be the average of all outputs. Therefore, in this study we accept a 3rd order Butterworth filter with cutoff frequency of 6Hz as the optimum filter (chapter5, section 5.3).

ii. To detect and eliminate the existence of the unwanted/crosstalk recordings from the signal of interest. The proposed method (detecting and comparing the onset/offset of both kinematics and sEMG) had the ability to determine the presence of the overlapped crosstalk measurements on the signal of interest. As these recording needs to be eliminated, the modified Butterworth filter successfully eliminated and reduced the crosstalk measurements by adaptively decreasing the cutoff frequency with accordance the contaminated crosstalk timing (chapter 5, section 5.5).

iii. To develop a model based HMM in order to relate the muscle activities with joint moment. On the other hand, the inverse dynamics model for both experiments protocol was developed to obtain the net joint moment to be compared with the joint moment obtained from the muscles. Accepted results between the two joint moments in term of waveform during chair-rise experiment while in the walking task, the waveform of was different. To attain a complete knee joint moment, the LS based optimization method showed good results to predict the knee joint moment produced by the muscles with good accuracy

iv. To implement the algorithm into a real time system as a preliminary application to an exoskeleton system. A full real time system was developed to include all above objectives in order to predict the knee joint moment and to track the motion of the individual. The system was tested on single link exoskeleton robot for sit to stand task. Even though the system is an open loop, it showed good tracking with the individual's motion.

6.3 Research Contribution

The contributions in this study appears in analyzing the sEMG in depth in term of filtering i.e. the design of the optimal filter along with the adaptive filter that removes the unwanted/crosstalk recordings for safety purposes. The process of obtaining the force generated by the muscles (Hill model-based) was also studied and transformed to the joint moment.

A real time algorithm was developed to record, filter, remove the unwanted measurements, normalize and transform the sEMG to the joint moment. Validation of the algorithm is also provided by implementing it in.

6.4 Future Work

In the future work, it is suggested to record and analyze other major muscles of the lower limb from healthy, adults and patients in order to evaluate the difference between them. Even though it is hard to stream multi-channels at a time, it is recommended to record every time two channels with the corresponding motion data. Using the methodology in this study will give each experiment an insight of the sEMG-motion pattern. With the help of getting the net moment using the inverse dynamic, one can predict the moment of the remaining muscles.

6.5 Recommendation

i. We recommend furthering this research by implementing the system in a developed real-time operating system such as QNX Neutrino, Linux operating system or xPc target using Matlab/Simulink software rather than using Windows as it can delay the execution time.
ii. Using more advanced motion sensor such as Inertial Measurement Unit (IMU) is crucial in order to avoid accumulated errors while calculating other physical parameters.
iii. Conducting the experiment on the treadmill has valuable benefits in 1) controlling the speed of the subjects during walking and 2) avoiding the

Bluetooth communication failure due to the distance between control station and the user while walking for instance.

iv. Further investigation on the Hill's Muscle Model (HMM) is most recommended.

v. Real time parameters estimation of the forces generated by the muscle is recommended.

UMP

REFERENCE

Aguirre-Ollinger, G., Colgate, J. E., Peshkin, M. A. and Goswami, A. (2007). Active-impedance control of a lower-limb assistive exoskeleton. *IEEE 10th International Conference on Rehabilitation Robotics,* pp. 188-195.

Artemiadis, P. K. and Kyriakopoulos, K. J. (2008) Estimating arm motion and force using EMG signals: On the control of exoskeletons. *IEEE/RSJ International Conference on Intelligent Robots and System*, pp. 279-284.

Barnes, C. (1991). *Disabled people in Britain and discrimination: A case for anti-discrimination legislation*. C. Hurst & Co. Publishers.

Blanco-Velasco, M., Cruz-Roldán, F., Moreno-Martínez, E., Godino-Llorente, J. I. and Barner, K. E. (2008). Embedded filter bank-based algorithm for ECG compression. *Signal Processing*, *88*(6), 1402-1412.

Blanco-Velasco, M., Weng, B., and Barner, K. E. (2008). ECG signal denoising and baseline wander correction based on the empirical mode decomposition. *Computers in biology and medicine*, *38*(1), 1-13.

Bogue, R. (2009). Exoskeletons and robotic prosthetics: a review of recent developments. *Industrial Robot: An International Journal*, *36*(5), 421-427.

Buchanan, T. S., Lloyd, D. G., Manal, K. and Besier, T. F. (2004). Neuromusculoskeletal modeling: estimation of muscle forces and joint moments and movements from measurements of neural command. *Journal of applied biomechanics*, *20*(4), 367.

Buchanan, T. S., Lloyd, D. G., Manal, K. and Besier, T. F. (2005). Estimation of muscle forces and joint moments using a forward-inverse dynamics model. *Medicine and Science in Sports and exercise*, *37*(11), 1911.

Burden, A. M., Trew, M. and Baltzopoulos, V. (2003). Normalisation of gait EMGs: a re-examination. *Journal of Electromyography and Kinesiology*, *13*(6), 519-532.

Burgar, C. G., Lum, P. S., Shor, P. C. and Van der Loos, H. M. (2000). Development of robots for rehabilitation therapy: the Palo Alto VA/Stanford experience. *Journal of rehabilitation research and development*, *37*(6), 663-674.

Clifford, D. G, (2009). Blind Source Separation (BSS) [Computer Program]. Available at http://stuff.mit.edu/~gari/CODE/BSS (Accessed 12/08/2013)

Conforto, S., D'Alessio, T. and Pignatelli, S. (1999). Optimal rejection of movement artefacts from myoelectric signals by means of a wavelet filtering procedure. *Journal of Electromyography and Kinesiology*, *9*(1), 47-57.

Cooper, R. A., Ohnabe, H. and Hobson, D. A. (2006). *An introduction to rehabilitation engineering*. CRC Press.

De Luca, C. J., Gilmore, L. D., Kuznetsov, M., and Roy, S. H. (2010). Filtering the surface EMG signal: Movement artifact and baseline noise contamination. *Journal of biomechanics*, *43*(8), 1573-1579.

De Luca, C. J., Gilmore, L. D., Kuznetsov, M. and Roy, S. H. (2010). Filtering the surface EMG signal: Movement artifact and baseline noise contamination. *Journal of Biomechanics*, *43*(8), 1573-1579.

Dehail, P., Bestaven, E., Muller, F., Mallet, A., Robert, B., Bourdel-Marchasson, I. and Petit, J. (2007). Kinematic and electromyographic analysis of rising from a chair during a "Sit-to-Walk" task in elderly subjects: role of strength. *Clinical Biomechanics*, *22*(10), 1096-1103.

Dellon, B. and Matsuoka, Y. (2007). Prosthetics, exoskeletons, and rehabilitation. *IEEE Robotics and Automation magazine*, *14*(1), 30.

Dietz, V., Colombo, G. and Müller, R. (2004). Single joint perturbation during gait: neuronal control of movement trajectory. *Experimental brain research*, *158*(3), 308-316.

Digiovine C, Hobson DA, Cooper R.A. 2007. Clinical practice of rehabilitation engineering. *An introduction to rehabilitation engineering*. pp. 19-45.

Ding, Q., Zhao, X., Xiong, A. and Han, J. (2011). A novel motion estimate method of human joint with EMG-driven model. *IEEE 5th International Conference on Bioinformatics and Biomedical Engineering*, pp. 1-5.

Disselhorst-Klug, C., Schmitz-Rode, T., and Rau, G. (2009). Surface electromyography and muscle force: limits in sEMG–force relationship and new approaches for applications. *Clinical Biomechanics*, *24*(3), 225-235.

Emken, J. L., and Reinkensmeyer, D. J. (2005). Robot-enhanced motor learning: accelerating internal model formation during locomotion by transient dynamic amplification. *IEEE Transactions on Neural Systems and Rehabilitation Engineering*, *13*(1), 33-39.

Englehart, K., Hudgin, B., and Parker, P. A. (2001). A wavelet-based continuous classification scheme for multifunction myoelectric control. *IEEE Transactions on Biomedical Engineering*, 48(3), 302-311

Farina, D., Arendt-Nielsen, L., Merletti, R., Indino, B., and Graven-Nielsen, T. (2003). Selectivity of spatial filters for surface EMG detection from the tibialis anterior muscle. *IEEE Transactions on Biomedical Engineering*, *50*(3), 354-364.

Farina, D., Févotte, C., Doncarli, C., and Merletti, R. (2004). Blind separation of linear instantaneous mixtures of nonstationary surface myoelectric signals. *IEEE Transactions on Biomedical Engineering*, *51*(9), 1555-1567.

Farina, D., Févotte, C., Doncarli, C., and Merletti, R. (2004). Blind separation of linear instantaneous mixtures of nonstationary surface myoelectric signals. *IEEE Transactions on Biomedical Engineering* , *51*(9), 1555-1567.

Fleischer, C., and Hommel, G. (2007). Calibration of an EMG-Based Body Model with six Muscles to control a Leg Exoskeleton. *IEEE International Conference on Robotics and Automation 2007*, pp. 2514-2519.

Fleischer, C., and Hommel, G. (2008). A human--exoskeleton interface utilizing electromyography. *IEEE Transactions on Robotics*, *24*(4), 872-882.

Gordon, K. E., and Ferris, D. P. (2007). Learning to walk with a robotic ankle exoskeleton. *Journal of biomechanics*, *40*(12), 2636-2644.

Gross, M. M., Stevenson, P. J., Charette, S. L., Pyka, G., and Marcus, R. (1998). Effect of muscle strength and movement speed on the biomechanics of rising from a chair in healthy elderly and young women. *Gait & posture*, *8*(3), 175-185.

Guizzo, E., and Goldstein, H. (2005). The rise of the body bots [robotic exoskeletons]. *IEEE Spectrum*, *42*(10), 50-56.

Günther, M., and Ruder, H. (2003). Synthesis of two-dimensional human walking: a test of the λ-model. *Biological cybernetics*, *89*(2), 89-106.

Haeufle, D. F. B., Günther, M., Bayer, A., and Schmitt, S. (2014). Hill-type muscle model with serial damping and eccentric force–velocity relation. *Journal of biomechanics*, *47*(6), 1531-1536.

Halaki, M., and Ginn, K. (2012). Normalization of EMG Signals: To Normalize or Not to Normalize and What to Normalize to?. *INTECH Open Access Publisher*

Han, J., Ding, Q., Xiong, A., and Zhao, X. (2015). A State-Space EMG Model for the Estimation of Continuous Joint Movements. *IEEE Transactions on Industrial Electronics*, *62*(7), 4267-4275.

He, H., and Kiguchi, K. (2007). A study on emg-based control of exoskeleton robots for human lower-limb motion assist. *6th IEEE International Special Topic Conference on Information Technology Applications in Biomedicine*, pp. 292-295

Hermens, H. J., Stegeman, D., Blok, J., and Freriks, B. (1998). State of the art on modelling methods for surface electromyography. *SENIAM project, Enschede, The Netherlands*.

Hersh. M. A. (2010). The design and evaluation of assistive technology products and devices Part 1: Design. *International Encyclopedia of rehabilitation*.

Hersh M. A, Johnson MA. (2008a). On modelling assistive technology systems part 1: modelling framework, Technology and Disability, *20*(3):193-215.

Hersh. M. A., and Johnson, M. A. (2008b). On modeling assistive technology systems-Part 2: Applications of the comprehensive assistive technology model. *Technology and Disability*, *20*(4), 251-270.

Hill, A. V. (1938). The heat of shortening and the dynamic constants of muscle. *Proceedings of the Royal Society of London B: Biological Sciences*, *126*(843), 136-195.

Hughes, J. (1972). Powered lower limb orthotics in paraplegia. *Paraplegia*, *9*(4), 191.

Jacobson, S. C., Knutti, D. F., Johnson, R. T., and Sears, H. H. (1982). Development of the Utah artificial arm. *IEEE Transactions on Biomedical Engineering,* (4), 249-269.

Jerard, R. B., Williams, T. W., and Ohlenbusch, C. W. (1974, May). Practical design of an EMG controlled above elbow prosthesis. *In Proc. of Conf. Engineering Devices for Rehabilitation*, pp. 73-73.

Jimenez-Fabian, R., and Verlinden, O. (2012). Review of control algorithms for robotic ankle systems in lower-limb orthoses, prostheses, and exoskeletons. *Medical engineering & physics*, *34*(4), 397-408.

Johnstone, D. (2012). *An introduction to disability studies*. 2nd ed. David Fulton Routledge.

Kadefors, R., Broman, H., and de Luca, C. J. (1980). Units, Terms and Standards in the Reporting of EMG Research.

Kerem Tuncay Özgünen Umut Çelik and Sanlı Sadi Kurdak, (2010). Determination of an optimal threshold value for muscle activity detection in EMG analysis. *Journal of Sports Science and Medicine*. 9,620-628

Khezri, M., and Jahed, M. (2008). Surface Electromyogram signal estimation based on wavelet thresholding technique. *30th Annual IEEE International Conference of the Engineering in Medicine and Biology Society,* pp. 4752-4755

Khushaba, R. N., Kodagoda, S., Takruri, M., and Dissanayake, G. (2012). Toward improved control of prosthetic fingers using surface electromyogram (EMG) signals. *Expert Systems with Applications*, *39*(12), 10731-10738

Kiguchi, K. and Hayashi, Y. 2012. An EMG based control for an upper limb power assist exoskeleton robot. *IEEE Transactions on systems, man, and cybernetics-part B. 42*(4), 1064-1071.

Kiguchi, K., Kariya, S., Watanabe, K., Izumi, K., and Fukuda, T. (2001). An exoskeletal robot for human elbow motion support-sensor fusion, adaptation, and control. *IEEE Transactions on, Systems, Man, and Cybernetics, Part B: Cybernetics, 31*(3), 353-361

Kinnaird, C. R., and Ferris, D. P. (2009). Medial gastrocnemius myoelectric control of a robotic ankle exoskeleton. *IEEE Transactions on Neural Systems and Rehabilitation Engineering*, *17*(1), 31-37.

Kistemaker, D. A., Van Soest, A. J. K., and Bobbert, M. F. (2007). A model of open-loop control of equilibrium position and stiffness of the human elbow joint. *Biological cybernetics*, *96*(3), 341-350.

Konrad, P. (2005). The abc of emg. *A practical introduction to kinesiological electromyography*, Noraxon U.S.A, Inc.1-61.

Kong, Y. K., Hallbeck, M. S., and Jung, M. C. (2010). Crosstalk effect on surface electromyogram of the forearm flexors during a static grip task. *Journal of Electromyography and Kinesiology*, *20*(6), 1223-1229.

Erer, K. S. 2007. Adaptive usage of the Butterworth filter. *Journal of Biomechanics*, 40(2007), 2934-2943

Kuiken, T. A., Stoykov, N. S., Popović, M., Lowery, M. and Taflove, A. (2001). Finite element modeling of electromagnetic signal propagation in a phantom arm. *IEEE Transactions on Neural Systems and Rehabilitation Engineering*, *9*(4), 346-354.

Lam H.Y.F, Analog and Digital Filters: Design and Realization, Prentice-Hall, Inc, Englewood Cliffs, New Jersey, 1979.

Lee, A. S., Cholewicki, J., and Reeves, N. P. (2007). The effect of background muscle activity on computerized detection of sEMG onset and offset. *Journal of biomechanics*, *40*(15), 3521-3526.

Lehman, G. J. and McGill, S. M. (1999). The importance of normalization in the interpretation of surface electromyography: a proof of principle. *Journal of manipulative and physiological therapeutics*, *22*(7), 444-446.

Lenzi, T., Rossi, S. M. M. D., Vitiello, N., and Carrozza, M. C. (2012). Intention-based EMG control for powered exoskeletons. *IEEE Transactions on Biomedical Engineering*, *59*(8), 2180-2190.

Lloyd, D. G. and Besier, T. F. (2003). An EMG-driven musculoskeletal model to estimate muscle forces and knee joint moments in vivo. *Journal of Biomechanics*, *36*(6), 765-776.

Lowery, M. M., Stoykov, N. S. and Kuiken, T. A. (2003). A simulation study to examine the use of cross-correlation as an estimate of surface EMG cross talk. *Journal of Applied Physiology*, *94*(4), 1324-1334.

Lu, G., Brittain, J. S., Holland, P., Yianni, J., Green, A. L., Stein, J. F. and Wang, S. (2009). Removing ECG noise from surface EMG signals using adaptive filtering. *Neuroscience letters*, *462*(1), 14-19.

Lucas, L., DiCicco, M. and Matsuoka, Y. (2004). An EMG-controlled hand exoskeleton for natural pinching. *Journal of Robotics and Mechatronics*, *16*, 482-488.

Malaysia. (2011). Annual Report Ministry of Health Malaysia.

Malmivuo, J and Plonsey, R. (1995). *Bioelectromagnetism principles and applications of bioelectric aand biomagnetic*. New York, Oxford University Press.

Manal, K. and Buchanan, T. S. (2003). A one-parameter neural activation to muscle activation model: estimating isometric joint moments from electromyograms. *Journal of Biomechanics*, *36*(8), 1197-1202.

Marras, W. S., and Davis, K. G. (2001). A non-MVC EMG normalization technique for the trunk musculature: Part 1. Method development. *Journal of Electromyography and Kinesiology*, *11*(1), 1-9.

Marras, W. S., Davis, K. G., and Maronitis, A. B. (2001). A non-MVC EMG normalization technique for the trunk musculature: Part 2. Validation and use to predict spinal loads. *Journal of electromyography and kinesiology*, *11*(1), 11-18.

Merletti, R., and Di Torino, P. (1999). Standards for reporting EMG data. *J Electromyogr Kinesiol*, *9*(1), 3-4.

Merlo, A., and Campanini, I. (2010). Technical aspects of surface electromyography for clinicians. *The open rehabilitation journal*, *3*(1).

Messier, C. F. E. (2010). *History and Future of Rehabilitation Robotics*. Bachelor Thesis. Worcester Polytechnic Institute. USA.

Mezzarane, R. A., and Kohn, A. F. (2009). A method to estimate EMG crosstalk between two muscles based on the silent period following an H-reflex. *Medical engineering & physics*, *31*(10), 1331-1336.

Micera, S., Vannozzi, G., Sabatini, A. M., & Dario, P. (2001). Improving detection of muscle activation intervals. *IEEE Engineering in Medicine and Biology Magazine*, *20*(6), 38-46.

Mogk, J. P., and Keir, P. J. (2003). Crosstalk in surface electromyography of the proximal forearm during gripping tasks. *Journal of Electromyography and Kinesiology*, *13*(1), 63-71.

Muscle (2016). In *Wikipedia*. Retrieved from https://en.wikipedia.org/wiki/Muscle

Neptune, R. R., Sasaki, K., & Kautz, S. A. (2008). The effect of walking speed on muscle function and mechanical energetics. *Gait & posture*, *28*(1), 135-143.

Oliver, M. (1996). *Fundamental Principles of Disability*. *Understanding Disability* (pp. 19-29). Macmillan Education UK.

Olree, K. S., and Vaughan, C. L. (1995). Fundamental patterns of bilateral muscle activity in human locomotion. *Biological cybernetics*, *73*(5), 409-414.

Özgünen, K. T., Çelik, U., and Kurdak, S. S. (2010). Determination of an optimal threshold value for muscle activity detection in EMG analysis. *Journal of sports science & medicine*, *9*(4), 620.

Pal, S., and Mitra, M. (2012). Empirical mode decomposition based ECG enhancement and QRS detection. *Computers in biology and medicine*, *42*(1), 83-92.

Phinyomark, A., Limsakul, C., and Phukpattaranont, P. (2009). A comparative study of wavelet denoising for multifunction myoelectric control. *IEEE International Conference on Computer and Automation Engineering*, pp. 21-25.

Phinyomark, A., Limsakul, C., and Phukpattaranont, P. (2009). A novel feature extraction for robust EMG pattern recognition. *Journal of Computing*, *1*(1), 71-80

Pons, J. L. (2010). Rehabilitation exoskeletal robotics. *IEEE Magazine in Engineering Medicine and Biology*, *29*(3), 57-63.

Pullman, S. L., Goodin, D. S., Marquinez, A. I., Tabbal, S., and Rubin, M. (2000). Clinical utility of surface EMG Report of the Therapeutics and Technology Assessment Subcommittee of the American Academy of Neurology. *Neurology*, *55*(2), 171-177.

Raasch, C. C., Zajac, F. E., Ma, B., and Levine, W. S. (1997). Muscle coordination of maximum-speed pedaling. *Journal of biomechanics*, *30*(6), 595-602.

Rainoldi, A., Melchiorri, G., and Caruso, I. (2004). A method for positioning electrodes during surface EMG recordings in lower limb muscles. *Journal of neuroscience methods*, *134*(1), 37-43.

Redfern, M. S., Hughes, R. E., and Chaffin, D. B. (1993). High-pass filtering to remove electrocardiographic interference from torso EMG recordings. *Clinical Biomechanics*, *8*(1), 44-48.

Robertson, D. G. E., and Dowling, J. J. (2003). Design and responses of Butterworth and critically damped digital filters. *Journal of Electromyography and Kinesiology*, *13*(6), 569-573.

Rodríguez-Carreño, I., Malanda-Trigueros, A., Gila-Useros, L., Navallas-Irujo, J., and Rodríguez-Falces, J. (2006). Filter design for cancellation of baseline-fluctuation in needle EMG recordings. *Computer Methods and Programs in Biomedicine*, *81*(1), 79-93

Rogers, S. S., Waigh, T. A., Zhao, X., and Lu, J. R. (2007). Precise particle tracking against a complicated background: polynomial fitting with Gaussian weight. *Physical Biology*, *4*(3), 220.

Rosen, J., Brand, M., Fuchs, M. B., and Arcan, M. (2001). A myosignal-based powered exoskeleton system. *IEEE Transactions on Systems, Man and Cybernetics, Part A: Systems and Humans*, *31*(3), 210-222.

Rowell. D. (2008), Introduction to Recursive Least Squares (RLS) Adaptive filters. *MIT OpenCourseWare*, Retreived from, http://ocw.mit.edu

Ruthenberg, Brent J, Wasylewski, Neil A., Beard, John. E. 1997. An experimental device for investigating the force and power requirements of a powered gait orthosis. *Journal of rehabilitation research and development*. *34*: 203-214

Sacco, I. C., Gomes, A. A., Otuzi, M. E., Pripas, D., and Onodera, A. N. (2009). A method for better positioning bipolar electrodes for lower limb EMG recordings during dynamic contractions. *Journal of neuroscience methods*. *180*(1), 133-137.

Ward, S. R., Eng, C. M., Smallwood, L. H., & Lieber, R. L. (2009). Are current measurements of lower extremity muscle architecture accurate?. Clinical orthopaedics and related research, 467(4), 1074-1082.

Sawicki, G. S. (2007). *Mechanics and energetics of walking with powered exoskeletons*. Doctoral dissertation, The University of Michigan.

Sawicki, G. S. (2007). *Mechanics and energetics of walking with powered exoskeletons*. Doctoral dissertation, The University of Michigan

Sawicki, G. S. and Ferris, D. P. (2008). Mechanics and energetics of level walking with powered ankle exoskeletons. *Journal of Experimental Biology*, *211*(9), 1402-1413.

Sawicki, G. S., Gordon, K. E. and Ferris, D. P. (2005). Powered lower limb orthoses: applications in motor adaptation and rehabilitation. *IEEE 9th International Conference on In.Rehabilitation Robotics*, pp. 206-211

Schulze, M., Calliess, T., Gietzelt, M., Wolf, K. H., Liu, T. H., Seehaus, F. and Marschollek, M. (2012). Development and clinical validation of an unobtrusive ambulatory knee function monitoring system with inertial 9DoF sensors. *IEEE Annual International Conference of the Engineering in Medicine and Biology Society*, pp. 1968-1971

Seireg, A. and Grundmann, J. G. (1981). Design of a multi-task exoskeletal walking device for paraplegics. *Biomechanics of Medical Devices*, 569-644.

Selvanayagam, V. S., Riek, S. and Carroll, T. J. (2012). A systematic method to quantify the presence of cross-talk in stimulus-evoked EMG responses: implications for TMS studies. *Journal of Applied Physiology*, *112*(2), 259-265.

Shao, Q., Bassett, D. N., Manal, K. and Buchanan, T. S. (2009). An EMG-driven model to estimate muscle forces and joint moments in stroke patients. *Computers in biology and medicine*, *39*(12), 1083-1088.

Singh, R. M., Chatterji, S. and Kumar, A. (2012). Trends and challenges in EMG based control scheme of exoskeleton robots-a review. *Int. J. Sci. Eng. Res*, *3*, 933-40.

Song, R., Tong, K. Y., Hu, X. and Zhou, W. (2013). Myoelectrically controlled wrist robot for stroke rehabilitation. *J Neuroeng Rehabil*, *10*(1), 52.

Sausa, A. S., and Tavares, J. M. R. (2012). Surface electromyographic amplitude normalization methods: a review. *Electromyography: New Developments, Procedures and Applications*.

Tilling, K., Sterne, J. A., Rudd, A. G., Glass, T. A., Wityk, R. J. and Wolfe, C. D. (2001). A new method for predicting recovery after stroke. *Stroke*, *32*(12), 2867-2873.

United Nations. Department of Economic. (2010). *World population ageing 2009* (Vol. 295). United Nations Publications.

Van Soest, A. J. and Bobbert, M. F. (1993). The contribution of muscle properties in the control of explosive movements. *Biological cybernetics*, *69*(3), 195-204.

Van Vugt, J. P. P. and Van Dijk, J. G. (2001). A convenient method to reduce crosstalk in surface EMG. *Clinical Neurophysiology*, *112*(4), 583-592.

Vaughan, C. L., Davis, B. L. and Jeremy, C. O. (1999). *Dynamics of human gait*.

Veneman, J. F., Kruidhof, R., Hekman, E. E., Ekkelenkamp, R., Van Asseldonk, E. H. and Van Der Kooij, H. (2007). Design and evaluation of the LOPES exoskeleton robot for interactive gait rehabilitation. *IEEE Transactions on Neural Systems and Rehabilitation Engineering*, *15*(3), 379-386.

Visser, J. J., Hoogkamer, J. E., Bobbert, M. F. and Huijing, P. A. (1990). Length and moment arm of human leg muscles as a function of knee and hip-joint angles. *European Journal of Applied Physiology and Occupational Physiology*, *61*(5-6), 453-460.

Ward, S. R., Eng, C. M., Smallwood, L. H. and Lieber, R. L. (2009). Are current measurements of lower extremity muscle architecture accurate? *Clinical Orthopaedics and Related Research*, *467*(4), 1074-1082.

WHO. (2013). Global action plan for the prevention and control of non-communicable diseases 2013-2020. World Health Organization.

WHO. (2001). International Classification of functioning, disability and health (ICF). World Health Organisation Publication, ISBN-13 9789241545426, ISBN-10 924 154 5429. Geneva (Switzerland): WHO.

WHO. (1980). International classification of impairments, disabilities and handicaps. Geneva (Switzerland): World Health Organisation.

Winter, D. A. (2009). *Biomechanics and motor control of human movement*. 4th edition, New Jersey, USA, John Wiley and Sons.

Winter, D. A. and Yack, H. J. (1987). EMG profiles during normal human walking: stride-to-stride and inter-subject variability. *Electroencephalography and clinical neurophysiology*, *67*(5), 402-411.

Winters, J. M. (1995). How detailed should muscle models be to understand multi-joint movement coordination?. *Human Movement Science*, *14*(4), 401-442.

Yamamoto, T., Tsujiuchi, N., Ito, A. and Koizumi, T. (2014). Motion discrimination technique by EMG signals using hyper-sphere model. *36th IEEE Annual International Conference of the Engineering in Medicine and Biology Society*, pp. 5-8

Zajac, F. E. (1988). Muscle and tendon: properties, models, scaling, and application to biomechanics and motor control. *Critical reviews in biomedical engineering*, *17*(4), 359-411.

Zardoshti-Kermani, M., Wheeler, B. C., Badie, K. and Hashemi, R. M. (1995). EMG feature evaluation for movement control of upper extremity prostheses. *IEEE Transactions on Rehabilitation Engineering*, *3*(4), 324-333.

Zoss, A. B., Kazerooni, H. and Chu, A. (2006). Biomechanical design of the Berkeley lower extremity exoskeleton (BLEEX). *IEEE/ASME Transactions on Mechatronics*, *11*(2), 128-138.

List of Publication

Zahari Taha, **Abdelhakim Deboucha**, NizamUddin Ahamed, Norhafizan Ahmed, Raja Ariffin Raja Ghazilla, IIR Filter Order and Cut-off Frequency Influences on sEMG Signal Smoothing, *Biomedical Research: vol* **26**(4): 616-620.

Zahari Taha, **Abdelhakim Deboucha**, 2013. Development of Synchronized Biomechanics Sensors Detection Software. *Advanced Materials Research. **706-708** (2013)*, 771-775.

Abdelhakim Deboucha, Zahari Taha and Nizam Uddin Ahamed, Designing an optimum filter for surface EMG smoothing, *Proceeding in MOHE conference 03rd Sept 2014.* Kuantan, Pahang.

Nizam Uddin Ahmad, Zahari Taha and **Abdelhakim Deboucha,** Age related Differences in the surface EMG signal on the Adolescent's muscle during contractions. Proceeding in the 2nd international Manufacturing Engineering conference (iMEC) 2015

Matiur Rahman, Nizam Uddin Ahamed, Md. Asraf Ali, Nurul Syahirahb, **Abdelhakim Deboucha** and Kenneth Sundaraj. Surface EMG-based Fatigue Analysis during Repetitive Work: A Review. NCON-PGR 2015. January , 2015, *UMP*.

Appendix A:

MATLAB-codes:

A.1. MATLAB code for filtering “Butterworth Filter”

```
%%  butterworth with cutoff fequency changing or adaptive cutoff
frequency
emg1=em1(:,2);emg1=emg1-mean(em1(:,2));
emg2=em2(:,2);emg2=emg2-mean(em2(:,2));
emg3=em3(:,2);emg3=emg3-mean(em3(:,2));
emg4=em4(:,2);emg4=emg4-mean(em4(:,2));
angvel=Gr2(:,2)-mean(Gr2(:,2));
Rawlength=[length(emg1),length(emg2),length(emg3),length(emg4),length(
angvel)];
samp=min(Rowlength);
w1=.2;w2=5;%lower and upper frequencies
%% generating a criteria cn
cnn=ones(samp,1);w0=0.2;
V  = tan(fc2 * pi/2);
Sp = V * [-1-1i, -1+1i -1+1i] / sqrt(2);
for k=1:length(V)
Sg(k) = V(k) ^ 3;% k1 coffiecient 1
  G(k) = real(Sg(k) / prod(1 - Sp(k,:)));
  P(k,:) = (1 + Sp(k,:)) ./ (1 - Sp(k,:));%bilinear transform
  B1(k,:) = G(k) * [1, 3, 3 1];
  A1(k,:) = real(poly(P(k,:)));
end
%% defining the upper lower corner of the frequencies non changing
freq
% corner
cn=((w2+1)*ones(length(emg3),1)-w1)/w2;
fc1=(w1+w2*cn)/512;
V  = tan(fc1 * pi/2);
Sp = V * [-1-1i, -1+1i -1+1i] / sqrt(2);
for k=1:length(V)
Sg(k) = V(k) ^ 3;% k1 coffiecient 1
  G(k) = real(Sg(k) / prod(1 - Sp(k,:)));
  P(k,:) = (1 + Sp(k,:)) ./ (1 - Sp(k,:));%bilinear transform
  B1(k,:) = G(k) * [1, 3, 3 1];
  A1(k,:) = real(poly(P(k,:)));
end
%% ========== filtering forward and
backward============================
%=========================================================================
=====
%% 1-1 Removing the DC Bias (DC offset coming from)===========
%=========================================================================
=====
Rawlength=[length(emg1),length(emg2),length(emg3),length(emg4),length(
angvel)];
samp=min(Rowlength);
angvel=angvel(1:samp);
Ms=[emg1(1:samp),emg2(1:samp),emg3(1:samp),emg4(1:samp)];
y0=abs(emg2(1:samp));
y=abs(emg3(1:samp));
y1=abs(emg4(1:samp));
y2=((-1)*angvel(1:samp));
```

```
lng=samp;
x=zeros(1,lng);x(1)=y(1); x(2)=y(1); x(3)=y(1);
x0=zeros(1,lng);x0(1)=y0(1); x0(2)=y0(1); x0(3)=y0(1);
x1=zeros(1,lng);x1(1)=y1(1); x1(2)=y1(1); x1(3)=y1(1);
x2=zeros(1,lng);x2(1)=y2(1); x2(2)=y2(1); x2(3)=y2(1);
for k=4:lng
 x(k)=B1(k,1)*y(k)+B1(k,2)*y(k-1)+B1(k,3)*y(k-2)+B1(k,4)*y(k-3) -
A1(k,2)*x(k-1)-A1(k,3)*x(k-2)-A1(k,4)*x(k-3); % forward filter
 x0(k)=B1(k,1)*y0(k)+B1(k,2)*y0(k-1)+B1(k,3)*y0(k-2)+B1(k,4)*y0(k-3) -
A1(k,2)*x0(k-1)-A1(k,3)*x0(k-2)-A1(k,4)*x0(k-3); % forward filter
 x1(k)=B1(k,1)*y1(k)+B1(k,2)*y1(k-1)+B1(k,3)*y1(k-2)+B1(k,4)*y1(k-3) -
A1(k,2)*x1(k-1)-A1(k,3)*x1(k-2)-A1(k,4)*x1(k-3); % forward filter
 x2(k)=B1(k,1)*y2(k)+B1(k,2)*y2(k-1)+B1(k,3)*y2(k-2)+B1(k,4)*y2(k-3) -
A1(k,2)*x2(k-1)-A1(k,3)*x2(k-2)-A1(k,4)*x2(k-3); % forward filter
end
%subplot(211);plot(x);grid on,subplot(212);plot(x1);grid on,
%
yy=zeros(1,lng); yy(lng)=x(lng); yy(lng-1)=x(lng-1); yy(lng-2)=x(lng-
2);yy(lng-3)=x(lng-3);
yy0=zeros(1,lng); yy0(lng)=x0(lng); yy0(lng-1)=x0(lng-1); yy0(lng-
2)=x0(lng-2);yy0(lng-3)=x0(lng-3);
yy1=zeros(1,lng); yy1(lng)=x1(lng); yy1(lng-1)=x1(lng-1); yy1(lng-
2)=x1(lng-2);yy1(lng-3)=x1(lng-3);
yy2=zeros(1,lng); yy2(lng)=x2(lng); yy2(lng-1)=x2(lng-1); yy2(lng-
2)=x2(lng-2);yy2(lng-3)=x2(lng-3);
for k=lng-3:-1:1
yy(k)= B1(k,1)*x(k)+B1(k,2)*x(k+1)+B1(k,3)*x(k+2)+B1(k,4)*x(k+3)+ -
A1(k,2)*yy(k+1)-A1(k,3)*yy(k+2)-A1(k,4)*yy(k+3); % backward filter
 yy0(k)=B1(k,1)*x0(k)+B1(k,2)*x0(k+1)+B1(k,3)*x0(k+2)+B1(k,4)*x0(k+3)+
- A1(k,2)*yy0(k+1)-A1(k,3)*yy0(k+2)-A1(k,4)*yy0(k+3); % backward
filter
 yy1(k)=B1(k,1)*x1(k)+B1(k,2)*x1(k+1)+B1(k,3)*x1(k+2)+B1(k,4)*x1(k+3)+
- A1(k,2)*yy1(k+1)-A1(k,3)*yy1(k+2)-A1(k,4)*yy1(k+3); % backward
filter
 yy2(k)=B1(k,1)*x2(k)+B1(k,2)*x2(k+1)+B1(k,3)*x2(k+2)+B1(k,4)*x2(k+3)+
- A1(k,2)*yy2(k+1)-A1(k,3)*yy2(k+2)-A1(k,4)*yy2(k+3); % backward
filter
end
out=yy;
subplot(411);plot(yy,'-k','LineWidth',2.0);grid on
subplot(412);plot(yy1,'-k','LineWidth',2.0);grid on
subplot(413);plot(yy2,'-k','LineWidth',2.0);grid on
subplot(414);plot(yy0,'-k','LineWidth',2.0);grid on
```

A.3. MATLAB code for filtering part “WAVELET FILTER”

```
function [approximations, details] = wavelet_decompose(signal, scale,
wavelet)

sig_length = length(signal);

approximations = zeros(sig_length, scale);
details = zeros(sig_length, scale);

[C,L] = wavedec(signal, scale, wavelet);

for i=1:scale,
  approximations(:,i) = wrcoef('a', C, L, wavelet, i);
  details(:,i) = wrcoef('d', C, L, wavelet, i);
end
```

A.4. MATLAB code for onset/offset detection (Offline Detection).

```
function[onoff,onset,restav,offset,yy,y10,x10]=emgonsetdet(emgraw,fs)
% base line wonder and DC offset removal
bsl=emgraw(1:length(emgraw));
[p,s,mu] = polyfit((1:numel(bsl))',bsl,15);
f_y = polyval(p,(1:numel(bsl))',[],mu);
%plot(f_y,'g');hold on
bsl1=f_y-bsl;
bsl1=bsl1-mean(bsl1);
fwlo = abs(bsl1);
fwlo=fwlo-mean(fwlo);
fwlo=abs(fwlo);
%% prepare for loop
% Get two ranges for resting emg (before & after burst) using ginput

w1=.1;w2=5;%emgraw=emg3;
cn=((w2+1)*ones(length(emgraw),1)-0.1)/w2;fc1=(w1+w2*cn)/512;
V  = tan(fc1 * pi/2);
Sp = V * [-1-1i, -1+1i -1+1i] / sqrt(2);
for k=1:length(V)
Sg(k) = V(k) ^ 3;% k1 coffiecient 1
  G(k) = real(Sg(k) / prod(1 - Sp(k,:)));
  P(k,:) = (1 + Sp(k,:)) ./ (1 - Sp(k,:));%bilinear transform
  B1(k,:) = G(k) * [1, 3, 3 1];
  A1(k,:) = real(poly(P(k,:)));
end
%Rowlength=[length(emg1),length(emg2),length(emg3),length(emg4),length
(angvel)];
%samp=min(Rowlength);
%angvel=angvel(1:samp);
%Ms=[emg1(1:samp),emg2(1:samp),emg3(1:samp),emg4(1:samp)];
%y0=abs(emg2(1:samp));
samp1=length(emgraw);
y=fwlo(1:samp1);
lng=length(y);
x=zeros(1,lng);x(1)=y(1); x(2)=y(1); x(3)=y(1);
for k=4:lng
    x(k)=B1(1,1)*y(k)+B1(1,2)*y(k-1)+B1(1,3)*y(k-2)+B1(1,4)*y(k-3) -
A1(1,2)*x(k-1)-A1(1,3)*x(k-2)-A1(1,4)*x(k-3); % forward filter
end
yy=zeros(1,lng); yy(lng)=x(lng); yy(lng-1)=x(lng-1); yy(lng-2)=x(lng-
2);yy(lng-3)=x(lng-3);
for k=lng-3:-1:1
yy(k)=B1(1,1)*x(k)+B1(1,2)*x(k+1)+B1(1,3)*x(k+2)+B1(1,4)*x(k+3)+ -
A1(1,2)*yy(k+1)-A1(1,3)*yy(k+2)-A1(1,4)*yy(k+3); % backward filter
end
f1 = figure;
plot(yy,'-k','LineWidth',2.0);grid on
%prepare for loop
% Get two ranges for resting emg (before & after burst) using ginput
%plot(yy);
[x10 y10] = ginput(4); %click four times: two for start/end of resting
emg before burst two for resting emg after burst
x10 = round(x10);
w1=.1;w2=5;%emgraw=emg3;
```

```
mvgav = zeros(x10(4)-x10(1),1);
onoff(1,1) = 0;
i=0;
restav = mean(yy(x10(1):x10(2))); %average value of rest EMG before ON
reststd = std(yy(x10(1):x10(2))); %std. dev. of rest EMG before ON
restav2 = mean(yy(x10(3):x10(4))); %average value of rest EMG after
OFF
reststd2 = std(yy(x10(3):x10(4))); %std. dev. of rest EMG after OFF
% restav3 = mean(yy(x10(5):x10(6))); %average value of rest EMG after
OFF
% reststd3 = std(yy(x10(5):x10(6))); %std. dev. of rest EMG after OFF
%% window size (in samples) = ws*fs e.g. 50ms*2400Hz = 120 samples
ws=50;
sws2 = fs*(0.001*ws);
sws = 0.5*(sws2);
sws = round(sws);
%% find "ON" index:
% for xi, change from x(1) to x(2) if you want to ignore any "blips"
% within the resting range.
%xi = x(1);
sd=1;
xi = x10(2); % start searching from the second point gig
xi = round(xi);
for n = 2:length(mvgav);
mvgav(n,1) = mean(yy((xi-sws):(xi+sws)));
ifmvgav(n) > restav+2*sd*reststd;
        i = i+1;
onoff(i,1) = xi;
break
end
    xi = xi+1;

end
%on1=onoff
%% find "OFF" index:
%clear n xi i
mvgav2=zeros(x10(4)-x10(1),1);
i=0;
xi=onoff(1,1)+(2/3)*(x10(3)-onoff(1,1)); %start OFF search approx. 1/2
way through ON burst.
%% OFF loop:
xi=round(xi);
for n=2:length(mvgav2);
    mvgav2(n,1)=mean(yy((xi-sws):(xi+sws)));
if mvgav2(n)<restav2+sd*reststd2;
        i=i+1;
onoff(i,2)=xi;
break
end
    xi=xi+1;

end
onoff1=onoff;
%% defining the index of the onset and the offset of the emg
% ind=ans;
 ton=onoff1(:,1);
toff=onoff1(:,2);
 ton=ton*[1;1];
toff=toff*[1;1];
%%toff=toff*[0.5;0.5];
%plot(emgraw,'LineWidth',2.0);grid on
```

```
%% Grid filtering
%%  butterworth with a changing cutoff fequency  or adaptive cutoff
frequency
hold on
onset=yy(onoff(1));offset=yy(onoff(2));
yrange=[0 max(yy)];
plot([ton toff],yrange,'--b','LineWidth',2.5)
```

A.5. MATLAB code for features extraction

```
%% absolute vector of emg4 and the integrated emg
emg44=emgtest;
clear IEMG4
%%#################1st Inegrated
EMG#######################################
seg=50;
for n=1:seg:length(emg4)-seg
    IEMG4(n)=sum(abs(emg4(n:n+seg)));
end
  IEMG4= IEMG4(IEMG4~=0);IEMG4=IEMG4/(max(IEMG4)+std(IEMG4));
  plot(IEMG4)
%% %#########################Mean Absolute
Value##############################
clear MAV
 MAV=1/length(IEMG4)*IEMG4;
 MAV=MAV/(max(MAV)+std(MAV));
 plot(MAV)

%% %######################Modified Mean Absolute Value 1#######
clear MMAV1
seg=50;
for n=2:seg:length(emg4)-seg
    if 0.25*length(emg4)<= n <=0.75*length(emg4)
        wn=1;
        MMAV1(n)=sum(wn*abs(emg4(n:n+seg)))/length(emg4);
    else
        wn=0.5;
        MMAV1(n)=sum(wn*abs(emg4(n:n+seg)))/length(emg4);
    end
end

 MMAV1= MMAV1(MMAV1~=0); MMAV1=MMAV1/(max(MMAV1)+std(MMAV1));
 plot(MMAV1)
%% ######## #####Modified Mean Absolute Value 2#######
seg=50;
clear MMAV2
for n=1:50:length(emg4)-seg
    if 0.25*length(emg4)<= n <=0.75*length(emg4)
        wn=1;
        MMAV2(n)=sum(wn*abs(emg4(n:n+seg)))/length(emg4);
    elseif n<0.25*length(emg4)
        wn(n)=n/length(emg4);
        MMAV2(n)=sum(wn(n)*abs(emg4(n:n+seg)))/length(emg4);
    else
        wn(n)=4*(n-length(emg4)/length(emg4));
        MMAV2(n)=sum(abs(emg4(n:n+seg)))/length(emg4);
    end
end
 MMAV2= MMAV2(MMAV2~=0);  MMAV2=MMAV2/(max(MMAV2)+std(MMAV2));
 plot(MMAV2)
```

```
%% ############### Mean Absolute Value Slope###################
clear MAVSLP
seg=50;
for n = 2:length(MAV)
    MAVSLP(n)=MAV(n)- MAV(n-1);
end
subplot(211);plot(MAVSLP,'r'),grid on;subplot(212);plot(MAV,'b');grid
on
%% ################### Simple Square Integral
############################
clear SSI
seg=50;
for n=1:seg:length(emg4)-seg
    SSI(n)= sum(abs(emg4(n:n+seg)))^2;

end
 SSI= SSI(SSI~=0);SSI=SSI/(max(SSI)+std(SSI));plot(SSI)
%% #################Variance of
EMG#####################################
clear VAR
seg=50;
for n=1:50:length(emg4)-seg
    VAR(n)=(1/(length(emg4)-1))*sum(emg4(n:n+seg));

end
 VAR= VAR(VAR~=0);plot(VAR)
%% ########################Root Mean Square ######################
clear RMS1
seg=50;
for n=1:seg:length(emg4)-seg
    RMS1(n)=sqrt(((1/seg)*sum(emg4(n:n+seg).^2)));
end
  RMS1= RMS1(RMS1~=0);RMS1=RMS1/(max(RMS1)+std(RMS1)); plot(RMS1)
%% ###### ############waveform length
###################################
for n=2:length(emg1);

    WL(n)=abs(emg1(1)-emg1(n-1));
end
WL;
%% ############## Zero crossing detector
#################################
%%
clear zeroNb
x=emg(1:end)';
zeroNb=0;
for i=1:length(x)-1 %length : get x size
if ((x(i)>=0 && x(i+1)<0) || (x(i)<=0 && x(i+1)>0))
     zeroNb=1+zeroNb;
end
end
```

A.6 Real time simulation Algorithm

```
%% this code calculate the average,the onset/offset acording to the
motion of the emg signal every 150 samples along
% the signal %%%%%%%% and return the onset of the emg signal
%x=emg;
%elapsedTime = 0;
tic;
```

```
x=yy; vel=abs(yy1);
 x = double(x);
if isvector(x)
    x = x(:);
end
[mx,nx] = size(x);%vel=abs(yy1);
%
clear y00 pks locs diff1 x_std sum1 newsum1 kk k ondiff newondiff
offdiff newoffdiff idvel_on idx_on
newdiff1=[];sum1=[];newsum1=[];onoff1(1,1) =
0;ont=[];offdiff=[];newoffdiff=[];
diff1=[];x_std=[];NS=150;i=0;ind1=[];newind1=[];ind2=[];newind2=[];ont
=[];
ondiff=[];newondiff=[];
% velocity
parameters=============================================================
%
=========================================================================
===
diff11=[];newdiff11=[];sum11=[];newsum11=[];vel_ont=[];ii=0;
vel_ondiff=[];vel_newondiff=[];ind11=[];ind22=[];newind22=[];
vel_offdiff=[];vel_newoffdiff=[];idx_on=[];idx_off=[];idvel_on=[];idve
l_off=[];
for k = 2:NS:length(vel)-NS
    % emg
processing=============================================================

%=========================================================================
=
    y00(:,k)=(1/NS)*sum(x(k:k+NS));% calculating the mean value  for
each segment
    %xy(:,k)=y00(:,k);
    locs=findpeaks(y00,0);% calculte the location of the peaks
    pks=y00(locs);%display the peaks
    newdiff1=(x(k:k+NS)-(1/NS)*sum(x(k:k+NS)));% calculate the
variance
    diff1=[diff1;newdiff1];
    newsum1=(sum(newdiff1)^2)*(1/(NS-1));
    sum1=[sum1;newsum1];%
    x_std=sqrt(sum1);%kk2=kk2+1; standard deviation calculation

% angular velocity
processing=============================================

%=========================================================================
=
    y001(:,k)=(1/NS)*sum(vel(k:k+NS));% mean value
    locs1=findpeaks(y001,0);
    pks1=y001(locs1);
    newdiff11=(vel(k:k+NS)-(1/NS)*sum(vel(k:k+NS)));
    diff11=[diff11;newdiff11];
    newsum11=(sum(newdiff11)^2)*(1/(NS-1));
    sum11=[sum11;newsum11];%xi = locs(3);xi = round(xi);
    vel_std=sqrt(sum11);%kk2=kk2+1;
    [B1,A1]=butter(3,6/512,'low');
    if y00(k)-y00(k-1)>0.0105+x_std
        i = i+1;%kk1=kk1+1;
        ont(i,1) = y00(k-NS);
        %ondiff=diff(ont(i,1));
        for kk=1:length(ont(:,1))-1
            if ont(kk,1)==0 && ont(kk+1,1)>0
```

```
                newondiff(kk,1)=(ont(kk+1,1))-ont(kk,1);
              end
              ondiff=newondiff;
              ondiff=ondiff(ondiff~=0);
           end
          %break
          [tf1, newind1] = ismember(ont(i,1), y00);
          ind1=[ind1;newind1];
      end
      for nn=1:length(ondiff)
         idx_on(nn)=(find(y00==ondiff(nn)));
      end
       if y001(k)-y001(k-1)>4.0 +vel_std(round((k+NS)/NS))
            ii = ii+1;%kk1=kk1+1;
            vel_ont(ii,1) = y001(k-NS);
            for kk=1:length(vel_ont(:,1))-1
                if vel_ont(kk,1)==0 && vel_ont(kk+1,1)>0
                  vel_newondiff(kk,1)=(vel_ont(kk+1,1))-vel_ont(kk,1);
                end
                vel_ondiff=vel_newondiff;
                vel_ondiff=vel_ondiff(vel_ondiff~=0);
%
            end
          %break
          [tf11, newind11] = ismember(vel_ont(i,1), y001);
          ind11=[ind11;newind11];
       end
       for nn=1:length(vel_ondiff)
         idvel_on(nn)=(find(y001==vel_ondiff(nn)));
       end
      if y00(k)-y00(k-1)<0.0105+x_std     %newont=y00(k);
            i=i+1;
            ont(i,2)=y00(k);
            %off10(i,:)=ont(i,2);%;ont(1,2)];
             for kk=1:length(ont(:,2))-1
                 if ont(kk,2)==0 && ont(kk+1,2)>0
                 newoffdiff(kk,1)=(ont(kk+1,2))-ont(kk,2);
                 end
                 offdiff=newoffdiff;
                 offdiff=abs(offdiff(offdiff~=0));
             end

             [tf2, newind2] = ismember(ont(i,2), y00);
            ind2=[ind2;newind2];
      end
      for nn=1:length(offdiff)
         idx_off(nn)=(find(y00==offdiff(nn)));

      end
       if y001(k)-y001(k-1)<4.0+vel_std(round((k+NS)/NS))
%newont=y001(k);
             ii=ii+1;
             vel_ont(ii,2)=y001(k);
            for kk=1:length(vel_ont(:,2))-1
                 if vel_ont(kk,2)==0 && vel_ont(kk+1,2)>0
                  vel_newoffdiff(kk,1)=(vel_ont(kk+1,2))-vel_ont(kk,2);
                 end
                 vel_offdiff=vel_newoffdiff;
                 vel_offdiff=(vel_offdiff(vel_offdiff~=0));
             end
```

```
            [tf22, newind22] = ismember(vel_ont(i,2), y001);
            ind22=[ind22;newind22];
     end
    for nn=1:length(vel_offdiff)
       idvel_off(nn)=(find(y001==vel_offdiff(nn)));

    end
    %==============================streching the signal======
    for k0=1:length(idvel_off)
    %emg_veldis_on1(:,k0)=idvel_on(k0)-idx_on(k0);
     if idvel_off(k0)-idx_off(k0)>20
        if k0==1
% =============baseline%
expanding=========================================
        x0=x(1:idx_on(k0));% I couldn't find it how it works
        x1=dct(x0);
        x1(length(x0):length(x0)+(idvel_on(k0)-idx_on(k0)))=0;
        xx_1=idct(x1);
% ==============1st burst
expanding=========================================
        x01=x(idvel_on(k0)+1:idx_off(k0));
        xx01=dct(x01);
        xx01(length(x01):length(x01)+(idvel_off(k0)-idx_off(k0)))=0;
        xx1=idct(xx01);
        else

        eval(sprintf('x0%d = x(idvel_on(k0)+1:(idx_off(k0)))', k0));

        eval(sprintf('in2%d = x(idvel_off(k0-1):idvel_on(k0)-1)',k0));

        eval(sprintf('yd%d = x(abs(idvel_off(k0-1)-idvel_on(k0)):-
1:1)',k0));

       if idvel_on(k0)-idx_on(k0)>40
        eval(['yhat' num2str(k0) '=filtadapt(yd' num2str(k0) ',in2'
num2str(k0) ');']);
       end

        eval(['xx0' num2str(k0) '=dct(x0' num2str(k0) ');']);

        eval(['x_' num2str(k0) '= (zeros(idvel_off(k0)-
idx_off(k0),1));']);

        eval(['xx_0' num2str(k0) '= [xx0' num2str(k0) ';x_'
num2str(k0) '];']);

        eval(['xx' num2str(k0) '=idct(xx_0' num2str(k0) ');']);

        zz_end=x(idvel_off(end)+1:end);


        end
     end
   end
end

toc
```

A.6. Real Time implementation correlation between the motion and muscle activities in real time process

```
function
[FiltEMG,GYFilt,MeanV,STDV,MGYRO,nSamp,idx_on,idx_off,idvel_on,idvel_o
ff]= cmd_realTime2(comPort1,comPort2,captureDuration,
fileName1,fileName2)
%% this code calculate the average of the emg signal every 150 samples
along
% the signal %%%%%%%% and return the onset of the emg signal
%elapsedTime = 0;
close all
DELAY_PERIOD =.2;
thisFilter.bufferedX=[];
thisFilter.bufferedX1=[];
thisFilter.samplingRate=512;

shimmer1 = ShimmerHandleClass(comPort1);
% Define shimmer as a ShimmerHandle Class instance with comPort1
shimmer2 = ShimmerHandleClass(comPort2);

firsttime = true;
 if (shimmer1.connect && shimmer2.connect)
%%%%%%%%%%%%%%%%%%%%%%%%%%%%%%%%%%%%%%%%%%%%%%%%%%%%%%%%%%%%%%%%%%%%%%%
%%%%%%%%%
% Define settings for shimmer



    shimmer1.setsamplingrate(512);
    shimmer1.setinternalboard('EMG'); % Set the shimmer internal
daughter board to 'None'
    shimmer1.setenabledsensors('EMG',1);

    shimmer2.setinternalboard('Gyro');
% Set the shimmer 2 internal daughter board to '9DOF', the default
setting is 'None'
    shimmer2.setenabledsensors('Gyro',1);  % Enable the shimmer 2
accelerometer and gyroscope, disable the magnetometer, AnEx_A0 and
AnEX_A7
    shimmer2.setsamplingrate(512);

    if (shimmer1.start && shimmer2.start)%
        calibDataShimmer1 = [];
        newData1 = [];

        calibDataShimmer2 = [];
        newData2 = [];

        storeData = [];
        MeanV=[];newMeanV=[];
        STDV=[];newSTDV=[];

        nSamp=[];sig=[];

        idx_on=[];idx_off=[];


        on=[];newondiff=[];ondiff=[];newoffdiff=[];offdiff=[];
```

```
        nSdiff=[];newSdiff=[];


        %%%% Gyro parameters %%%%%%%%%%%%%%%
        GYFilt=[];
        MGYRO=[];newMGYRO=[];MGYRO1=[];newMGYRO1=[];
        sig1=[];MnGyro=[];
        idvel_on=[];idvel_off=[];
        STDGYRO=[];newSTDGYRO=[];nSamp1=[];

onGY=[];newonGYdiff=[];onGYdiff=[];newoffGYdiff=[];offGYdiff=[];
        nSdiff1=[];newSdiff1=[];

        h.figure1=figure('Name','Shimmer ');
% Create a handle to figure for plotting data from shimmer

        elapsedTime = 0;    i0=0;    i1=0;
% Reset to 0
        tic;

        while (elapsedTime < captureDuration)

            pause(DELAY_PERIOD);
% Pause for this period of time on each iteration to allow data to
arrive in the buffer

            %%%EMG data shimmer sensor ################

[newData1,signalNameArray,signalFormatArray,signalUnitArray]=
shimmer1.getdata('EMG','c');

            if (firsttime==true)
                signalNamesString = char(signalNameArray(1,1));
% Create a single string, signalNamesString
                signalFormatsString = char(signalFormatArray(1,1));
% Create a single string, signalFormatsString
                signalUnitsString = char(signalUnitArray(1,1));
% Create a single string, signalUnitsString
                signalNamesString=[char('EMG'), char(9),
char('EMG_Filtered'), char(9)]; % create a single string,
signalNamesString
                dlmwrite(fileName1, signalNamesString, '%s');
            end

            if ~isempty(newData1)
% TRUE if new data has arrived

               %dlmwrite(fileName1, newData1, '-append', 'delimiter',
'\t'); % Append the new data to the file in a tab delimited format
                calibDataShimmer1 = [calibDataShimmer1; newData1];
                EMGDataFiltered=(calibDataShimmer1(:));
                % filter
design==============================================
                nSamples = length(calibDataShimmer1(:));
                bufferSize = thisFilter.samplingRate*2;
                if isempty(thisFilter.bufferedX)
```

```
                    thisFilter.bufferedX =
[newData1(1)*ones(bufferSize,1); calibDataShimmer1(:)];
                else
                    thisFilter.bufferedX =
[thisFilter.bufferedX(nSamples+1:end); calibDataShimmer1(:)];
                end
                  % filter coeffecient
                B=[6.000067137988330e-06,1.800020141396499e-
05,1.800020141396499e-05,6.000067137988330e-06];
                A=[1,-2.921919417911570,2.846514484228639,-
0.924560688648323];

                Y = filtfilt(B,A,abs(thisFilter.bufferedX));
                EMGDataFiltered = Y(end-nSamples+1:end);

                %%%%%%%%%%%%%%%%%%%%%%%%%%%%%%%%%%%%%%%%%%%%%%%%
                newstoreData = [calibDataShimmer1 EMGDataFiltered];
                storeData = [storeData; newstoreData];
                dlmwrite(fileName1, newData1, '-append', 'delimiter',
'\t');
                Seg=nSamples/150;

                newMeanV=mean(EMGDataFiltered(end-Seg+1:end));%(end-
Seg+1:end));% The mean values for each requested coming filtered data
                nSamp=[nSamp;nSamples];k0=0;
                MeanV=[MeanV(:);newMeanV(:)];

                newSTDV=std(EMGDataFiltered(end-Seg+1:end));% The
standard diviation for each segment
                STDV=[STDV(:);newSTDV(:)];
                FiltEMG=EMGDataFiltered(nSamp(1)-100:end);
                FiltEMG1=abs(FiltEMG-newMeanV);
                if length(nSamp)>1
                    k0=k0+1;
                    newSdiff(k0)=nSamp(length(nSamp))-
nSamp(length(nSamp)-1);
                    nSdiff=[nSdiff;newSdiff];
                    newsig=zeros(newSdiff,1);newsig(end)=newMeanV;
                    sig=[sig;newsig];
                end


                if length(MeanV)>1
                     i0=i0+1;
                     if MeanV(length(MeanV))> 3*MeanV(1)+
1*STDV(length(STDV))%&&
                         on(i0,1)=MeanV(length(MeanV)-1);
                         %on1=on(i0,1);
                       for kk=1:length(on(:,1))-1
                          if on(kk,1)==0 && on(kk+1,1)>0
                            newondiff(kk,1)=(on(kk+1,1))- on(kk,1);
                            %newondiff(i0)=on1(length(on)+1)-
on(length(on));
                            ondiff=[newondiff];
                          end
                          ondiff=ondiff(ondiff~=0);
                       end
                     end
                    for nn=1:length(ondiff)
                       idx_on(nn)=(find(sig==ondiff(nn)));
```

```
                    end
                      if MeanV(length(MeanV)) <
3*MeanV(1)%+STDV(length(STDV))
                          on(i0,2)=MeanV(length(MeanV));
                          for kk=1:length(on(:,2))-1
                           if on(kk,2)==0 && on(kk+1,2)>0
                             newoffdiff(kk,2)=(on(kk+1,2))- on(kk,2);
                             %newondiff(i0)=on1(length(on)+1)-
on(length(on));
                             offdiff=[newoffdiff];
                           end
                           offdiff=abs(offdiff(offdiff~=0));
                          end
                      end
                      for n0=1:length(offdiff)
                       idx_off(n0)=(find(sig==offdiff(n0)));
                      end

                end

                 set(0,'CurrentFigure',h.figure1);
% Create subplot
                 subplot(211); plot(FiltEMG);
                 x=FiltEMG;
            end
            %%%%%%%%%%%%%%%%%%%%%%%%GYRO SHIMMER %%%%%%%%%%%%%%%%%%%%
```

```
                dlmwrite(fileName2, newData2, '-append', 'delimiter',
'\t'); % Append the new data to the file in a tab delimited format

                calibDataShimmer2 = [calibDataShimmer2; newData2];
                GYDataFiltered=calibDataShimmer2(:,1);

                gyroData = [calibDataShimmer2(:,1),
calibDataShimmer2(:,2), calibDataShimmer2(:,3)];
                % filter design for the Gyro sensor
                nSamples1 = length(calibDataShimmer2(:,1));
                bufferSize1 = thisFilter.samplingRate*2;
                if isempty(thisFilter.bufferedX1)
                   thisFilter.bufferedX1 =
[newData2(1,1)*ones(bufferSize1,1); calibDataShimmer2(:,1)];
                else
                   thisFilter.bufferedX1 =
[thisFilter.bufferedX1(nSamples1+1:end); calibDataShimmer2(:,1)];
                end
                %                   % filter coeffecient
                B=[6.000067137988330e-06,1.800020141396499e-
05,1.800020141396499e-05,6.000067137988330e-06];
                A=[1,-2.921919417911570,2.846514484228639,-
0.924560688648323];
                YY = filtfilt(B,A,thisFilter.bufferedX1);
                GYDataFiltered = YY(end-nSamples1+1:end);
                GYDataFiltered1= abs(YY(end-nSamples1+1:end));
                 Seg1=nSamples1/150;

               %(end-Seg+1:end));% The mean values for each requested
coming filtered data
                newMGYRO= mean(GYDataFiltered(end-Seg1+1:end));
                GYFilt=GYDataFiltered-newMGYRO;
                MGYRO=[MGYRO;newMGYRO];

                newSTDGYRO=std(GYDataFiltered1(end-Seg1+1:end));% The
standard diviation for each segment
                STDGYRO=[STDGYRO;newSTDGYRO];
                nSamp1=[nSamp1;nSamples1];k1=0;
                if length(nSamp1)>1
                    k1=k1+1;
                    newSdiff1(k1)=nSamp1(length(nSamp1))-
nSamp1(length(nSamp1)-1);
                    nSdiff1=[nSdiff1;newSdiff1];
                    newsig1=zeros(newSdiff1,1);newsig1(end)=
(newMGYRO);
                    sig1=[sig1;newsig1];
                    sig1=abs(sig1);
                end
                %%%%%%%%%%%%%%%%%%%%GYRO MEAN and
%%%%%%%%%%%%%%%%%%%%%%%%
                if length(MGYRO)>1
                     i1=i1+1;
                     if abs(MGYRO(length(MGYRO)))> 7+1*abs(MGYRO(2)) +
1*STDGYRO(length(STDGYRO))%&&
                         onGY(i1,1)=abs(MGYRO(length(MGYRO)-1));
                         %on1=on(i0,1);
                        for k=1:length(onGY(:,1))-1
                           if onGY(k,1)==0 && onGY(k+1,1)>0
                             newonGYdiff(k,1)=(onGY(k+1,1))-
onGY(k,1);
```

```
                                %newondiff(i0)=on1(length(on)+1)-
on(length(on));
                                onGYdiff=[newonGYdiff];
                              end
                              onGYdiff=onGYdiff(onGYdiff~=0);
                           end
                        end

                        for n1=1:length(onGYdiff)
                          idvel_on(n1)=(find(sig1==onGYdiff(n1)));
                        end


%
%%%%%%%%%%%%%%%%%%%%%%%%%%%%%%%%%%%%%%%%%%%%%%%%%%%%%%%%%%%%%%%
                        if abs(MGYRO(length(MGYRO))) <
4+1*abs(MGYRO(2))%+STDV(length(STDV))
                           onGY(i1,2)=abs(MGYRO(length(MGYRO)));
                           for k=1:length(onGY(:,2))-1
                            if onGY(k,2)==0 && onGY(k+1,2)>0
                              newoffGYdiff(k,2)=(onGY(k+1,2))-
onGY(k,2);
                              %newondiff(i0)=on1(length(on)+1)-
on(length(on));
                              offGYdiff=[newoffGYdiff];
                            end
                            offGYdiff=abs(offGYdiff(offGYdiff~=0));
                           end
                        end
                        for n2=1:length(offGYdiff)
                         idvel_off(n2)=(find(sig1==offGYdiff(n2)));
                        end
%
                  end


              % Extract only the columns of gyroscope data
              set(0,'CurrentFigure',h.figure1);
% Create subplot
              subplot(212); plot(GYFilt);
              %xx=[x1,x2,x3];
              %subplot(212); plot(x1);%hold on;plot(x2,'g');hold
on;plot(x3,'r')
              end


              %%% Finding the delays between the two signals / expanding
              %%% or/shortening the signal whenever is needed to be???
     for k2=1:length(idvel_off)
%     %emg_veldis_on1(:,k0)=idvel_on(k0)-idx_on(k0);
      if idvel_off(k2)-idx_off(k2)>20
         if k2==1
% % =============baseline%
expanding=========================================
         x0=x(1:idx_on(k2));% I couldn't find it how it works
         x1=dct(x0);
         x1(length(x0):length(x0)+(idvel_on(k2)-idx_on(k2)))=0;
         xx_1=idct(x1);
% % =============1st burst
expanding=========================================
         x01=x(idvel_on(k2)+1:idx_off(k2));
```

```
          xx01=dct(x01);
          xx01(length(x01):length(x01)+(idvel_off(k2)-idx_off(k2)))=0;
          xx1=idct(xx01);
         else

         eval(sprintf('x0%d = x(idvel_on(k2)+1:(idx_off(k2)))', k2));

         eval(sprintf('in2%d = x(idvel_off(k2-1):idvel_on(k2)-1)',k2));

         eval(sprintf('yd%d = x(abs(idvel_off(k2-1)-idvel_on(k2)):-
1:1)',k2));

        if idvel_on(k2)-idx_on(k2)>40
         eval(['yhat' num2str(k2) '=filtadapt(yd' num2str(k2) ',in2'
num2str(k2) ');']);
        end

         eval(['xx0' num2str(k2) '=dct(x0' num2str(k2) ');']);

         eval(['x_' num2str(k2) '= (zeros(idvel_off(k2)-
idx_off(k2),1));']);

         eval(['xx_0' num2str(k2) '= [xx0' num2str(k2) ';x_'
num2str(k2) '];']);

         eval(['xx' num2str(k2) '=idct(xx_0' num2str(k2) ');']);

          end
       end
     end

            elapsedTime = elapsedTime + toc;
% Stop timer and add to elapsed time
            tic;
         end

          elapsedTime = elapsedTime + toc;
% Stop timer

          fprintf('The percentage of received packets: %d
\n',shimmer1.getpercentageofpacketsreceived(calibDataShimmer1(:,1)));
          fprintf('The percentage of received packets: %d
\n',shimmer1.getpercentageofpacketsreceived(calibDataShimmer2(:,1)));
% Detect loss packets

          shimmer1.stop;
          shimmer2.stop;

     end
      shimmer1.disconnect;
      shimmer2.disconnect;

 end
```

A.7 Passive force-length relationship

```
function Fp=fp_l(n_lm)
fmax=974;
```

```
for k=1:length(n_lm)
Fp (k) =exp(10*n_lm(k)-15);
end
figure
plot(fmax*Fp)
end
```

A.8 Active force-Fiber length relationship

```
function Fa=fa_l(n_lm)
%This is the force-length equation for the bicep. (pg 88)
%For the equation to not equal 0, the muscle length must be between
.075 and .225.
q0= -2.06; q1 = 6.16;  q2 = -3.13;fmax=974;
for k=1:length(n_lm)
    if n_lm(k)>=0.5 & n_lm(k)<=1.5
    Fa(k) = q0+ q1*n_lm(k)+ q2*n_lm(k).^ 2;
    else
    Fa(k)=0;
    end% k1 coffiecient 1

end

plot(fmax*Fa)

end
```

A.8 sEMG raw to muscle force-joint moment transformation

```
%% EMG to neural activation
gama1=0.23;gama2=0.28;
beta1=gama1+gama2;beta2=gama1*gama2;
alpha = beta1+beta2+1;d=40e-3;

n_emg1_fil=BF_M';
u0=n_emg1_fil(1);
u=u0*ones(1,1201);u(1)=n_emg1_fil(1); u(2)=n_emg1_fil(2);d=40e-
3;Fs=512;

for i=21:1:length(u)
    u(i)=alpha*n_emg1_fil(i-round(d*Fs))- beta1*u(i-1)-beta2*u(i-2);
end
plot(u)
%% BF optimal muscle length
A=-1.78;
lm0=10.09;%(cm) for the lower limb BF muscle

for k=1:length(RF_M)
    aa(k)=(exp(A*u(k))-1)/(exp(A)-1);
    lm(k) = lm0*(0.15*(1- aa(k))+1);
    n_lm(k)=lm(k)/lm0;
end
plot(aa)
hold on
plot(u,'r');plot(n_emg1_fil(1:1201),'k')
figure
plot(n_lm)
%% active muscle force normalized to the length of the muscle FA
fmax=1312; % from literature
for k=1:length(RF_M)
```

```
    FA(k)=aa(k)*Fa(k);
end
FA;

FA_t=fmax*(FA+Fp);
```

A.9 Moment Arm code

```
% the following coeffiecient are adapted from J.J. Visser et.al 1990

coef1=[-0.02345 0.24222 -0.00059]; %RF_knee angle coeff
coef2=[-0.01966 -0.15041    0.00044];% RF_Hip angle coeff
coef3=[0.19826  -0.04600    0.00000];%BF_knee angle coeff
coef4=[0.16644  0.31078 0.00061]; %BF_hip angle coeff
coef5=[-0.08268 -0.08028    -0.00013]; %Gas_knee angle coeff

%theta1=ang1;
seg=46.1;% upper seg length (cm);

for kk=1:length(theta1)

A0=coef1(1);
A1=coef1(2);
A2=coef1(3);

lmt(kk,1)=coef3(1)+coef3(2)*theta1(kk,1) + coef3(3)*(theta1(kk,1))^2;
MA1_RFw(kk,1)= coef1(2)+2*coef1(3)*theta1(kk,1);
MA1_BFw(kk,1)= coef3(2)+2*coef3(3)*theta1(kk,1);
MA1_Gasw(kk,1)= coef5(2)+2*coef5(3)*theta1(kk,1);
end
```

A.9 Moment generated by the muscles

```
%% muscle tendon length measurments of the RF BF and Gas and moment
arm
% Estimation of the RF length with reagrds to the hip movement
%parameter

for nn=1:length(RF_M)
    Mt1(nn)=FA_t(nn)*MA1(nn);%% BF muscle
    Mt2(nn)=FA_t1(nn)*MA(nn);%% RF muscle
end
MT_t=Mt1+Mt2;
plot(MT_t)
```

A.11 Inverse dynamics moment for sit to stand, stand to sit anf walking

```
% simulation parameters
m1=7.1;m2=48.14; l1=0.461;l2=0.29;g=9.81;
I1=0.132;I2=1.145;
%theta2=-(3/2)*theta1 + (3*pi
%% standing up model
for nn=1:length(acc)
Mk(nn)=acc(nn)*(-(1/8)*m2*l2^2+(1/4)*m1*l1^2 +m2*l1^2 -
(1/4)*m2*l1*l2*sin((3/2)*theta1(nn))+I1- 1/2*I2)...
       -(3/8)*m2*l1*l2*cos((3/2)*theta1(nn))*vel(nn)^2 +
0.5*m1*g*l1*sin(theta1(nn))...
```

```
       +m2*g*l1*sin(theta1(nn))-0.5*m2*g*l2*cos(0.5*theta1(nn));
end
plot(Mk)
%% sitting down model
%%%%=========================%%%%%%%===============
%P1=0.5*m1*g*l1*cos(theta1);P2=m2*g*(l1*cos(theta1)-
0.5*l2*sin(theta1/2));
%x=l1*sin(theta1)-0.5*l2*cos(theta1/2);y=l1*cos(theta1)-
0.5*l2*sin(theta1/2);
clear DLk DLp
for nn=1:length(acc)
   K1(nn)=0.5*vel(nn)^2*(0.25*m1*l1^2+I1);
   DLk(nn)= acc(nn)*(0.25*m1*l1^2+I1+0.25*I2) +
0.5*m2*acc(nn)*(4*l1.^2+0.25*l2.^2 - l1*l2*sin(theta1(nn)/2))-
0.5*l1*l2*vel(nn).^2*cos(theta1(nn)./2);
   DLp(nn)=0.5*g*l1*(m1-
2*m2)*cos(theta1(nn))+0.25*m2*g*l2*cos(theta1(nn)./2);
   Mk2(nn)=DLk(nn)-DLp(nn);
end
 plot(Mk2,'r')
%% walking experiment inverse dynamics

% simulation parameters
m1=3.2;m2=7.1; l1=0.43;l2=0.46;g=9.81;
I1=0.064;I2=0.1345;

%theta1=-(heel_angtr3*pi./180);
theta0=(theta3*pi/180);
%ang=theta1;
clear vel1 vel2
for kk=1:length(theta1)-1;
    vel1(kk)=512*(theta1(kk+1)-theta1(kk));
    vel2(kk)=512*(theta0(kk+1)-theta0(kk));
end

plot(vel1);
%%
clear acc1 acc2

for k=1:length(vel1)-1;
   acc1(k)=512*(vel1(k+1)- vel1(k));
   acc2(k)=512*(vel2(k+1)- vel2(k));
end
plot(acc2)
%% walking inverse dynamic
clear Mkw Dlp Dkw
for nn=1:length(acc1)
    Dlk(nn)=(acc1(nn)*(0.25*m1*l1^2+I1))+
0.5*I2*(acc1(nn)+acc2(nn))+0.5*m2*(4*l1^2*acc1(nn)+l2^2*(acc1(nn)+acc2
(nn))+l1*l2*(2*acc1(nn)+acc2(nn))*cos(theta0(nn))-
l1*l2*(2*vel1(nn)*vel2(nn)+(vel1(nn)^2))*sin(theta0(nn)));
    Dlp(nn)= -(0.5*m1*g*l1*cos(theta1(nn)) + m2*g*l1*cos(theta1(nn))+
0.5* m2*g*l2*cos(theta1(nn)+theta0(nn)));
    Mkw(nn)=Dlk(nn)-Dlp(nn);

end
```

A.11 fitting polynomials for the sit to stand, stand to sit anf walking

```
function p = polyfit2(aa1,aa2,z)
% polyfit2.m
% --------------------
% By D.HAKIM (2016)
%
% Usage aa1 and aa2 aa3 are the muscle activation dynamics
% z is the inverse dynamic moment
% ------

% sense. P is a row vector of length (N+1)*(N+2)/2 containing the
% polynomial coefficients in ascending powers, 0th order first.
%
%   P = [ p11 p12 p13 p21 p22]
%
% e.g. For a 3rd order fit,
% the regression problem is formulated in matrix format as:
%   [x  y  x^2  y^2  x^3   y^3] [p11
%                                p12
%                                p13
%                                p21
%                                p22
%                                p23]
%
%


clear V

x=aa1';y=aa2';
x = x(:);
y = y(:);

lx=length(x);
ly=length(y);
y=y*ones(1,lx);
x=ones(ly,1)*x';
x = x(:);
y = y(:);
z = z(:);
%w = w(:);
F0Bf=1312;F0RF=974;F0Gas=2225;% are the max forces at isometric
contraction
%pts=lx*ly;
%pts=length(z);
V(:,1)=diag(F0Bf*x(:)*MA1_BF');V(:,2)=diag(F0Bf*diag(x*x')*MA1_BF');V(
:,3)=diag(F0Bf*diag(diag(x*x')*x')*MA1_BF');
V(:,4)=diag(F0RF*y(:)*MA1_RF');V(:,5)=diag(F0RF*diag(y*y')*MA1_RF');V(
:,6)=diag(F0RF*diag(diag(y*y')*y')*MA1_RF');
V(:,7)=diag(F0Gas*z(:)*MA1_Gasw');V(:,8)=diag(F0Gas*diag(z*z')*MA1_Gas
w');V(:,9)=diag(F0Gas*diag(diag(z*z')*z')*MA1_Gasw');

% Solve least squares problem.
[Q,R] = qr(V,0);
ws = warning('off','all');
p = R\(Q'*(z));    % Same as p = V\(w.*z);

%r = z - (V*p)./w;
p = p.';          % Polynomial coefficients are row vectors by
convention.
```

Appendix B

More simplification on equation (4.46) has been made; the force generated by a muscle is rewritten as

$$F^m(k) = F_0^m[\mathrm{K}_1 a(k) + \mathrm{K}_2 a^2(k) + \mathrm{K}_3 a^3(k) + \mathrm{K}_4 \mathrm{e}^{\mathrm{K}_5 a(k)}] \quad \text{(B.1)}$$

where,

$\mathrm{K}_1 = l_0^{2m}(1+2\eta+\eta^2) + \mathrm{C}_0 + \mathrm{C}_1(l_0^m + l_0^m\eta)$, $\mathrm{K}_2 = (2\mathrm{C}_2(l_0^m\eta - l^{2m}_0\eta^2) - \mathrm{C}_1 l_0^m\eta)$,

$\mathrm{K}_3 = l_0^{2m}\eta^2$

$\mathrm{K}_4 = \mathrm{e}^{10(l_0^m\eta + l_0^m) - 15}$ and $\mathrm{K}_5 = -10 l_0^m\eta$

Since l_0^m and η are known see (chapter 4, **Table 4.3**) for each muscle, one can calculate the coefficients K3, K4 and K5 in which are listed in table 5.4. These coefficients are constant with all types of experiment.

Let,

$$F_{BF}^m(k) = [\mathrm{K}_{1\mathrm{BF}} a_1(k) + \mathrm{K}_{2\mathrm{BF}} a_1^2(k) + \mathrm{K}_{3\mathrm{BF}} a_1^3(k) + \mathrm{K}_{4\mathrm{BF}} \mathrm{e}^{\mathrm{K}_{5\mathrm{BF}} a_1(k)}] \quad \text{(B.2)}$$

$$F_{RF}^m(k) = [\mathrm{K}_{1\mathrm{RF}} a_2(k) + \mathrm{K}_{2\mathrm{RF}} a_2^2(k) + \mathrm{K}_{3\mathrm{RF}} a_2^3(k) + \mathrm{K}_{4\mathrm{RF}} \mathrm{e}^{\mathrm{K}_{5\mathrm{RF}} a_2(k)}] \quad \text{(B.3)}$$

$$F_{Gas}^m(k) = [\mathrm{K}_{1\mathrm{Gas}} a_3(k) + \mathrm{K}_{2\mathrm{Gas}} a_3^2(k) + \mathrm{K}_{3\mathrm{Gas}} a_3^3(k) + \mathrm{K}_{4\mathrm{Gas}} \mathrm{e}^{\mathrm{K}_{5\mathrm{Gas}} a_3(k)}] \quad \text{(B.4)}$$

the forces generated by the BF, RF and Gas muscles, $a_1(k)$, $a_2(k)$, and $a_3(k)$ are the muscle activities for the BF, RF and Gas muscle at time sample k, respectively.

$\mathrm{K}_{i\mathrm{BF}}$ with i =1,2….,5 are the coefficients of force generated by the BF muscle, $\mathrm{K}_{i\mathrm{RF}}$ are the coefficients of force generated by the RF muscle and $\mathrm{K}_{i\mathrm{Gas}}$ are the coefficients of force generated by the Gas muscle.

Appendix C:

Table C.1
Wavelet and Butterworth correlation

Butterworth order	Wavelet levels	Correlation
8	6	0.9864
	7	0.9568
	8	0.9283
	5	0.9801
	4	0.9222
7	4	0.9229
	5	0.9805
	6	0.9866
	7	0.9571
	8	0.9286
6	4	0.9237
	5	0.9812
	6	0.9868
	7	0.9575
	8	0.9290
5	4	0.9250
	5	0.9820
	6	0.9872
	7	0.9580
	8	0.9295
4	4	0.9267
	5	0.9830
	6	0.9874
	7	0.9587
	8	0.9302
3	4	0.9298
	5	0.9847
	6	0.9879
	7	0.9601
	8	0.9315
2	4	0.9352
	5	0.9862
	6	0.9878
	7	0.9624
	8	0.9339
1	4	0.9480
	5	0.9851
	6	0.9847
	7	0.9657
	8	0.9393

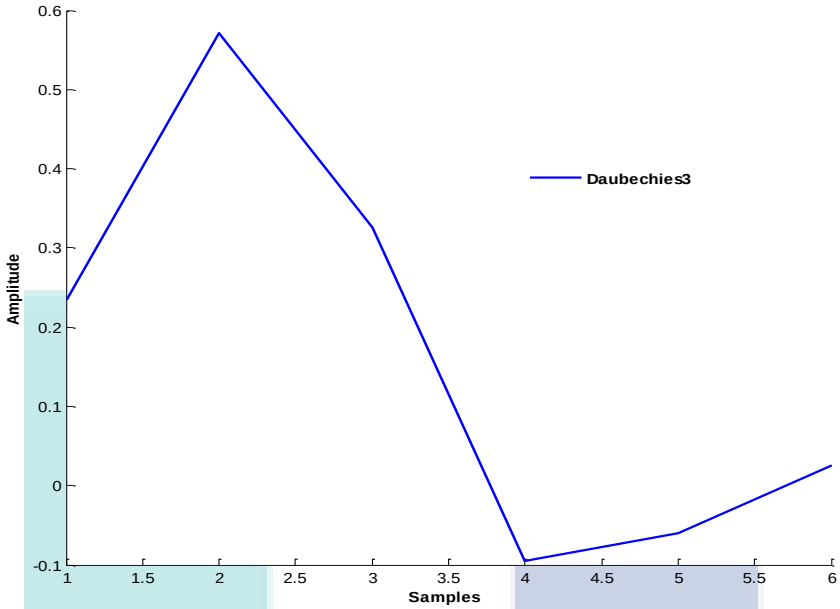

Figure C.2. Daubechies mother wavelet waveform.